1991

Spectrophotometric determination of dissolved manganese in natural waters : in situ chemical mapping in hydrothermal plumes, with concurrent measurements of total dissolved iron

Carol Sue Chin
San Jose State University

Order Number 1345791

Spectrophotometric determination of dissolved manganese in natural waters: *In situ* chemical mapping in hydrothermal plumes, with concurrent measurements of total dissolved iron

Chin, Carol Sue, M.S.

San Jose State University, 1991

U·M·I
300 N. Zeeb Rd.
Ann Arbor, MI 48106

SPECTROPHOTOMETRIC DETERMINATION OF DISSOLVED MANGANESE IN NATURAL WATERS: *IN SITU* CHEMICAL MAPPING IN HYDROTHERMAL PLUMES, WITH CONCURRENT MEASUREMENTS OF TOTAL DISSOLVED IRON

A Thesis

Presented to

The Faculty of Moss Landing Marine Laboratories

In Partial Fulfillment

of the Requirements for the Degree

Master of Sciences

in

Marine Sciences

By

Carol Sue Chin

August, 1991

APPROVED FOR MOSS LANDING MARINE LABORATORIES

Kenneth S Johnson

Dr. Kenneth S. Johnson, Professor

Kenneth H. Coale

Dr. Kenneth H. Coale, Researcher

Dr. John H. Martin, Professor

APPROVED FOR THE UNIVERSITY

Serena M. Stanford

ABSTRACT

Spectrophotometric Determination of Dissolved Manganese in Natural Waters:
In Situ Chemical Mapping in Hydrothermal Plumes,
with Concurrent Measurements of Total Dissolved Iron

by Carol Sue Chin

A spectrophotometric method using 1-(2-pyridylazo)-2-naphthol (PAN) was developed for the determination of dissolved manganese in natural waters. Additionally, the colorimetric ferrozine technique for the determination of dissolved Fe(II) was modified by adding ascorbic acid as a reductant, allowing for the determination of total dissolved iron (Fe(II) plus Fe(III)). These two techniques were adapted for use on a submersible chemical analyzer (Scanner) for analyses *in situ*. Continuous measurements of manganese and iron were performed *in situ* in submarine hydrothermal plumes along the Juan de Fuca Ridge using the Scanner, which was mounted on a CTD/Transmissometer/rosette (CTDT/rosette) sampler. Deployments of this instrument package produced the first near real time analyses of manganese and iron from a hydrothermal plume environment. The detailed distributions of these two metals, and their relationship to the temperature anomaly produced by venting, were used to examine processes within the plumes sampled; as well as to predict the types of source waters contributing to the dispersing plumes.

ACKNOWLEDGMENTS

I wish to extend my sincere gratitude to my adviser Dr. Ken Johnson who has provided support and guidance throughout my tenure at Moss Landing Marine Labs. I am flattered that he trusted me with a project of such magnitude. I would also like to thank Dr. John Martin for participating as a member of my committee, and for his interest in this research.

I feel very fortunate to have worked with and learned from Dr. Kenneth Coale. He has been both a mentor and a friend; serving as a constant source of encouragement, enthusiasm, and humor.

Ginger Elrod and Kenneth Coale deserve special thanks for the month that we spent at sea aboard the NOAA Ship Discoverer -- enduring rubber chickens, voodoo dolls, intriguing fragrances, and enjoying many laughs...

This project was a collaborative effort and could not have been completed without Gary Massoth, Ed Baker, Dick Feely, Sharon Walker, Kevin Roe and Geoff Lebon of the NOAA/Pacific Marine Environmental Laboratory who graciously accommodated us on the VENTS cruise, 1989; and who have provided us with a wealth of supporting data, valuable insight, and critical, encouraging discussions and comments.

I am also indebted to Lynn McMasters who prepared several of the figures included in this manuscript and its resulting publications, as well as others used in

the presentation of this work at scientific meetings; and to Sheila Baldridge and Sandi O'Neil for all of their assistance in conducting literature searches.

Finally, I would like to thank Mom, Dad and Timmy who have supported me in a variety of ways, even providing invaluable suggestions in my research. This work is dedicated to the memory of my late grandmother, Mock Shee Chin.

I would like to express my appreciation to the David and Lucille Packard Foundation for funding the presentation of this work at the AGU-ASLO Ocean Sciences Meeting, February, 1990; and to The Oceanography Society for funding the presentation of this work at the Second Scientific Meeting, March, 1991. This research was supported by the Ocean Sciences Division of the NSF grant OCE-8609437 to K. Johnson, the Office of Naval Research grant N00014-89-J-1010 to K. Johnson and K. Coale, and the NOAA VENTS Program.

PREFACE

This thesis presents the study of manganese and iron distributions and geochemistry in hydrothermal vent plumes. It begins with an introduction to the characteristics of hydrothermal venting processes and hydrothermal plume chemistry and physics (Chapter 1). The development of a method for the determination of dissolved manganese in natural waters is then described (Chapter 2). The thesis concludes with a discussion of the distributions and geochemical cycling of dissolved Mn and Fe in near field hydrothermal plumes along the Cleft and Endeavour Segments of the Juan de Fuca Ridge (Chapter 3). An appendix which also describes some of these results is included. The method and these results have been presented at three international meetings and the chapters and appendix have been (or will be soon be) submitted for publication. The chemical results are interpreted together with measurements of physical properties (temperature anomaly, beam attenuation anomaly, and potential density) and provide a unique database from which the age, mixing dynamics, and sources of the sampled hydrothermal plumes are inferred.

The format of each chapter reflects the format required by each journal to which chapters are submitted. Chapter 2, in press in *Marine Chemistry*, presents a technique for the determination of dissolved manganese in natural waters. Most of this chapter describes the development of this technique, and includes a discussion of the laboratory experiments performed to test and verify this method. A brief description of the field application of this technique to the determination of Mn *in*

situ also appears. The third chapter describes the application of this method to the determination of dissolved manganese in submarine hydrothermal plumes at both the Cleft and Endeavour Segments, along with the simultaneous determination of total dissolved iron (Fe(II) plus Fe(III)). This chapter is to be submitted to *Deep-Sea Research*. The appendix is a shorter paper which serves as a brief presentation of some of the key results of this study, and is in press in *Nature*.

CONTENTS

LIST OF FIGURES

Figure Page

Chapter 3

Figure Page

Chapter 4

LIST OF TABLES

CHAPTER 1

Introduction

Since the discovery of both low temperature, diffuse flow and high temperature, "black smoker" type submarine hydrothermal venting in the late 1970s (Corliss et al., 1979; Spiess et al., 1980), such phenomena have changed the way that oceanographers think about various aspects of the ocean environment including deep-sea communities, abyssal circulation, heat and chemical budgets, and depositional patterns of metal-rich sediments. Some of the most sensational findings have focused on the chemosynthetic based animal/bacterial communities which inhabit the venting sites, mediating the reaction of the highly reducing hydrothermal vent waters and the oxygenated bottom waters for use as their energy source. Of equal importance and of greater geochemical significance is the influence that hydrothermal venting has had upon the chemistry of the midwaters, and the distribution of metalliferous sediments world wide. This thesis project will elucidate some of the chemical processes of this important biogeochemical phenomenon.

Submarine hydrothermal venting delivers an estimated 4.9×10^{19} calories of heat to the world's ocean every year (Jenkins et al., 1978). This hydrothermal heat flux represents approximately 25% of the total annual heat loss from the earth (Sclater et al., 1981). As a result, this geothermal heating is believed to contribute to abyssal circulation (Hautala and Riser, 1989; Stommel, 1982). Stommel (1982) notes that a turbulent ascending hydrothermal plume would act as a sink for bottom waters from which seawater is entrained and warmed, and would also act as a source to

layers higher in the water column where the rising water would reach buoyancy equilibrium with the surrounding water, at a height of several hundred meters, and begin to spread laterally (Lupton and Craig, 1981; Lupton et al., 1985; Baker et al., 1985; Baker and Massoth, 1986; 1987).

Approximately 1.2 x 10^{14} kg of high temperature fluids are produced by hydrothermal venting every year. In terms of volume, this is less than 1% of the annual global water runoff (Palmer and Edmond, 1989). Nonetheless, concentrations of chemicals in these fluids may be extremely high. Thus, hydrothermal vents are also a major source of iron, manganese, copper, lithium, lead, and rubidium, and also contribute substantially to the input of calcium, barium, and silica to the ocean (Edmond et al., 1979; 1982). Edmond et al. (1982) note that the fluxes of these elements from venting processes are often comparable with or greater than those estimated for all other inputs. Table 1 presents a comparison of hydrothermal, fluvial, and atmospheric fluxes of elements to the world's oceans. These fluxes have been compiled from available data (Edmond et al., 1979a, b; Von Damm et al., 1985; Kadko et al., 1987; Shimmield and Price, 1988; Chester and Murphy, 1990; Feely et al., 1990; Trefry and Metz, 1990). The atmospheric fluxes are presented as net global total atmospheric input, rather than total soluble input, except where noted. Column 6 (Table 1) presents the relative hydrothermal contribution in percent of total input. Hydrothermal solutions are particularly enriched in manganese and iron, and it is estimated that these effluents contribute approximately 73% of the total input of Fe

and 69% of the total input of Mn to the ocean (Table 1). All of these estimates are, however, only approximate. The hydrothermal flux estimates are limited by the present knowledge and understanding of the number and distribution of hydrothermal vents as well as the magnitude (activity and strength) of venting processes. Despite this uncertainty, this table demonstrates the importance of hydrothermal venting both as a major source and as a significant removal mechanism for chemical constituents of the world's oceans.

The lateral dispersal pattern of hydrothermal plumes over the East Pacific Rise is coincident with the observed distribution of metalliferous sediments along the ridge crest (Klinkhammer and Hudson, 1986). This suggests that the particulate phases precipitated from these plumes (primarily iron oxides and hydroxides) contribute to these deposits of metalliferous sediments along the crests and flanks of mid-ocean ridges. In addition, the particulate phases within hydrothermal plumes have been found to scavenge phosphorus, vanadium, chromium, arsenic, lead, polonium, uranium, thorium, protactinium, and a number of rare earth elements from seawater (Table 1; Feely et al., 1990; Trefry and Metz, 1990; Kadko et al., 1987; Shimmield and Price, 1988; Klinkhammer et al., 1983; German et al., 1990).

Hydrothermal venting sites occur along the crests of mid ocean ridges. Only a small percentage of the possible sites have been discovered and sampled (Rona, 1988) (Fig. 1). The chemistries and temperatures (Edmond et al., 1979; Canadian American Seamount Expedition, 1985; Von Damm, 1985; USGS Juan de Fuca Study

Group, 1986; Macdonald et al., 1980; Converse et al., 1984) of venting fluids have been sampled directly using submersibles at fewer than 25 sites. The buoyant and neutrally buoyant plumes have been sampled both by submersible and tethered instrument packages at only a few locations in the Pacific and Atlantic.

Direct observations at vents are difficult because they require expensive, manned submersibles. Spatial and temporal variability and the extreme thermal conditions at individual vents can also make it difficult to determine mass fluxes by direct observation. However, hydrothermal plumes integrate this variability and can be used to estimate thermal and chemical fluxes from vent fields (Baker and Massoth, 1986; Rosenberg et al., 1988). Thus, mapping of hydrothermal plumes is one of the most effective strategies for locating hydrothermal venting sites and assessing their mass and thermal budgets.

The physical characteristics of hydrothermal plumes have been mapped through the examination of the distributions of conductivity, temperature, and light attenuation, using a towed CTD/Transmissometer/rosette (CTDT/rosette) instrument package (Baker and Massoth, 1986). Until now, the chemical distributions in the plumes have only been studied using discrete samples collected in Niskin bottles and returned to the laboratory for analysis. The chemical characteristics of the dispersing plumes remain poorly understood due to undersampling. Discrete sampling techniques that have been used in past studies limit the number of samples per deployment to 12 on a typical rosette. This small

number fails to indicate, with much confidence, the range and variability in the concentrations of metals in plumes, or details of their relationship to excess heat (Coale et al., 1991).

Chemical tracers in vent plumes have great potential both for locating vent fields and also as remote indicators of the geochemical characteristics of the hydrothermal sources. Manganese is one of the most sensitive chemical indicators of hydrothermal activity (Bolger et al., 1978; Klinkhammer, 1980; Lupton et al., 1980; Baker et al., 1985). The concentration of manganese in hydrothermal source waters (black smoker vents; 4.48 mM, Von Damm, 1990) is up to 22 million fold enriched over the ambient seawater concentrations of 0.2 nM (Landing and Bruland, 1980; 1987; Martin et al., 1985), and it behaves nearly conservatively within near field hydrothermal plumes (Lupton et al., 1980; Jenkins et al., 1978; Klinkhammer et al., 1977; Weiss, 1977). As a result of this large input, hydrothermally derived anomalies in the seawater concentration of manganese have been detected thousands of kilometers from hydrothermal sources (Klinkhammer and Hudson, 1986).

Manganese and iron analyses are usually performed using column extraction followed by graphite furnace atomic absorption detection (Klinkhammer, 1980). Recently, K. Johnson and co-workers have reported reliable shipboard methods for the determination of dissolved Mn (Chapin et al., 1991) and dissolved iron(II) and total iron (Elrod et al. 1991) using flow injection analysis with chemiluminescence

detection. To date, however, all of these methods require modes of sample manipulation or detection that are not readily amenable to analysis *in situ*.

The goals of this research were to develop a simple colorimetric chemical technique that could be used for sensitive Mn analyses and to use this chemistry to map the *in situ* distribution of Mn in hydrothermal plumes. A submersible chemical analyzer (Scanner) has been used to study sulfide and oxygen distributions in hydrothermal vent fields (Johnson et al., 1986a; 1986b). The Scanner was designed to perform two colorimetric analyses simultaneously *in situ*. For this study it was necessary to adapt or develop colorimetric methods for the determination of metals (Fe and Mn) for use with the Scanner. The ferrozine method for the colorimetric determination of dissolved Fe(II) (Stookey, 1970) was adapted for the determination of total dissolved iron (Fe(II) plus Fe(III)) using ascorbic acid to reduce Fe(III) to Fe(II). Next, a method for the colorimetric determination of dissolved manganese was developed in the laboratory and then also adapted for use on the Scanner (Chin et al., 1990; 1991). The Scanner was secured to a CTDT/rosette sampler, and this instrument package was deployed on both vertical casts and "tow-yos" over the Juan de Fuca Ridge hydrothermal system. During the tow-yos, the Scanner/CTDT/rosette was raised and lowered in a sawtooth pattern while towed from a surface ship at a speed of 1 to 2 knots.

These deployments produced the first near real time analyses of dissolved Mn and Fe, together with measurements of physical properties including the temperature and light attenuation anomalies, in a hydrothermal plume environment.

References

Baker E. T. and G. J. Massoth (1986) Hydrothermal plume measurements: a regional perspective. Science, **234**, 980-982.

Baker E. T. and G. J. Massoth (1987) Characteristics of hydrothermal plumes from two vent fields on the Juan de Fuca Ridge, northeast Pacific Ocean. Earth and Planetary Science Letters, **85**, 59-73.

Baker E. T., J. W. Lavelle and G. J. Massoth (1985) Hydrothermal particle plumes over the Juan de Fuca Ridge. Nature, **316**, 342-344.

Baker E. T., G. J. Massoth and R. A. Feely (1987) Cataclysmic hydrothermal venting on the Juan de Fuca Ridge. Nature, **329**, 149-151.

Bolger G. W., P. R. Betzer and V. V. Gordeev (1978) Hydrothermally-derived manganese suspended over the Galapagos Spreading Center. Deep-Sea Research, **25**, 721-733.

Boström K., M. N. P. Peterson, O. Joensuu and D. E. Fisher (1969) Aluminum-poor ferromanganoan sediments on active oceanic ridges. Journal of Geophysical Research, **74**, 3261-3270.

Canadian American Seamount Expedition (1985) Hydrothermal vents on an axis seamount of the Juan de Fuca Ridge. Nature, **313**, 212-214.

Chapin T. P., K. S. Johnson and K. H. Coale (1991) Rapid determination of manganese in seawater by flow injection analysis with chemiluminescence detection. Analytica Chimica Acta, in press.

Chin C., K. Coale, K. Johnson, G. Massoth, E. Baker and R. Feely (1990) Development and application of an *in situ* spectrophotometric method for the determination of manganese in hydrothermal vent plumes. EOS, **71**, 143.

Chin C. S., K. S. Johnson and K. H. Coale (in press) Spectrophotometric determination of dissolved manganese in natural waters with 1-(2-pyridylazo)-2-naphthol: application to analysis *in situ* in hydrothermal plumes. Marine Chemistry.

Coale K. H., C. S. Chin, G. J. Massoth, K. S. Johnson and E. T. Baker (1991) *In situ* chemical mapping of dissolved iron and manganese in hydrothermal plumes. Nature, **352**, 325-328.

Collier R. and J. Edmond (1984) The trace element geochemistry of marine biogenic particulate matter. Progress in Oceanography, **13**, 113-199.

Converse D. R., H. D. Holland and J. M. Edmond (1984) Flow rates in the axial hot springs of the East Pacific Rise (21°N): implications for the heat budget and the formation of massive sulfide deposits. Earth and Planetary Science Letters, **69**, 159-175.

Corliss J. B., J. Dymond, L. I. Gordon, J. M. Edmond, R. P. von Herzen, R. D. Ballard, K. Green, D. Williams, A. Bainbridge, K. Crane and T. H. van Andel

(1979) Submarine thermal springs on the Galapagos Rift. Science, **203**, 1073-1083.

Craig H., W. B. Clark and M. A. Beg (1975) Excess *3*He in deep water on the East Pacific Rise. Earth and Planetary Science Letters, 26, 125-132.

Edmond J. M., C. Measures, R. E. McDuff, L. H. Chan, R. Collier, B. Grant, C. I. Gordon and J. B. Corliss (1979) Ridge crest hydrothermal activity and the balances of the major and minor elements in the ocean: the Galapagos data. Earth and Planetary Science Letters, **46**, 1-18.

Edmond J. M., K. L. Von Damm, R. E. McDuff and C. I. Measures (1982) Chemistry of hot springs on the East Pacific Rise and their effluent dispersal. Nature, **297**, 187-191.

Elrod, V. A., K. S. Johnson and K. H. Coale (1991) Determination of subnanomolar levels of iron(II) and total dissolved iron in seawater by flow injection analysis with chemiluminescence detection. Analytical Chemistry, **63**, 893-898.

Feely R. A., G. J. Massoth, E. T. Baker, J. P. Cowen, M. F. Lamb and K. A. Krogslund (1990) The effect of hydrothermal processes on midwater phosphorus distributions in the northeast Pacific. Earth and Planetary Science Letters, **96**, 305-318.

German, C. R., G. P. Klinkhammer, J. M. Edmond, A. Mitra and H. Elderfield (1990) Hydrothermal scavenging of rare-earth elements in the ocean. Nature, **345**, 516-518.

Hautala S. and S. Riser (1989) A simple model for abyssal circulation, including effects of wind, buoyancy and topography. Journal of Physical Oceanography, **19**, 596-611.

Jenkins W. J., J. M. Edmond and J. B. Corliss (1978) Excess ^{3}He and ^{4}He in Galapagos submarine hydrothermal waters. Nature, **272**, 156-158.

Johnson K. S., C. L. Beehler and C. M. Sakamoto-Arnold (1986a) A submersible flow analysis system. Analyt. Chim. Acta, **179**, 245-257.

Johnson K. S., C. L. Beehler, C. M. Sakamoto-Arnold and J. J. Childress (1986b) *In Situ* measurements of chemical distributions in a deep-sea hydrothermal vent field. Science, **231**, 1139-1141.

Kadko D., M. P. Bacon and A. Hudson (1987) Enhanced scavenging of ^{210}Pb and ^{210}Po by processes associated with the East Pacific Rise near 8°45'N. Earth and Planetary Science Letters, **81**, 349-357.

Klinkhammer G. P. (1980a) Observations of the distribution of manganese over the East Pacific Rise. Chemical Geology, **29**, 211-226.

Klinkhammer G. (1980b) Determination of manganese in seawater by flameless atomic absorption spectrometry after pre-concentration with 8-hydroxyquinoline in chloroform. Analytical Chemistry, **52**, 117-120.

Klinkhammer G. and A. Hudson (1986) Dispersal patterns for hydrothermal plumes in the South Pacific using manganese as a tracer. Earth and Planetary Science Letters, **79**, 241-249.

Klinkhammer G., H. Elderfield and A. Hudson (1983) Rare earth elements in seawater near hydrothermal vents. Nature, **305**, 185-188.

Klinkhammer G. P., M. Bender and R. F. Weiss (1977) Hydrothermal manganese in the Galapagos Rift. Nature, **269**, 319-320.

Landing W. M. and K. W. Bruland (1980) Manganese in the North Pacific. Earth and Planetary Science Letters, **49**, 45-56.

Landing W. M. and K. W. Bruland (1987) The contrasting biogeochemistry of iron and manganese in the Pacific Ocean. Geochimica et Cosmochimica Acta, **51**, 29-43.

Lupton J. E. and H. Craig (1981) A major helium-3 source at 15°S on the East Pacific Rise. Science, **214**, 13-18.

Lupton J. E., J. R. Delaney, H. P. Johnson and M. K. Tivey (1985) Entrainment and vertical transport of deep-ocean water by buoyant hydrothermal plumes. Nature, **316**, 621-623.

Lupton J. E., G. P. Klinkhammer, W. R. Normark, R. Haymon, K. C. MacDonald, R. F. Weiss and H. Craig (1980) Helium-3 and manganese at the 21°N East Pacific Rise hydrothermal site. Earth and Planetary Science Letters, **50**, 115-127.

Macdonald K. C., K. Becker, F. N. Speiss and R. D. Ballard (1980) Hydrothermal heat flux of the "black smoker" vents on the East Pacific Rise. Earth and Planetary Science Letters, **48**, 1-7.

Martin J. H., G. A. Knauer and W. W. Broenkow (1985) VERTEX: the lateral transport of manganese in the northeast Pacific. Deep-Sea Research, **32**, 1405-1427.

Palmer M. R. and J. M. Edmond (1989) The strontium isotope budget of the modern ocean. Earth and Planetary Science Letters, **92**, 11-26.

Rona P. A. (1988) Hydrothermal mineralization at oceanic ridges. Canadian Mineralogist, **26**, 431-465.

Sclater J. G., C. Jaupart and D. Galson (1981) Journal of Geophysical Research, **86**, 11535-11552.

Shimmield G. B. and N. B. Price (1988) The scavenging of U, ^{230}Th and ^{231}Pa during pulsed hydrothermal activity at 20°S, East Pacific Rise. Geochimica et Cosmochimica Acta, **52**, 669-677.

Spiess F. N., K. C. Macdonald, T. Atwater, R. Ballard, A. Carranza, D. Cordoba, C. Cox, V. M. Diaz Garcia, J. Francheteau, J. Guerrero, J. Hawkins, R. Haymon, R. Hessler, T. Juteau, M. Kastner, R. Larson, B. Luyendyk, J. D. Macdougall, S. Miller, W. Normark, J. Orcutt and C. Rangin (1980) East Pacific Rise: Hot springs and geophysical experiments. Science, 207, 1421-1432.

Stommel H. (1982) Is the South Pacific helium-3 plume dynamically active? Earth and Planetary Science Letters, **61**, 63-67.

Stookey L. L. (1970) Ferrozine -- A new spectrophotometric reagent for iron. Analytical Chemistry, **42**, 779-781.

Trefrey J. H. and S. Metz (1990) Role of hydrothermal precipitates in the geochemical cycling of vanadium. Nature, **342**, 531-533.

U.S.G.S. Juan de Fuca Study Group (1986) Submarine fissure eruptions and hydrothermal vents on the southern Juan de Fuca Ridge: preliminary observations from the submersible *Alvin*. Geology, **14**: 823-827.

Von Damm K. L., J. M. Edmond, B. Grant, C. I. Measures, B. Walden and R. F. Weiss (1985) Chemistry of submarine hydrothermal solutions at 21°N, East Pacific Rise. Geochimica et Cosmochimica Acta, **49**, 2197-2220.

Von Damm K. L. (1990) Seafloor hydrothermal activity: black smoker chemistry and chimneys. Annual Review of Earth and Planetary Sciences, **18**, 173-204.

Weiss R. F. (1977) Hydrothermal manganese in the deep sea: scavenging residence time and $Mn/^{\beta}He$ relationships. Earth and Planetary Science Letters, **37**, 257-262.

Figure Captions

Figure 1) Map of the world's oceans showing locations of known, sampled hydrothermal venting sites (stars), and the distribution of metalliferous sediment coverage where Al/Al+Fe+Mn < 60 (indicating the vast extent of hydrothermally derived sediments; after Boström et al., 1969).

Table 1: Comparison of hydrothermal, fluvial, and atmospheric fluxes (moles year^{-1}).

	Hydrothermal Contributions				Relative Hydrothermal Contribution[g]
	Source Fluids 21°N, EPR[a]	Other Venting Sites	Fluvial Input[b]	Atmospheric Deposition[c]	
Li	1.2→1.9x10^{11}	9.5→16x10^{10}[d]	1.4x10^{10}		91
Na	-8.6→1.9x10^{12}	+,- [d,k]	6.9x10^{12}		-76
K	-1.9→2.3x10^{12}	1.3x10^{12}[d]	1.9x10^{12}		-20
Rb	3.7→4.6x10^{9}	1.7→2.8x10^{9}[d]	5x10^{6}		99
Be	1.4→5.3x10^{5}	1.6→5.3x10^{6}[d]	3.3x10^{7}		5
Mg	-7.5x10^{12}	-7.7x10^{12}[d]	5.3x10^{12}		-143
Ca	2.4→15x10^{11}	2.1→4.3x10^{12}[d]	1.2x10^{13}		14
Sr	-3.1→+1.4x10^{9}	0[d]	2.2x10^{10}		-4
Ba	1.1→2.3x10^{9}	2.5→6.1x10^{9}[d]	1.0x10^{10}		23
F	-1.0x10^{10}		1.6x10^{11}		-6
Cl	0→-1.2x10^{13}	-31→+7.8x10^{12}[d]	6.9x10^{12}		-212
SiO_2	2.2→2.8x10^{12}	3.1x10^{12}[d]	6.4x10^{12}		30
Al	5.7→7.4x10^{8}		6.0x10^{12}	2.4x10^{11}	<0.1
SO_4	-4.0x10^{12}	-3.8x10^{12}[d]	3.7x10^{12}		-105
H_2S	9.4→12x10^{11}	+[d]			
ΣS	-2.8→3.1x10^{11}	-[d]			

	Hydrothermal Contributions				Relative Hydrothermal Contribution[g]
	Source Fluids 21°N, EPR[a]	Other Venting Sites	Fluvial Input[b]	Atmospheric Deposition[c]	
Mn	$1.0 \rightarrow 1.4 \times 10^{11}$	$5.1 \rightarrow 16 \times 10^{10}$[d]	4.9×10^{10}	1.3×10^{9}	69
Fe	$1.1 \rightarrow 3.5 \times 10^{11}$	+[d]	2.3×10^{10}	6.3×10^{10}	73
Co	$3.1 \rightarrow 32 \times 10^{6}$		1.1×10^{8}	4.1×10^{7}	10
Cu	$0 \rightarrow 6.3 \times 10^{9}$	-[d]	5.0×10^{9}	5.5×10^{8}	36
Zn	$5.7 \rightarrow 15 \times 10^{9}$		1.4×10^{10}	3.0×10^{9}	38
Ag	$0 \rightarrow 5.4 \times 10^{6}$		8.8×10^{7}		3
Cd	$2.3 \rightarrow 26 \times 10^{6}$	-[d]	2.8×10^{7}	$<3.0 \times 10^{7}$	20
Pb	$2.6 \rightarrow 5.1 \times 10^{7}$		1.5×10^{8}	1.3×10^{9}	3
V		-1.4×10^{8}[e]*	5.0×10^{8}[e]	$<6.9 \times 10^{8}$	-12
Cr		-[d], -[e]*	3.5×10^{8}	$<9.5 \times 10^{8}$	-
Ni		-[d]	4.9×10^{8}	$<1.2 \times 10^{9}$	-
P		-4.2×10^{9}[f]*	3.2×10^{10}[f]	3.2×10^{9}[f]	-12
As	$0 \rightarrow 6.5 \times 10^{7}$	-[e]*	7.2×10^{8}		4
Se	$0 \rightarrow 1.0 \times 10^{7}$	-[d]	7.9×10^{7}		6
^{3}He		≤ 1080[h]		~ 1080[h]	+
^{210}Pb ^{210}Po		-[i]			-
^{234}U ^{238}U		-[i]			
^{230}Th ^{231}Pa		-[i]			
		-[i]			
		-[i]			
REE		-[j]			-

Footnotes to Table 1

[a]EPR data from Von Damm et al. (1985).

[b]Fluvial fluxes from Von Damm et al. (1985) and Edmond et al. (1979a,b) and references therein.

[c]Atmospheric fluxes from Chester and Murphy (1990) and references therein. These values represent net global total atmospheric input, and are not corrected for % soluble.

[d]GSC data from Edmond et al.(1979a,b).

[e]MAR data from Trefry and Metz (1990) and references therein.

[f]JDFR data from Feely et al. (1990) and references therein. Atmospheric value is soluble P in atmospheric particulates.

[g]Relative hydrothermal contribution calculated as follows: where HT contribution is positive, Relative hydrothermal contribution = (HT source/all sources)x100, and all sources = hydrothermal + fluvial + atmospheric. Where HT contribution is negative, Relative hydrothermal contribution = (HT sink/all sources)x100, and all sources = fluvial + atmospheric.

[h]Data from Craig et al. (1975). The studies of Clarke et al. (1969), Craig et al. (1975), Lupton and Craig (1975; 1981), and Craig and Lupton (1976) have indicated that hydrothermal venting is a major source of ^{3}He to the world's ocean.

[i]These radionuclides have a strong *in situ* production term from the radiodecay of their parent isotopes. Hydrothermal source fluids, fluvial, and atmospheric input are small in comparison (Kadko et al., 1987; Shimmield and Price, 1988).

[j]Data from Klinkhammer et al. (1983) and German et al. (1990).

[k] + = gain, - = loss, * = removal mechanism is scavenging by hydrothermal precipitates in plumes.

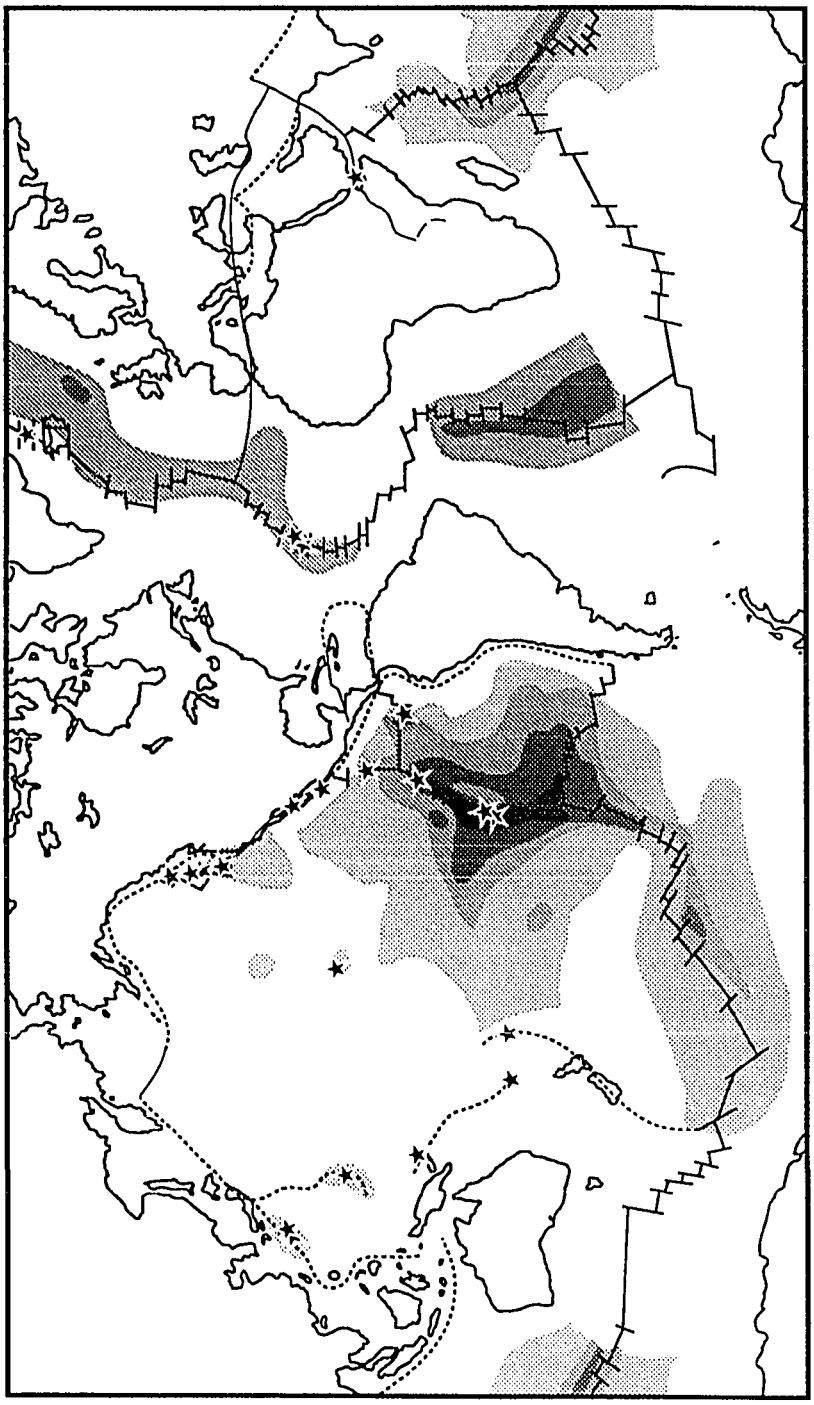

in press: *Marine Chemistry*

CHAPTER 2

Spectrophotometric Determination of Dissolved Manganese in Natural Waters with 1-(2-Pyridylazo)-2-naphthol: Application to Analysis *In Situ* in Hydrothermal Plumes

Abstract

A spectrophotometric method using the complexing reagent 1-(2-pyridylazo)-2-naphthol (PAN) was developed for the determination of dissolved manganese in seawater. A detection limit of approximately 22 nM was obtained when the analyses were performed *in situ* with a submersible chemical analyzer (Scanner). Color formation was rapid (< 1 second), which permitted the technique to be used in flow injection and continuous flow systems. An investigation of possible interferences revealed that the only significant interferant to manganese determinations in seawater (hydrothermal plumes) was iron. The iron specific chelating agent desferrioxamine B was used to mask this interference. Temperature and pressure did not adversely affect the sensitivity of the technique, which made it amenable to applications *in situ* to depths of 3000 meters. This method was tested by measuring dissolved manganese concentrations *in situ* in submarine hydrothermal plumes using a submersible chemical analyzer (Scanner). Scanner deployments over the Juan de Fuca Ridge produced the first near real time analyses of manganese from a hydrothermal plume environment. Estuarine samples have also been successfully analyzed in the laboratory and the results confirmed by an independent method.

Introduction

Manganese is a useful tracer of a wide variety of biogeochemical processes in the marine environment. In particular, manganese is among the most sensitive indicators of hydrothermal activity. Its concentration in hydrothermal source waters ("black smoker" vents) is up to 22 million fold enriched over the ambient seawater concentrations (0.2 nM) (Von Damm, 1990). In some cases, manganese is a better tracer of hydrothermal emissions than is water temperature (Lupton et al., 1980). For example, hydrothermally derived manganese has been detected thousands of kilometers from hydrothermal sources (Klinkhammer and Hudson, 1986). It has been observed that the lateral dispersal pattern of hydrothermal plumes over the East Pacific Rise is coincident with the observed distribution of metalliferous sediments along the ridge crest. This implies that hydrothermal emissions are an important contributor to this sedimentary signature (Klinkhammer and Hudson, 1986).

The distributions of conductivity, temperature, and light scattering in nearfield hydrothermal plumes have been mapped in earlier studies using a towed CTD/transmissometer/rosette package (CTDT/rosette) (Baker and Massoth, 1987). This sampling strategy allows only 12 discrete seawater samples to be collected on each deployment. This small number of discrete samples fails to resolve the range and variability in the metal concentrations in the plumes, or details of their relationship to excess heat (Coale et al., 1991). In addition, discrete sampling

techniques cannot provide the resolution necessary to discriminate processes such as chemical reaction and multiple source mixing, which complicate the chemical distributions within plumes. In order to distinguish these processes with more certainty, it was necessary to develop a technique for the determination of manganese which had sufficient sensitivity to detect low nanomolar concentrations of manganese, and which could be performed continuously *in situ* with a submersible chemical analyzer (Scanner) developed by K. Johnson and coworkers (Johnson et al., 1986a; 1986b).

There are numerous catalytic kinetic methods for the determination of manganese which show both high selectivity and sensitivity (Chiswell et al., 1990). These methods, however, are complicated, the reactions are slow, and some have strong temperature dependencies which make them undesirable for analyses performed *in situ* at variable temperatures. Colorimetric analyses based on the formation of colored Mn-reagent complexes are the simplest reactions for Mn detection. As a result, they are well suited for use *in situ*. The most common analytical reagent used for the determination of manganese in natural waters is formaldoxime (Brewer and Spencer, 1971). The formaldoxime method, however, has the disadvantages of low sensitivity, with a molar extinction coefficient of 11,000 L $mol^{-1} cm^{-1}$ (Chiswell et al., 1990), and a significant iron interference (McArthur and Osborn, 1989).

The reagent 1-(2-pyridylazo)-2-naphthol (PAN) has been used for colorimetric manganese determinations (Betteridge et al., 1963; Donaldson and Inman, 1966). The molar extinction coefficient for the PAN-manganese complex (44,000 L mol^{-1} cm^{-1}) is four times higher than that of the formaldoxime-manganese complex (Chiswell et al., 1990), suggesting that greater sensitivity is possible with PAN than can be obtained with the formaldoxime method. However, studies of manganese determinations using PAN have generally been limited to non-aqueous systems because of its low solubility in water. Watanabe (1974) demonstrated that PAN could be solubilized by the surfactant Triton X-100 and used as an effective colorimetric reagent in aqueous systems. Thus, with the use of surfactants, PAN is a good candidate for manganese determinations in natural waters. PAN has also been used for the determination of zinc, nickel, cobalt, and copper in non-aqueous systems (Betteridge et al., 1963; Cheng and Bray, 1955; Watanabe, 1974). These metals can potentially interfere with manganese analyses. In hydrothermal plumes, however, interferences from these metals are negligible because their concentrations are low compared to manganese (Edmond et al., 1982; Von Damm et al., 1985). On the other hand, iron is a significant interferant when present in concentrations greater than those of manganese, as found in hydrothermal emissions. Goto et al. (1977) suppressed the interference from iron in the analysis of manganese by using cyanide as a masking agent.

In this study PAN was used to determine manganese in seawater using the solubilization method of Watanabe (1974). The iron specific chelating agent desferrioxamine B (Prelog and Walser, 1962; Perrin, 1970) was used to suppress interference from iron.

Methods

Reagents

Desferrioxamine B solution: A 250 mM solution of this Fe(III)-specific chelating agent was prepared by adding 3.05 mL of deionized water, purified using a Millipore Milli-Q system (MQ water) to 500 mg of the pharmaceutical grade of desferrioxamine B (Desferal®; required a prescription, FW 656.79) in a glass ampoule. 400 μL of this solution was added to 250 mL of the PAN reagent, giving a final concentration of 400 μM desferrioxamine B. This effectively chelated all interfering iron to concentrations as high as 2 μM Fe. The effectiveness of this chelating agent was highly sensitive to its age and the grade used. Whereas 400 μM desferrioxamine B (pharmaceutical grade) in the PAN reagent was sufficient to mask 2 μM interfering iron, 6,000 μM reagent grade desferrioxamine B (deferoxamine mesylate; Sigma, FW 656.1) was required to produce a similar result.

Borate buffer, pH 10: 0.618 g H_3BO_3 was dissolved in 100 mL 0.1 N NaOH, prepared in MQ water. Reagent grade NaOH (GFS Chemicals) was used for all solutions.

PAN mixed reagent: A 0.8 mM PAN (FW 249.28) solution was prepared by adding 0.05 g PAN and 5 mL Triton X-100 to approximately 50 mL of MQ water. The mixture was stirred with a magnetic stir bar and heated to approximately 80°C until the PAN dissolved (usually about 8 hours). 100 mL of the borate buffer was added and the solution brought up to 250 mL. The pH of the resulting solution was between 9.7 and 10.0. 400 μL of the desferrioxamine B solution was added only after the PAN had cooled as the sideramine will degrade very quickly when warmed. Due to the short working lifetime of the iron binding reagent (approximately 1.5 days after its addition to the PAN mixed reagent), an effort was made to add the desferrioxamine B solution immediately before use so that insignificant decomposition would occur during analyses.

Standards: Manganese working standards were prepared both by dilution of a 1000 ppm AA standard and also by dilution of a stock solution of 5 mM Mn to the desired working standard concentrations. The stock solution was prepared gravimetrically by dissolving 0.8451 g $MnSO_4 \cdot H_2O$ in 10 mL concentrated HNO_3 and diluting to 1 L. Working standards and blank solutions were prepared using both MQ water and a bulk supply of low Mn seawater ($\approx$1 nM). For the analyses performed *in situ* using the Scanner, a bulk supply of ambient seawater was collected during the cruise and used both for the preparation of standards and also as a blank solution. This seawater had a Mn concentration of approximately 4 nM.

Carrier: For analyses performed in the laboratory using flow injection analysis, a bulk supply of low Mn seawater was used for the carrier stream. When the standards and blanks were prepared using MQ water, a MQ water carrier was used (see below).

Apparatus

Most of the laboratory experiments were performed using flow injection analysis (FIA). A block diagram of the equipment used for the FIA system is shown in Figure 1. The reaction manifold was made from 0.5 mm i.d. PTFE (Teflon) tubing. A Gilson peristaltic pump with PVC pump tubing was used to propel the sample/carrier, and PAN reagent at 0.8 and 0.15 mL/min., respectively. A rotary injection valve (Rheodyne Type 50 Teflon rotary valve) with a pneumatic actuator was used to inject 300 μL of sample into a seawater carrier stream. The sample and carrier were merged with the reagent at a T fitting. Since the formation of the PAN-manganese complex occurred rapidly, it was not necessary to further increase the reaction (residence) time. However, because of the high viscosity of the surfactant, Triton X-100, a 50 cm glass bead column was used to promote mixing of the PAN reagent with the sample. This mixing column was made of 0.8 mm teflon tubing filled with 0.45 to 0.5 mm diameter glass beads (van den Berg et al., 1980; Reijn et al., 1981). The resulting colored solution was pumped through a 2 cm path length flow-through cuvette, where its absorbance was measured with a Lachat System IV

colorimeter (model 1000-300) with a 560 nm filter. Some of the calibration experiments, and determinations of absorption spectra, were performed manually with a Hewlett-Packard diode array spectrophotometer (HP 8452A). For these manual experiments, reagents and samples were mixed in batch in the same proportions that were obtained in the FIA system.

The reaction manifold used on the Scanner for determinations of manganese *in situ* is shown in Figure 2. The Scanner is described in detail elsewhere (Johnson et al., 1986a, 1989). The flow rates for the samples and reagent were the same as those used on the FIA system, 0.8 and 0.15 mL/min for sample and PAN, respectively. The PTFE tubing was 0.5 mm i.d., except for the PVC pump tubing and the mixing column. The glass bead column was used on this system as well. Two standards and a blank were programmed to be run at selected time intervals by switching selection valves on the Scanner (Fig. 2). A 10 μm filter on the sample inlet was used to exclude large particles. A solid state, flow-through photometric detector (Betteridge et al., 1978) with a green LED as the light source (569 nm maximum emission, 28 nm bandwidth) was used to detect the color in the solution due to the PAN-Mn complex. Data were recorded digitally and stored in RAM for retrieval upon recovery of the instrument package. The signal can also be retrieved in real time through a CTD cable, or through the hull fitting of a submersible (Johnson et al., 1986b).

The Scanner was adapted for deployment on the NOAA/PMEL rosette sampler as part of the VENTS '89 cruise aboard the NOAA ship Discoverer. The system consisted of three components. An electronics module, containing the selection valve circuitry, signal processing and storage capabilities, was secured to the bottom circular frame of the CTDT/rosette package. A chemistry module, which contained the pump, selection valves, detectors, and reagents occupied one of the twelve, 30 L sampling bottle positions; and a battery pack occupied another. This instrument package was deployed on both vertical casts and "tow-yos" (Baker and Massoth, 1987). During the "tow-yos," the instrument package was raised and lowered over a depth range from 1700 to 2300 m while the ship steamed at a speed of approximately 1-2 knots.

Results and Discussion

Laboratory Results

Laboratory experiments showed that a concentration between 0.8 to 1.0 mM PAN was sufficient for samples with manganese concentrations on the order of 0.25 to 50 μM. Reagent concentrations <0.8 mM produced lower absorbances. Higher concentrations of the PAN reagent did not appear to increase the sensitivity, but they did increase baseline noise. A concentration of 0.8 mM PAN was used for determinations made with the Scanner, where concentrations of manganese ranged from 0.2 to 650 nM.

The absorption spectra of the PAN reagent, and the PAN-Mn complex in MQ water and in seawater at pH values of 8.0, 9.5, and 11.0 are shown in Figures 3a and 3b. The absorption peak of the PAN-Mn complex appears as a shoulder at 560 nm on the spectrum of the PAN reagent alone. This is due to a bathochromic shift as the PAN-Mn complex is formed (Fig. 3b). The optimal pH for the determination of Mn is 9.5, where the difference in absorbance between the PAN and the PAN-Mn complex at 560 nm is greatest. An additional bathochromic shift in the spectrum of PAN in seawater appears at pH values greater than about 10 (Fig. 3b). This shift was not observed in standards prepared with MQ water (Fig. 3a). We attribute this feature to an interference caused by Ca^{2+} and Mg^{2+} in seawater as the PAN reagent loses specificity at higher pH, and the possible precipitation of magnesium hydroxides at high pH, thus producing this broad spectrum increase in absorbance.

The 0.01 M borate buffer was used to control the pH of the reaction mixtures. It maintained the PAN mixed reagent at a pH of 9.7 to 10.0. This was within the optimum range of 9.0 to 10.0 (Fig. 4). The actual pH of the reaction mixture is slightly lower due to the lower pH of the carrier and standards. It is expected, based on pH measurements of the effluent from the FIA system, that the reaction pH is no more than 0.5 pH units less than the pH of the PAN mixed reagent. Weaker buffer solutions may be used when analyzing seawater at natural pH. However, the buffer described here provided adequate pH control when analyzing both standards on the

Scanner that had been acidified to pH values as low as 5.5, as well as samples at their natural pH (7.5 to 8.0).

Large differences in salinity between the sample and carrier stream create a refractive index gradient that produces a detector signal (Betteridge et al., 1978). Such a refractive index signal can obscure the signal due to the PAN-Mn complex. Therefore, bulk seawater was used as the carrier for the injected sample when seawater samples were analyzed, to minimize the difference in refractive index between the sample and the carrier. In addition, standards were prepared using this same bulk supply of seawater. A MQ water carrier was used for standards prepared in MQ water. When estuarine samples were analyzed it was necessary to adjust the salinity of the carrier so that it was similar to that of the sample. This was accomplished by diluting the seawater carrier with MQ water.

Standards prepared in seawater show a linear response with this technique (r^2 = 0.999), as do standards prepared in MQ water (r^2 = 0.996), to concentrations of manganese as high as 20 μM (Fig. 5). Absorbances greater than 1.2 were obtained at concentrations above 35 μM. Concentrations greater than 35 μM produced a non-linear calibration curve. Shorter path length cells, or dilution of the sample, would extend the upper concentration limit of this technique. Figure 5 also shows results for standards prepared in MQ water using the same PAN reagent at pH 9.8. Differences in the signal obtained for standards prepared in seawater versus standards prepared in MQ water may be due to the lower pH of the MQ water

standards at very high manganese concentrations. Where seawater and MQ water standards of similar pH were determined (the lower standards on the curve, Fig. 5) absorbances were similar, and a salt effect, if any, was negligible.

The effects of potential interferences were determined by analyzing standards prepared with a suite of metals whose concentrations may be elevated in hydrothermal solutions. Zinc, nickel, and copper standards all produce absorbances that are greater than 50 percent of the absorbance of an equimolar Mn standard (Fig. 6). However, Fe(III) and Fe(II) are the primary potential interferants (Fig. 7) at the predicted plume water concentrations that were extrapolated from "black smoker" endmember concentrations (Von Damm et al., 1985). These relative plume water concentrations were calculated based on conservative mixing of the "black smoker" waters with ambient seawater. Other chemical removal processes such as natural precipitation and scavenging of elements from plume waters (Feely et al., 1990; German et al., 1990; Trefry and Metz, 1989; Kadko et al., 1987) were not considered. Therefore, these calculations represent an upper limit on the potential of these metals to interfere within the hydrothermal plume environment.

In riverine and estuarine waters where concentrations of zinc may reach micromolar levels, there is a potential for significant interference in this technique. However, in these natural waters the predominant chemical form of zinc, and other metals that show substantial interference (nickel, copper, and cobalt, Fig. 6), is that of a strongly bound organic complex (van den Berg et al., 1987; Bruland, 1989;

Nimmo et al., 1989; Coale and Bruland, 1988; Zhang et al., 1990). This complexation by natural organic ligands limits the availability of these metal ions for complexation with the PAN ligand, thus suppressing the interference. The extent of this natural competitive suppression, however, is difficult to estimate and such a study remains to be performed. None of the metals examined should cause an interference greater than 10%.

Although the PAN-Fe(III) complex has an extinction coefficient that is only 20 percent of that of the PAN-Mn(II) complex (Fig. 6), iron can be present at a 4 fold excess over Mn in vent solutions. Thus, for application of this technique in the nearfield plume environment, the iron interference must be suppressed. The iron-specific chelating agent used here, desferrioxamine B, eliminated any interference from iron (Fig. 7).

The pharmaceutical grade of desferrioxamine B used in this study, deferoxamine mesylate or Desferal®, is a synthetic analog of the sideramine desferrioxamine B (Prelog and Walser, 1962; Perrin, 1970). The iron chelate, ferrioxamine B, was first isolated from *Streptomyces pilosus* in 1960 (Bickel et al., 1960). All ferrioxamines, or sideramines, occur only in bacteria and have three hydroxamic acid groups as iron-binding centers which occupy all six positions about the ferric ion. The thermodynamic formation constant for the iron(III) complex is $10^{30.6}$ (Perrin, 1970; Harris, 1982). Desferrioxamines have a powerful iron(III) chelating ability with a relatively weak affinity for most other cations, and a negligible affinity for complexing

Mn(II) (Perrin, 1970; Martell and Smith, 1977; Morel, 1983). Desferrioxamine B is specific for Fe(III) but also masks Fe(II), perhaps by shifting the equilibrium between Fe(II) and Fe(III) in solution.

Field Results

The accuracy of manganese analyses with PAN was determined by comparing the results obtained *in situ* with this method with results from discrete samples that were collected concurrently. The discrete samples were analyzed on shore at PMEL by column extraction followed by graphite furnace atomic absorption spectrometry (GFAAS). The Scanner data and discrete samples were collected during the 1989 NOAA/VENTS cruise to the Juan de Fuca Ridge hydrothermal system (USGS Juan de Fuca Study Group, 1986). Normally, the Scanner allows for *in situ* calibrations at pre-programmed, user-determined intervals on every cast. Such a calibration sequence during a tow-yo along the Cobb Segment of the Juan de Fuca Ridge (tow XT-3) is shown in Figure 8. The upward rise in the detector response with time reflects the slow expansion of the tubing, at *in situ* temperatures and pressures, after the selection valves (pinch valves) have opened. The maximum signal for each standard is close to the plateau value, as determined by a comparison of the slope from the *in situ* calibration with the slope from calibrations conducted in the laboratory. However, after tow XT-3, the valves that select standards or sample malfunctioned. Since the detector response was stable and reproducible between

deployments, the calibrations from tow XT-3 were, therefore, applied to other casts to determine manganese throughout the remainder of the cruise. Because only a weak hydrothermal signal was encountered during tow XT-3 (<7 nM Mn), intercomparisons were made between Scanner and discrete data collected at the North Cleft Segment of the Juan de Fuca Ridge during tow XT-10 and vertical cast X-4, later in the cruise.

Manganese concentrations determined *in situ* by the PAN method and in the laboratory by extraction/GFAAS for tow XT-10 and for the vertical cast X-4 are plotted versus temperature anomaly (d-theta) in Figures 9a and b, respectively. There was good agreement between the Scanner PAN method and the column extraction/GFAAS analysis of the discrete samples. A comparison of the linear least squares regressions of Scanner Mn versus d-theta and discrete Mn versus d-theta at XT-10 shows no significant difference between slopes or intercepts (95% confidence interval, Snedecor and Cochran, 1967). This agreement suggests that any interferences from iron or other metals were negligible.

A buoyant plume was sampled at station X-4, north of the XT-10 tow-yo, on the North Cleft Segment. Here, the Scanner results provide a more representative sampling of the full range of Mn:heat values within this turbulent plume. A statistical comparison of the manganese concentrations measured *in situ* at X-4 and discrete samples collected concurrently is not as simple as that for XT-10 because the relationship between manganese and d-theta in this plume is complicated by multiple

source mixing (Coale et al., 1991). The agreement between the Scanner data and discrete sample values can, however, be seen from the plot of manganese versus d-theta for X-4 (Fig. 9b).

An additional comparison was made between the results of the FIA application of the PAN technique and of a chemiluminescence technique using FIA, also developed in our laboratory (Chapin et al., in press). Analyses were performed on an estuarine water sample collected from Elkhorn Slough (Smith, 1974), adjacent to Monterey Bay. The colorimetric PAN and chemiluminescence techniques yielded concentrations of 392 ± 10 nM and 389 ± 11 nM Mn (1 S.D.), respectively, indicating no significant difference between the two methods. Again, agreement between the values obtained by these two techniques suggests that interferences in this method from iron or other metals was negligible.

The detection limit for this technique, defined as three times the standard deviation of replicate measurements, depended on the environment in which it was applied. Analyses performed *in situ* generally gave lower detection limits than were obtained in laboratory experiments. The standard deviation of replicate measurements performed *in situ* with the Scanner was determined by examining the relationship between manganese and temperature anomaly (Fig. 9a). A least squares line (Mn versus temperature anomaly) was fit to each of the 15 vertical casts in the XT-10 tow-yo, an average of 250 data points each. The range of the standard error in the manganese concentration was from 6 to 10 nM, yielding a range in the

detection limit (3 S.D.) from 15 to 30 nM, with an average of 22 nM. Although XT-10 was chosen for its stability and uniformity in the metal:heat relationship, these are conservative estimates of the detection limit since some of the changes in the Mn:heat relationship may have been due to natural variability, such as multiple source mixing (Coale et al., 1991). The detection limit observed in the laboratory was 48 nM, based on the concentration of Mn which produces a signal equal to three times the noise level of the baseline. We attribute the difference between the two detection limits to the increased stability of the baseline on the Scanner because the pressure *in situ* eliminated problems with air bubbles in the system.

Conclusions

This technique was sufficiently sensitive to detect nanomolar levels of manganese in seawater. It has been adapted for the analysis of discrete samples by flow injection analysis (with a higher detection limit). It was also used on the Scanner with continuous flow analysis *in situ*. In this configuration, the Scanner provides chemical data with the resolution necessary to elucidate important processes and relationships in hydrothermal plumes. Samples can also be analyzed by manually mixing the reagent and sample in batch. Because of the high sensitivity of this technique, it would not be practical to use the Scanner, in its present configuration, to determine manganese directly in vent waters at their source ("black smokers"). However, the Scanner manifold could be adapted for determinations of source fluids

in situ by decreasing the flow cell length, by adding a sample dilution line, or by decreasing the concentration of the PAN reagent and increasing its flow rate, and decreasing the flow rate of the sample inlet.

Continuous measurements of dissolved manganese performed *in situ* with the Scanner in hydrothermal vent plumes yield high resolution chemical data in near real-time at a low cost. This detection capability provides a more representative sampling of hydrothermal plumes over large spatial scales.

Acknowledgments

We wish to extend our sincere thanks to H. P. Chin for suggesting the use of desferrioxamine B, Desferal®, as a masking agent; V. Elrod for laboratory assistance; Chief Scientist E. Baker for his patience and encouragement; E. Baker and S. Walker for providing CTD/T data; G. Massoth and K. Roe for providing results of the discrete sample analyses; R. Feely for accommodating our participation in the NOAA/PMEL VENTS '89 expedition; G. Lebon for modifications to the PMEL rosette to accommodate the Scanner; the David and Lucille Packard Foundation for funding the presentation of this work at the AGU-ASLO Ocean Sciences Meeting, February, 1990; The Oceanography Society for funding the presentation of this work at the Second Scientific Meeting, March 1991; and the crew and officers of the NOAA Ship *Discoverer*, R/V *Ricketts*, and R/V *Point Sur*. This work was supported by NSF grant OCE-8609437 to K. Johnson. C.S.C. wishes to dedicate this work to the memory of her grandmother Mock Shee Chin.

References

Baker, E. T. and Massoth, G. J., 1987. Characteristics of hydrothermal plumes from two vent fields on the Juan de Fuca Ridge, northeast Pacific Ocean. Earth Planet. Sci. Lett. 85: 59-73.

Betteridge, D., Dagless, E. L., Fields, B. and Graves, N. F., 1978. A highly sensitive flow-through phototransducer for unsegmented continuous-flow analysis demonstrating high-speed spectrophotometry at the parts per 10^9 level and a new method of refractometric determinations. Analyst, 103: 897-908.

Betteridge, D., Fernando, Q. and Freiser, H., 1963. Solvent extraction of certain transition metal ions with 1-(2-pyridylazo)-2-naphthol: A study of complex formation and distribution equilibria. Anal. Chem., 35: 294-298.

Bickel, H., Hall, G. E., Keller-Schierlein, W., Prelog, V., Vischer, E. and Wettstein, A., 1960. Über die Konstitution von Ferrioxamin B. Helv. Chim. Acta, 43: 2129-2138.

Brewer, P. G. and Spencer, D. W., 1971. Colorimetric determination of manganese in anoxic waters. Limnol. Oceanogr., 16: 107-110.

Bruland, K. W., 1989. Complexation of zinc by natural organic ligands in the central North Pacific. Limnol. Oceanogr., 34: 269-285.

Chapin, T. P., Johnson, K. S. and Coale, K. H., 1991. Determination of manganese in seawater by flow injection analysis with chemiluminescence detection. Anal. Chim. Acta, in press.

Cheng, K. L. and Bray, R. H., 1955. 1-(2-pyridylazo)-2-naphthol as a possible analytical reagent. Anal. Chem., 27: 782-785.

Chiswell, B., Rauchle, G. and Pascoe, M., 1990. Spectrophotometric methods for the determination of manganese, Talanta 37, 237-259.

Coale, K. H. and Bruland, K. W., 1988. Copper complexation in the Northeast Pacific. Limnol. Oceanogr., 33: 1084-1101.

Coale, K. H., Chin, C. S., Massoth, G. J., Johnson, K. S. and Baker, E. T., 1991. *In situ* chemical mapping of dissolved iron and manganese in hydrothermal plumes. Nature, **352**, 325-328.

Donaldson, E. M. (P.) and Inman, W. R., 1966. Determination of manganese in high-purity niobium, tantalum, molybdenum and tungsten metals with PAN. Talanta, 13: 489-497.

Feely, R., Massoth, G. J., Baker, E. T., Cowen, J. P., Lamb, M. F. and Krogslund, K. A., 1990. The effect of hydrothermal processes on midwater phosphorus distributions in the northeast Pacific. Earth Planet. Sci. Lett., 96: 305-318.

German, C. R., Klinkhammer, G. P., Edmond, J. M., Mitra, A. and Elderfield, H., 1990. Hydrothermal scavenging of rare-earth elements in the ocean. Nature, 345: 516-518.

Goto, K., Tagudhi, S. Fukue, Y. Ohta, K. and Watanabe, H., 1977. Spectrophotometric determination of manganese with 1-(2-pyridylazo)-2-naphthol and a non-ionic surfactant. Talanta, 24: 752-753.

Harris, D. C., 1982. Quantitative Chemical Analysis. W. H. Freeman and Company, New York, 748 pp.

Johnson, K. S., Sakamoto-Arnold, C. M., and Beehler, C. L. 1989. Continuous determination of nitrate concentrations in situ. Deep-Sea Research, 36: 1407-1413.

Johnson, K. S., Beehler, C. L. and Sakamoto-Arnold, C. M., 1986a. A submersible flow analysis system. Analyt. Chim. Acta, 179: 245-257.

Johnson, K. S., Beehler, C. L., Sakamoto-Arnold, C. M. and Childress, J. J., 1986b. *In situ* measurements of chemical distributions in a deep-sea hydrothermal vent field. Science, 231: 1139-1141.

Kadko, D., Bacon, M. P. and Hudson, A., 1987. Enhanced scavenging of ^{210}Pb and ^{210}Po by processes associated with the East Pacific Rise near 8°45'N. Earth Planet. Sci. Lett., 81: 349-357.

Klinkhammer, G. and Hudson, A., 1986. Dispersal patterns for hydrothermal plumes in the South Pacific using manganese as a tracer. Earth Planet. Sci. Lett., 79: 241-249.

Lupton, J. E., Klinkhammer, G. P., Normark, W. R., Haymon, R., MacDonald, K. C., Weiss, R. F. and Craig, H., 1980. Helium-3 and manganese at the 21°N East Pacific Rise hydrothermal site. Earth Planet. Sci. Lett., 50: 115-127.

Martell, A. E. and Smith, R. M., 1977. Critical Stability Constants, Vol. 3, Other Organic Ligands. Plenum, New York, 495 pp.

McArthur, J. M. and Osborn, A. T., 1989. Manganese analysis by the formaldoxime method: Problems with iron interference. Mar. Chem., 26: 81-85.

Morel, F. M. M., 1983. Principles of Aquatic Chemistry. John Wiley and Sons, New York, 446 pp.

Nimmo, M., van den Berg, C. M. G. and Brown, J., 1989. The chemical speciation of dissolved nickel, copper, vanadium and iron in Liverpool Bay, Irish Sea. Estuarine Coastal Shelf Sci., 29: 57-74.

Perrin, D. D., 1970. Chemical Analysis, Vol. 33, Masking and Demasking of Chemical Reactions. John Wiley and Sons, New York, 211 pp.

Prelog, V. and Walser, A., 1962. Über die Synthese der Ferrioxamine B und D_1. Helv. Chim. Acta, 45: 631-637.

Reijn, J. M., van der Linden, W. E. and Poppe, H., 1981. Dispersion in open tubes and tubes packed with large glass beads: The single bead string reactor. Anal. Chim. Acta, 123: 229-237.

Smith, R. E., 1974. Hydrography of Elkhorn Slough, a Shallow California Coastal Embayment. M.S. Thesis, Moss Landing Marine Laboratories, 88 pp.

Snedecor, G. W. and Cochran, W. G. 1967. Statistical Methods. Sixth edition, Iowa State University Press, Ames, 593 pp.

Trefry, J. H. and Metz, S., 1989. Role of hydrothermal precipitates in the geochemical cycling of vanadium. Nature, 342: 531-533.

U. S. G. S. Juan de Fuca Study Group, 1986. Submarine fissure eruptions and hydrothermal vents on the southern Juan de Fuca Ridge: Preliminary observations from the submersible *Alvin*. Geology, 14: 823-827.

van den Berg, C. M. G., Merks, A. G. A. and Duursma, E. K., 1987. Organic complexation and its control of the dissolved concentrations of copper and zinc in the Scheldt Estuary. Estuarine Coastal Shelf Sci., 24: 785-797.

van den Berg, J. H. M., Deelder, R. S. and Egberink, H. G. M., 1980. Dispersion phenomena in reactors for flow analysis. Anal. Chim. Acta, 114: 91-104.

Von Damm, K. L., 1990. Seafloor hydrothermal activity: Black smoker chemistry and chimneys. Annu. Rev. Earth Planet. Sci., 18: 173-204.

Von Damm, K. L., Edmond, J. M., Grant, B., Measures, C. I., Walden, B. and Weiss, R. F., 1985. Chemistry of hydrothermal solutions at 21°N, East Pacific Rise. Geochim. Cosmochim. Acta, 49: 2197-2220.

Watanabe, H., 1974. Spectrophotometric determination of cobalt with 1-(2-pyridylazo)-2-naphthol and surfactants. Talanta, 21: 295-302.

Weiss, R. F., 1977. Hydrothermal manganese in the deep sea: scavenging residence time and $Mn/^{\beta}He$ relationships. Earth Planet. Sci. Lett. 37: 257-262.

Zhang, H., van den Berg, C. M. G. and Wollast, R., 1990. The determination of interactions of cobalt(II) with organic compounds in seawater using cathodic stripping voltammetry. Mar. Chem., 28, 285-300.

Figure Captions

Figure 1) Schematic of the FIA manifold for the colorimetric determination of Mn in the laboratory. The structure of the PAN ligand is shown at the bottom.

Figure 2) Schematic of the Scanner manifold for the determination of dissolved Mn *in situ*. Selection valves were used to perform a calibration sequence *in situ* at pre-programmed time intervals. Absorbance was measured at 560 nm.

Figure 3 a) Plot of the PAN absorption spectrum at pH 8.0, 9.5, and 11.0 for 10 μM Mn standards prepared in MQ water, and MQ blank solutions (<0.01 nM Mn). b) Plot of the PAN absorption spectrum at pH 8.0, 9.5, and 11.0 for 10 μM Mn standards prepared in seawater, and seawater blank solutions (<1.0 nM Mn).

Figure 4) Plot of the absorbance at 560 nm of a 2 μM manganese standard in seawater versus the pH of the PAN mixed reagent.

Figure 5) Plot of absorbance (at 560 nm) versus concentration for standards prepared in both seawater and MQ water. Both sets of standards show a linear response to concentrations of Mn as high as 20 μM (r^2 = 0.999 for SW standards; r^2 = 0.996 for MQ water standards).

Figure 6) Absorbances (measured at 560 nm) of PAN-metal complexes relative to an equimolar Mn standard, indicating Zn, Ni, and Cu as the greatest potential interferants on an equimolar basis.

Figure 7) Relative absorbances (measured at 560 nm) of PAN-metal complexes at calculated plume water concentration ratios, based on conservative dilution of the source water with ambient seawater. The ratios do not reflect the natural precipitation or scavenging of the more particle and redox reactive elements.

Figure 8) Detector response, in detector voltage units, vs time in minutes for an *in situ* calibration sequence performed using the Scanner during the tow-yo XT-3 over the Cobb Segment, Juan de Fuca Ridge. The Scanner was programmed to run a seawater blank (ambient deep water, ≈4 nM Mn), 1.0 μM Mn, and 2.0 μM Mn standards once every hour of operation. The upward rise in the detector response with time is due to the slow expansion of the selection valve (pinch valve) tubing. The detector response at each calibration concentration was determined by averaging the last 5 detector voltage measurements.

Figure 9 a) Manganese (nM) vs temperature anomaly (°C) for the tow-yo XT-10 across the North Cleft Segment. Scanner Mn concentrations were determined colorimetrically using PAN, whereas discrete samples were analyzed by column

extraction/GFAAS at PMEL. Where discrete samples were collected concurrently, analyses show excellent agreement with the Scanner manganese data versus temperature anomaly. b) Manganese vs temperature anomaly for the vertical cast X-4. Again, where there are concurrent determinations, there is very good agreement between the Scanner and discrete Mn values. Negative temperature anomaly values reflect the difficulty in choosing a "background" potential temperature (theta) value for the calculation of this anomaly. Although sometimes negative, this anomaly is still valid in a relative sense. The negative manganese concentrations are due to small fluctuations in detector response at concentrations near zero.

FIA Manifold Configuration for Manganese Determination

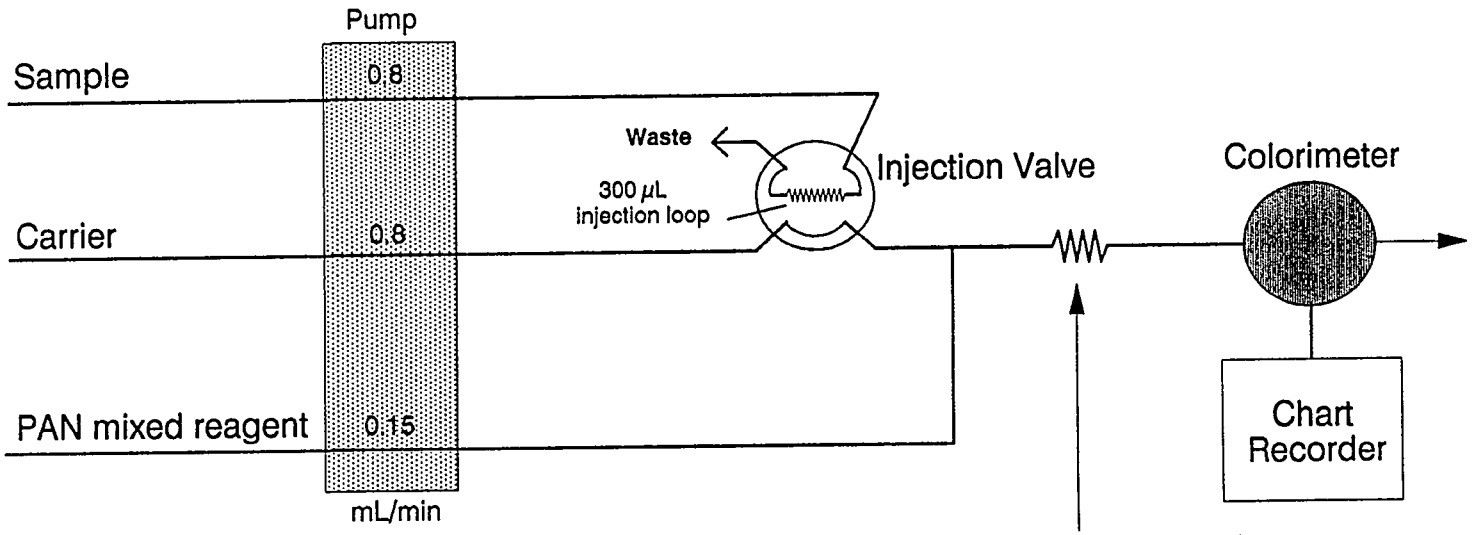

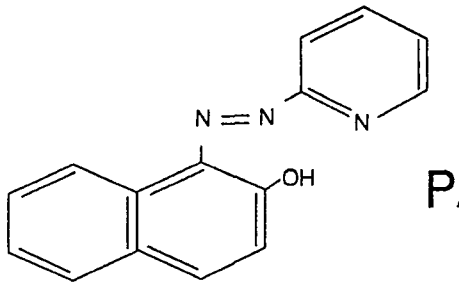

PAN + Mn ⟶ PAN-Mn

Absorbance measured at 560 nm

Scanner Manifold Configuration for Manganese Determination

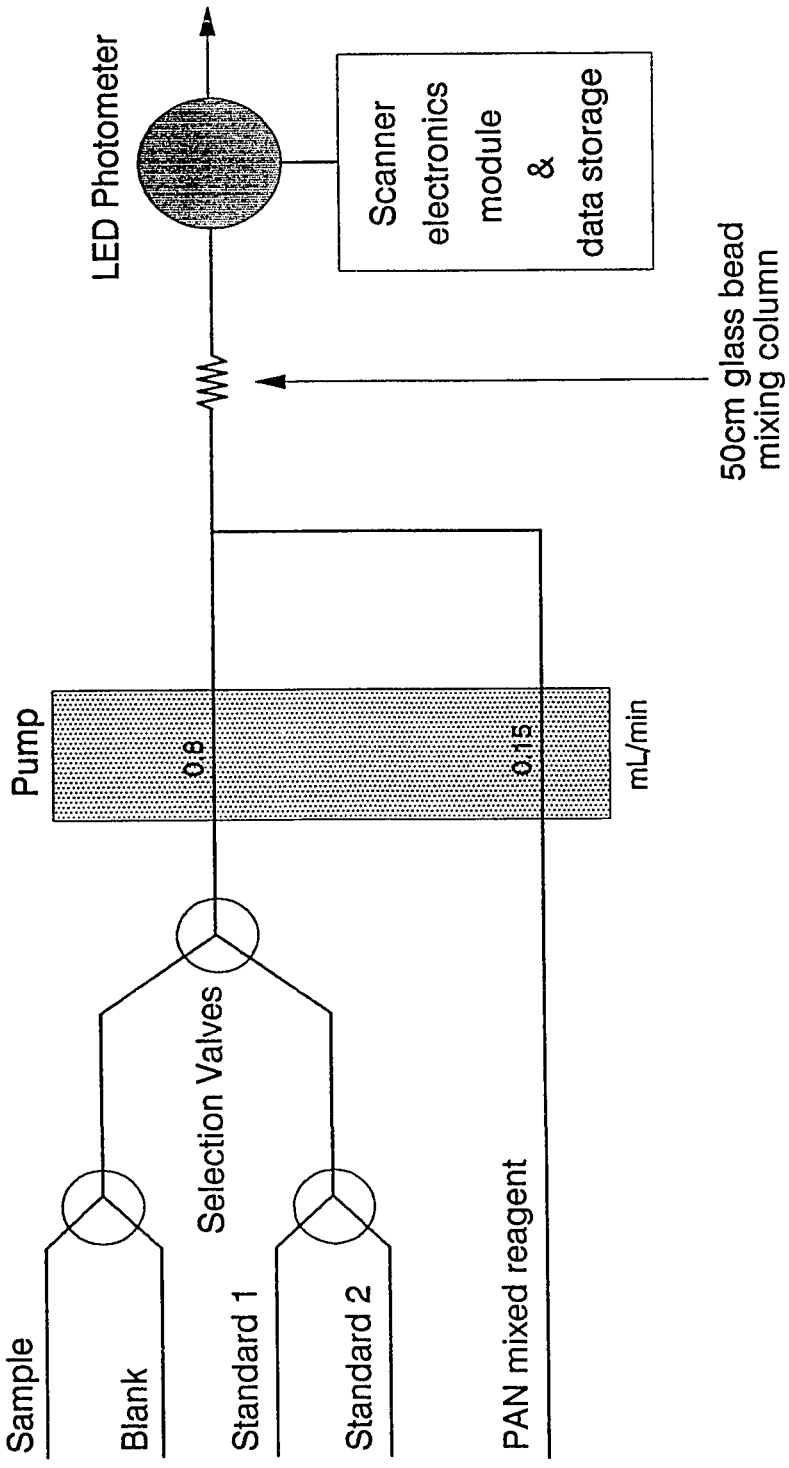

Spectra of PAN–Mn Complex in Milli–Q Water

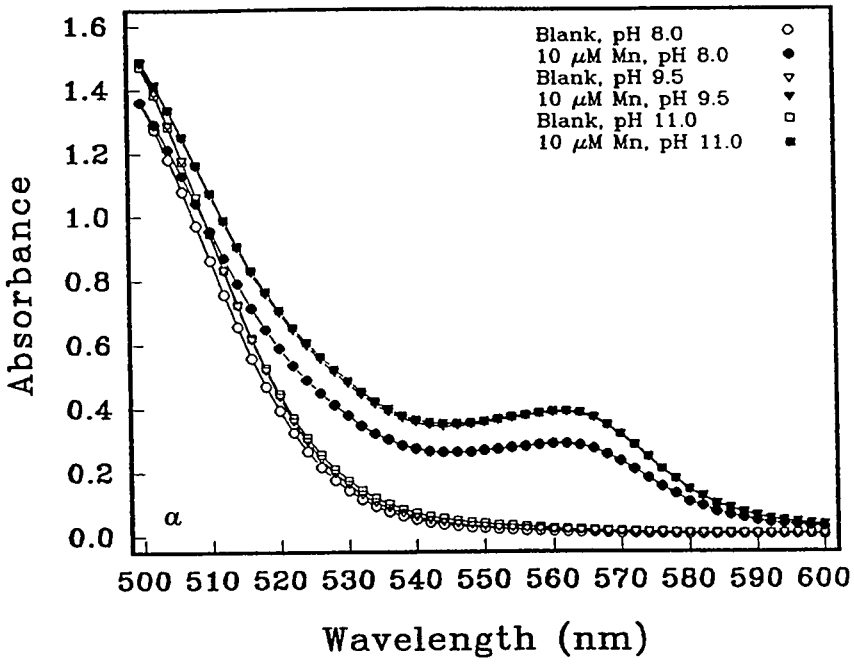

Spectra of PAN–Mn Complex in Seawater

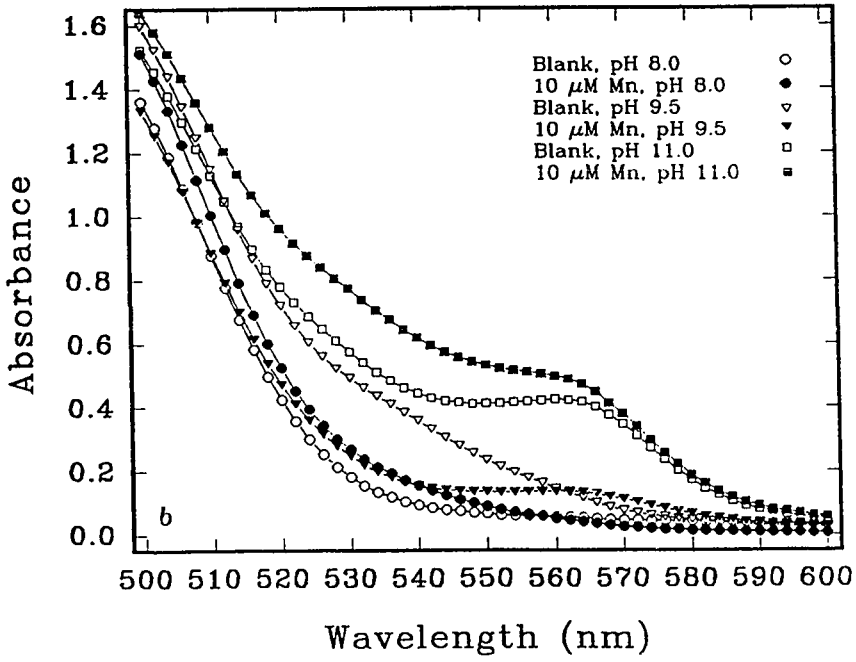

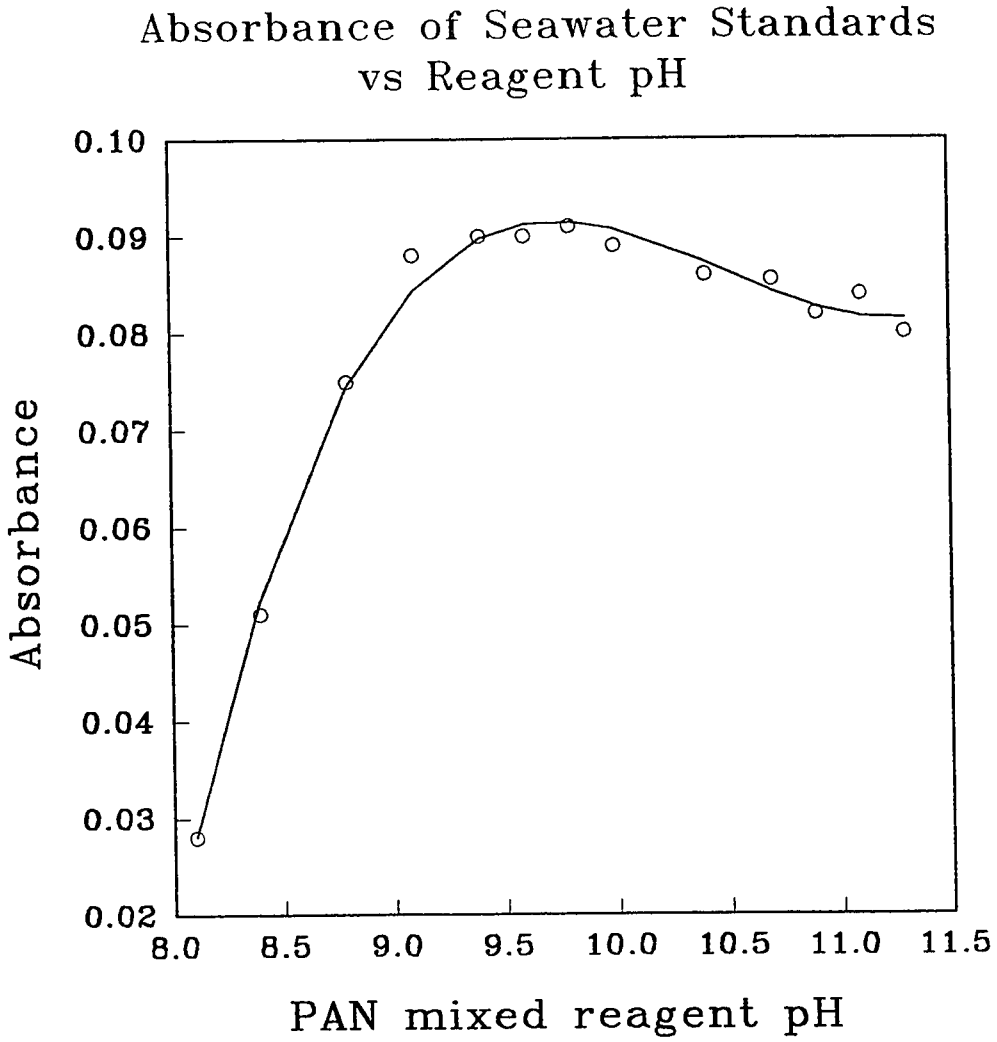
Absorbance of Seawater Standards
vs Reagent pH
Absorbance
0.10
0.09
0.08
0.07
0.06
0.05
0.04
0.03
0.02
8.0
8.5
9.0
9.5
10.0
10.5
11.0
11.5
PAN mixed reagent pH

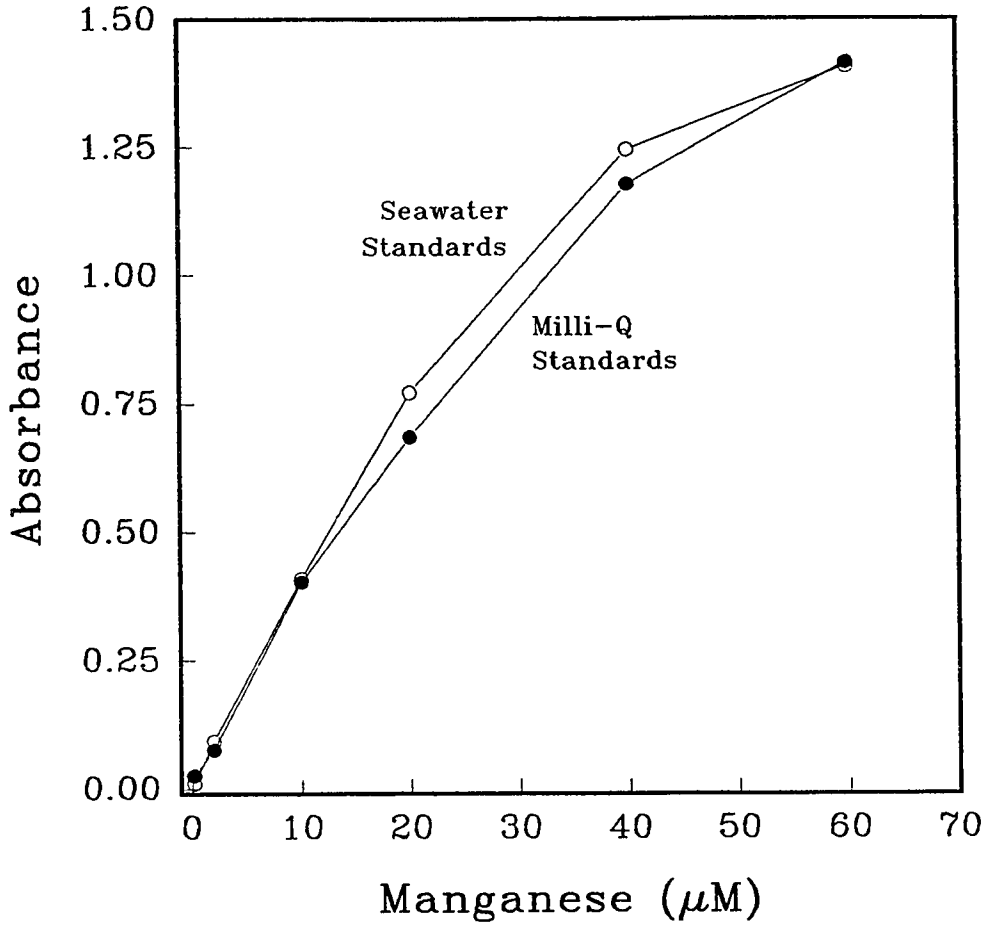
1.50
1.25
1.00
0.75
0.50
0.25
0.00
Absorbance
Seawater
Standards
Milli-Q
Standards
0
10
20
30
40
50
60
70
Manganese (μM)

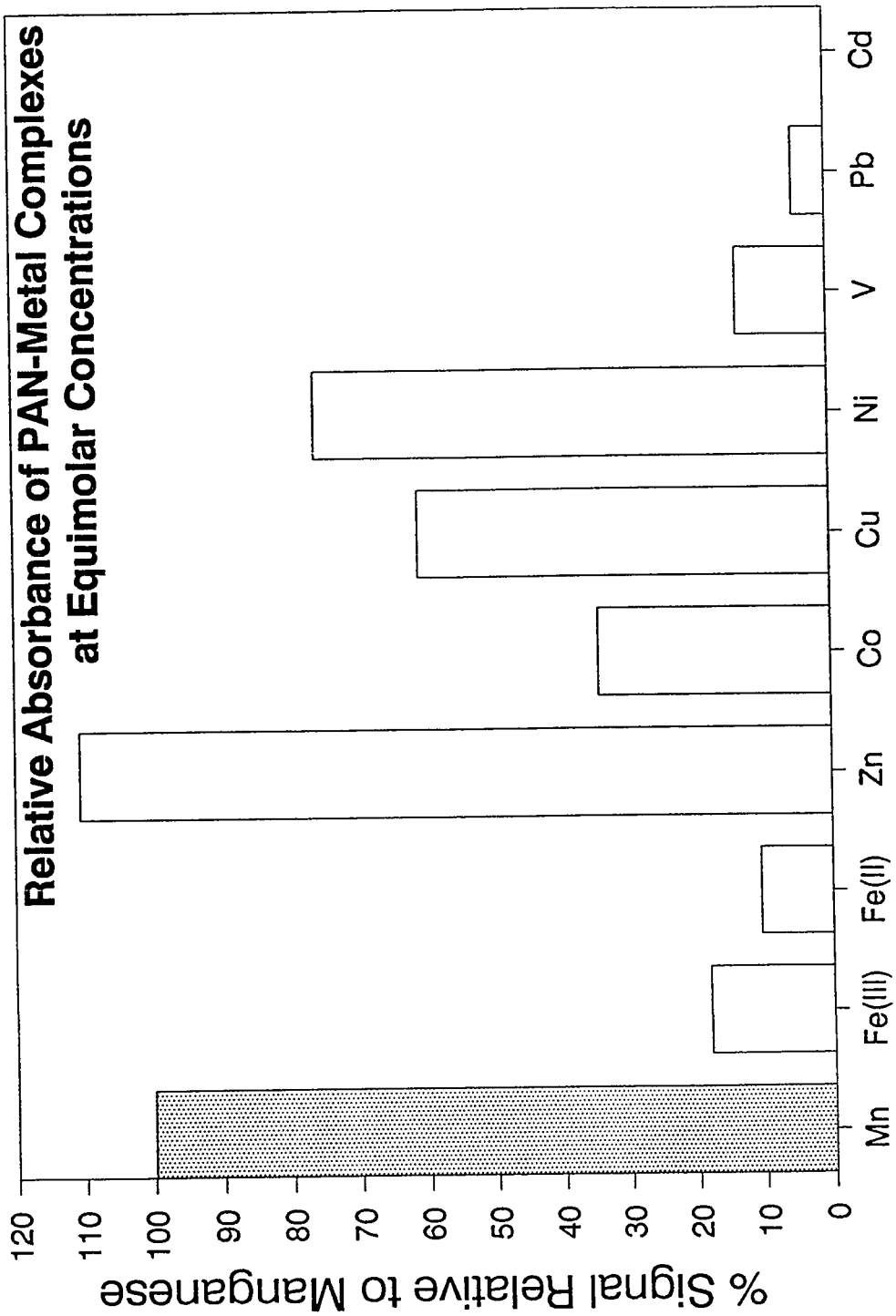
Relative Absorbance of PAN-Metal Complexes
at Equimolar Concentrations
% Signal Relative to Manganese
120
110
100
90
80
70
60
50
40
30
20
10
0
Mn
Fe(III)
Fe(II)
Zn
Co
Cu
Ni
V
Pb
Cd

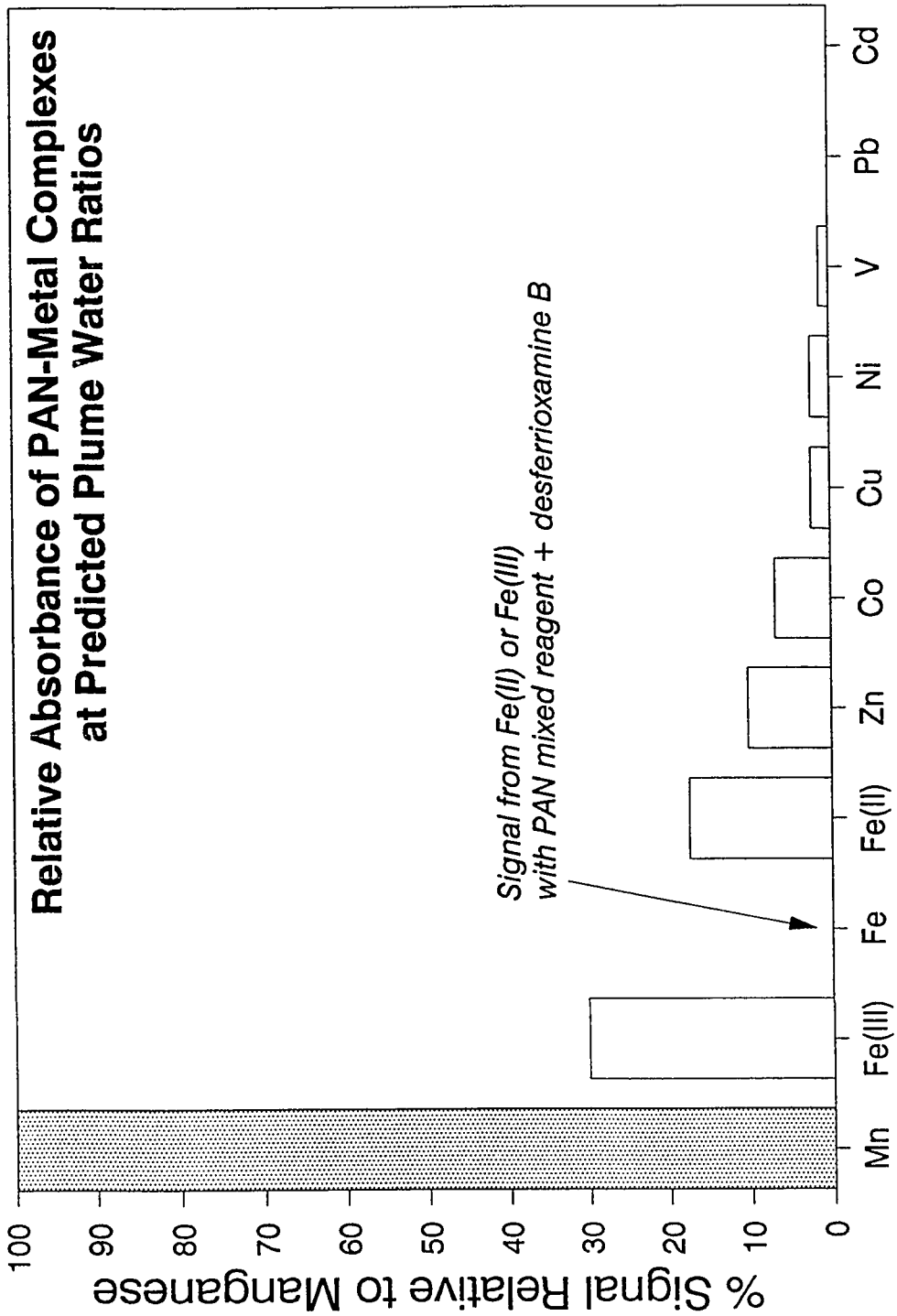
Relative Absorbance of PAN-Metal Complexes
at Predicted Plume Water Ratios
% Signal Relative to Manganese
100
90
80
70
60
50
40
30
20
10
0
Mn
Fe(III)
Fe
Fe(II)
Zn
Co
Cu
Ni
V
Pb
Cd
Signal from Fe(II) or Fe(III)
with PAN mixed reagent + desferrioxamine B

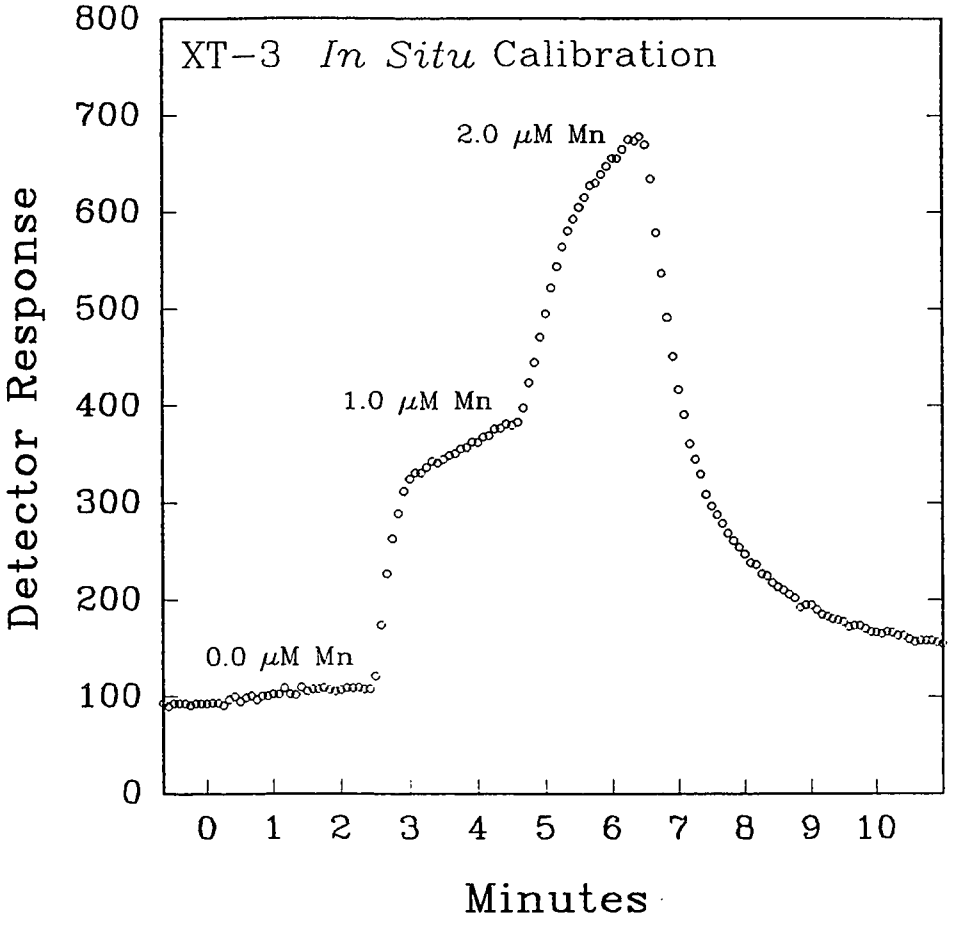
XT−3 *In Situ* Calibration
2.0 μM Mn
1.0 μM Mn
0.0 μM Mn
Detector Response
800
700
600
500
400
300
200
100
0
0 1 2 3 4 5 6 7 8 9 10
Minutes

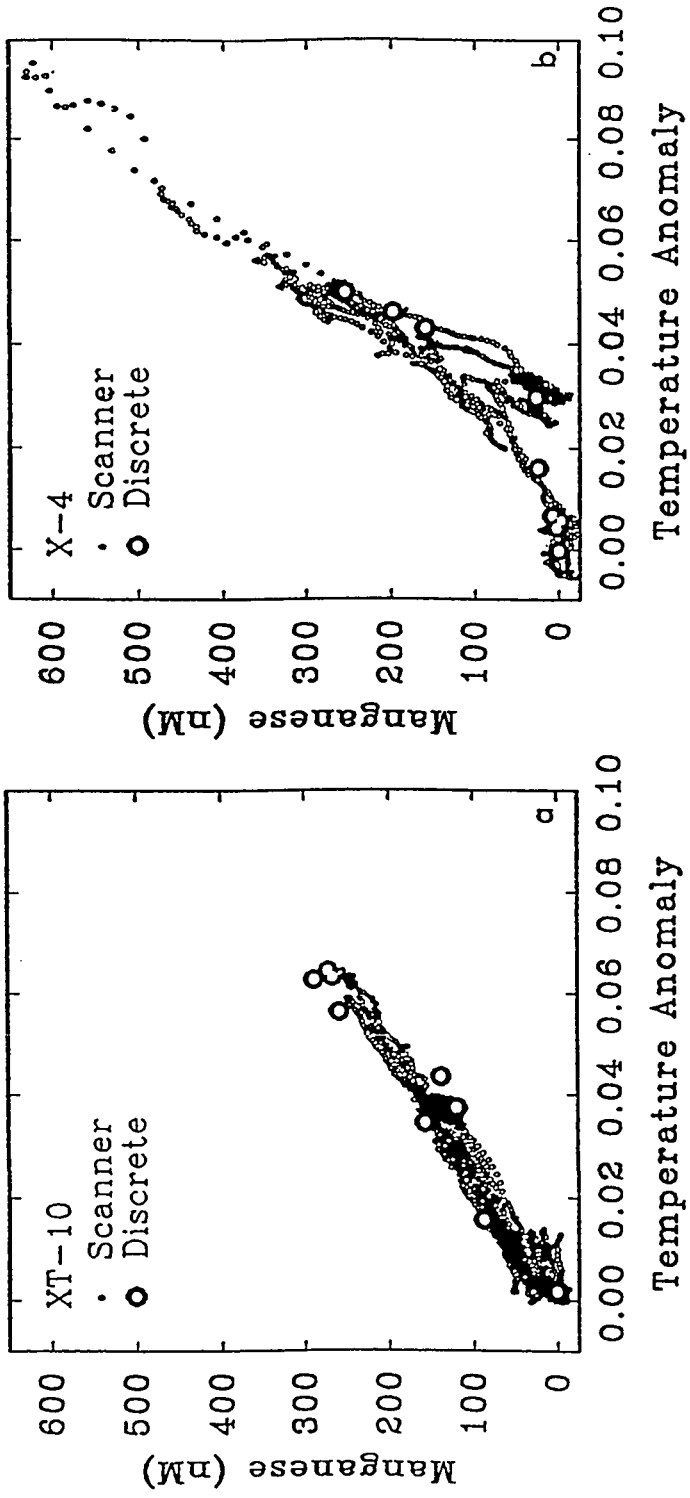
XT-10
Scanner
Discrete
a
X-4
Scanner
Discrete
b
Manganese (nM)
Temperature Anomaly
0
100
200
300
400
500
600
0.00
0.02
0.04
0.06
0.08
0.10

CHAPTER 3

High Resolution *In Situ* Determination of Dissolved Iron and Manganese in Hydrothermal Plumes, Juan de Fuca Ridge

Abstract

High resolution measurements of dissolved manganese and total dissolved iron (Fe(II) plus Fe(III)) were conducted *in situ* in submarine hydrothermal plumes along the Juan de Fuca Ridge hydrothermal system using a submersible chemical analyzer (Scanner). Dissolved manganese was measured colorimetrically using 1-(2-pyridylazo)-2-naphthol (PAN). Total dissolved iron (Fe(II)+(III)) was also measured colorimetrically using ferrozine, with ascorbic acid as the reductant.

The Scanner was deployed as part of a CTD/Transmissometer/rosette (CTDT/rosette) instrument package on both tow-yos and vertical casts during the PMEL/NOAA VENTS cruise, 1989. High resolution transects of dissolved manganese and total dissolved iron concentrations, along with temperature and light attenuation anomalies, were mapped in near real time. By comparing the chemical distributions to the nearly conservative temperature anomaly produced by the venting, these measurements were used to examine physical and chemical processes within plumes, as well as to predict the types of sources contributing to the dispersing plumes. Constant Mn:heat ratios observed in one plume at the North Cleft Segment indicated uniform mixing of two endmembers (ambient seawater and one hydrothermal source) in an older, more mature plume. A vertical cast conducted in the same region revealed that a plume from a younger event had penetrated into this existing, well-mixed plume. Variability in the Mn:heat ratios in a plume sampled 12

km to the north indicated the presence of at least two distinct hydrothermal sources. Tight interleaving of various Mn:heat ratios measured during two vertical casts suggested that turbulent entrainment of these two hydrothermal endmembers had occurred within the ascending plume.

Introduction

Ridge crest hydrothermal vents are a major source of dissolved iron and manganese to the ocean (Edmond et al., 1979; 1982), contributing 73% and 69% of the total input of these metals to the ocean (Table 1). The concentrations of iron and manganese in hydrothermal source waters (black smoker vents) is, respectively, up to 23 and 22 million fold enriched (Von Damm, 1990) over the ambient seawater concentrations (0.8 nM Fe and 0.2 nM Mn; Landing and Bruland, 1987; Martin and Gordon, 1988; Landing and Bruland, 1980; Martin et al., 1985). These inputs significantly influence the chemistry of the mid-depths. Iron and manganese precipitate upon oxidation in the plumes, forming hydroxide and oxyhydroxide particulate mineral phases and Mn-rich bacterial capsules (Cowen et al., 1986). The particulate phases precipitating from these plumes are a dominant constituent within metalliferous sediments deposited for thousands of kilometers from the hydrothermal sources (Boström et al., 1969; Bolger et al., 1978; Lupton and Craig, 1981; Klinkhammer and Hudson, 1986). These iron- and manganese-rich particles scavenge significant amounts of other elements, including phosphorus, vanadium, chromium, arsenic, lead, polonium, uranium, thorium, protactinium, and a number of rare earth elements from seawater (Feely et al., 1990; Trefry and Metz, 1990; Kadko et al., 1987; Shimmield and Price, 1988; Klinkhammer et al., 1983; German et al., 1990).

Many constituents and properties of vent fluids have been studied in order to characterize these effluents, and to understand the magnitude and rates of chemical transformations associated with the plume environment. Physical properties such as temperature anomaly, light attenuation (beam transmission), and potential density have been used to locate and map hydrothermal plumes (Lupton et al., 1985; Baker et al., 1985). Radiotracers such as ^{222}Rn have been used to constrain the ages of plumes, as well as to estimate heat and chemical fluxes from the vents (Kadko et al., 1990; Rosenberg et al., 1988). Probably the most conservative tracer of hydrothermal emissions is ^{3}He, a primordial isotope trapped in the mantle at the formation of the earth which is injected into deep water by hydrothermal processes. Measurements of ^{3}He in plumes make it possible to study the chemical reactivity of other key constituents in hydrothermal emissions through their relationship to ^{3}He (Kadko et at., 1990; Lupton et al., 1980; Lupton and Craig, 1981). It has been shown that ^{3}He and manganese are highly correlated in Galapagos vent waters (Weiss, 1977), and Lupton et al. (1980) state that these two tracers are more sensitive indicators of hydrothermal activity than any other property, including temperature (Klinkhammer et al., 1977; Weiss, 1977; Jenkins et al., 1978). The analysis of ^{3}He requires elaborate gas stripping apparatus coupled to a mass spectrometer and, therefore, is not amenable to shipboard determination. The analysis of Mn typically proceeds via column extraction followed by graphite furnace atomic absorption detection. Although this method is time and labor intensive and not readily amenable to

shipboard analysis, it has been performed at sea (Klinkhammer et al., 1980b, 1986). Recently, K. Johnson and co-workers have reported reliable shipboard methods for the determination of dissolved Mn (Chapin et al., 1991) and dissolved iron(II) and total iron (Elrod et al. 1991) using flow injection analysis with chemiluminescence detection. Until now, chemical tracers have only been sampled discretely and only physical properties could be determined at high resolution in real time.

We present here the first application of a submersible chemical analyzer (Scanner) to the analysis of dissolved manganese and iron *in situ* in hydrothermal plumes. The Scanner was adapted for deployment as part of the Pacific Marine Environmental Laboratory (PMEL) CTD/Transmissometer/ rosette sampler (CTDT/rosette) during the NOAA VENTS '89 cruise (July 27 to August 25, 1989) aboard the NOAA Ship *Discoverer.* The Scanner/CTDT/rosette package was deployed on both vertical casts and "tow-yos" (Baker and Massoth, 1987). During the tow-yos, the instrument package was raised and lowered over a depth range from 1700 to 2300 m while the ship steamed at a speed of approximately 1-2 knots. In this way detailed distributions of physical and chemical characteristics within the plumes were mapped in near real time.

Methods

Apparatus

Chemical analyses were performed *in situ* with a Scanner. The Scanner was

developed to perform two continuous colorimetric analyses *in situ* simultaneously to depths over 3000 m (Johnson et al., 1986a; 1986b). Reagents and standards were held in pressure compensated reservoirs (disposable baby bottles). A solid state, flow-through photometric detector (Betteridge et al., 1978) with a green LED as the light source (569 nm maximum emission, 28 nm bandwidth) was used to detect the color in the solution due to the reagent-metal complexes. Data were recorded digitally and stored in computer memory for retrieval upon recovery of the instrument package. The Scanner was deployed on the Pacific Marine Environmental Laboratory (PMEL) CTDT/rosette sampler. The electronics module, which contained the selection valve circuitry, signal processing, and data storage capabilities, was secured to the bottom frame of the instrument package. The chemistry module, which contained the pump, selection valves, LED detectors, reaction manifolds, and reagent reservoirs, occupied one of the twelve, 30 L sampling bottle positions. A battery pack occupied an adjacent bottle position. Details of the Scanner, its configuration, software, and data acquisition capabilities, as well as data reduction methods are discussed elsewhere (Johnson et al., 1986a; 1989).

Total dissolved iron and dissolved manganese were determined *in situ* by unsegmented continuous flow analysis with colorimetric detection. A schematic of the Scanner manifold for the determination of Mn and Fe is shown in Figure 1. Sample was drawn through a 10 μm filter at 0.8 mL/min and merged continuously with the reagents. Flow rates for the 1-(2-pyridylazo)-2-naphthol (PAN), ferrozine,

and ascorbic acid reagents were 0.15, 0.15, and 0.2 mL/min, respectively (Fig. 1). Selection valves were used to perform a calibration sequence *in situ*, which consisted of two standards and a blank (Fig. 2). Glass bead columns (van den Berg et al., 1980; Reijn et al., 1981) were used to insure complete mixing of the sample with the reagent. The teflon manifold tubing was 0.5 mm i. d. throughout, except for the glass bead columns, which were 0.8 mm i. d.

Dissolved Mn

Manganese was determined colorimetrically using the complexing reagent 1-(2-pyridylazo)-2-naphthol (PAN) in the presence of a nonionic surfactant, Triton X-100, which was used to solubilize the PAN ligand. An iron(III) specific chelating agent, desferrioxamine B, masked any potential interferences from iron in the sample. Details of the method for the determination of manganese, together with intercomparison results, are discussed elsewhere (Chin et al., 1990; 1991).

Total Dissolved Fe

The colorimetric method for the determination of iron in seawater was a modification of the ferrozine method (Stookey, 1970), using ascorbic acid to reduce Fe(III) to Fe(II) and thus allowing the determination of total iron.

Iron Reagents

Ferrozine. 1.25 g Ferrozine was dissolved in 100 mL of 2 M acetic acid/sodium

acetate buffer and diluted to 250 mL with deionized water, purified using a Millipore Milli-Q system (MQ water).

Ascorbic Acid. 12.5 g ascorbic acid was dissolved in 250 mL MQ water, in a separatory funnel. Approximately 50 mL of diethyl ether was then added to the funnel. The diethyl ether extraction was performed to remove iron contamination in the ascorbic acid, and was found to reduce the baseline. After shaking vigorously for 1 minute, the ether was allowed to separate for several hours. After phase separation, the ascorbic acid was drained from the funnel and 5 mL of 6 N hydrochloric acid was added to this reagent. The contaminant iron remained with the ether fraction.

Results and Discussion

Instrument Calibration

Calibrations of these methods were performed both *in situ* with the Scanner and through comparison of the Scanner results with analyses of discrete samples that were performed in the laboratory and at sea. The Scanner could be programmed to run a series of calibrations *in situ* at user-determined intervals. These calibrations generally consisted of the analysis of a blank solution, mid-standard, and high standard for 2 minutes each, at 1 hour intervals. A calibration sequence (Fig. 2), consisting of a seawater blank (<0.5 nm Mn), 1.0 μM Mn, and 2.0 μM Mn, was performed *in situ* during the tow-yo XT-3 along the Cobb Segment of the Juan de

Fuca Ridge. Normally the Scanner allows for such *in situ* calibrations on each deployment. After this particular tow, however, the valves which select sample or standards failed. Because of the stability and reproducibility of the detector response, within single casts as well as between different casts, calibrations from tow-yos XT-2 and XT-3, along the Endeavour and Cobb Segments, were applied to other casts to determine Mn and Fe throughout the remainder of the cruise.

The detection limits for Mn and Fe were determined by calculating 3 times the standard deviation of the metal concentration data from a straight line fitted by least squares regression to the temperature anomaly measured during a single cast (one vertical cast on tow-yo XT-10, n≈250) over which the metal/temperature anomaly ratio was constant. The detection limit for the manganese analysis, depending on the cast, ranged from 15 to 30 nM (average = 22). The range in the detection limit for total iron was 12 to 38 nM (average = 25). These detection limits are operationally defined and, therefore, reflect both instrumental and environmental variability.

The *in situ* calibrations were verified by comparing the Scanner results with shipboard and laboratory analyses of discrete dissolved samples collected concurrently using 30 L Niskin bottles mounted on the rosette (Elrod et al., 1990; 1991; Massoth, pers. comm.). The discrete samples were filtered through 0.2 μm Nucleopore polycarbonate membrane filters immediately after the rosette was returned to the surface. In the following sections, Scanner data, plotted together with discrete sample values from both the Cleft and Endeavour Segments, show excellent

agreement between the Scanner results and the conventional discrete sample analyses performed by column extraction followed by graphite furnace atomic absorption spectrometry (GFAAS). This agreement indicates that the colorimetric methods used to perform analyses *in situ* do not detect metals in the particulate phase.

The chemical and temperature data were smoothed to reduce noise and numerically filtered to correct for the different response rates of the various sensors. The Scanner data were smoothed with a simplified 13-point quadratic least squares algorithm using the convolutes of Savitzky and Golay (1964). The temperature data were difficult to compare directly with the chemical data because the thermistor had a much higher response rate than did the chemical channels (response time of ≈ 10 seconds; Johnson et al., 1989). The five second averaged CTDT data were "smeared" numerically to match the smearing of the chemical signal. The numerical filter used to smear the temperature anomaly ($\Delta\theta$) data was

$$\Delta\theta_i^f = \Delta\theta_{i-1} + 0.1(\Delta\theta_i - \Delta\theta_{i-1}^f) \qquad (1)$$

where $\Delta\theta_i^f$ is the sequential filtered temperature anomaly, $\Delta\theta_i$ is unfiltered temperature anomaly, $\Delta\theta_{i-1}^f$ is the previous filtered temperature anomaly value in a sequence. This 10 percent filter is consistent with smearing of the chemical data as determined by the rise time of the standards analyzed *in situ*. The filtered temperature anomaly was used in all the comparisons discussed below.

Field Results

Study area

The data discussed here are the results of studies conducted along the Cleft and Endeavour Segments of the Juan de Fuca Ridge. The Juan de Fuca Ridge is an active spreading center located approximately 600 km off the coast of Oregon and Washington (Fig. 3) (Vine and Wilson, 1965; Raff and Mason, 1961; Wilson, 1965). The average spreading rate along the ridge is 6 cm yr^{-1} (full rate; Atwater, 1970). The Juan de Fuca Ridge spans a distance of approximately 500 km, between the Blanco (to the south) and the Sovanco (to the north) Fracture Zones; and separates the Pacific Plate from the Juan de Fuca Plate.

Most of the work described here was performed over the Cleft Ridge Segment. This segment is located at the southern end of the Juan de Fuca Ridge, extending approximately 55 km northward from the Blanco Fracture Zone (Fig. 3). It is named for the continuous cleft which splits the otherwise smooth floor along the axial valley of the southern most section of Cleft Ridge (South Cleft, see below). Detailed descriptions of this area have been reported by Normark et al. (1983), Kappel and Ryan (1986) and Kappel and Normark (1987). The Cleft Segment is characterized by a 2.5 km wide crest trending N 20°E. The floor of the axial valley reaches depths of 2300 meters, while the walls of the valley rise to approximately 2150 meters (water depth). The first 20 km of the ridge extending north from the Blanco Fracture Zone is known as the South Cleft Segment. The geologic setting of this segment of the

ridge has been described by the USGS Juan de Fuca Study Group (1986) and Normark et al. (1987). The remaining 35 km of this segment is known as the North Cleft Segment, and has been described by Embley et al. (1988).

Steady state plumes, defined as those produced by continuous venting of compositionally uniform hydrothermal fluids, have been sampled at South Cleft each year beginning in 1985 (Baker and Massoth, 1986; Cowen et al., 1986; Massoth et al., 1988; Massoth et al., 1990). In contrast, plumes indicating episodic and sudden large scale emissions of hydrothermal fluids, such as the 1986 megaplume (Baker et al., 1987; Baker et al., 1989) and the "non-steady-state" plume sampled in 1989 (Massoth et al., 1990; and this work) have been observed at North Cleft. High temperature vent fields have been reported for South Cleft Segment (Von Damm and Bischoff, 1987), whereas the venting sources for the plumes at North Cleft have only recently been discovered and sampled (Massoth, pers. comm.).

The Endeavour Segment is located at the northern most end of the Juan de Fuca Ridge (Fig. 3). This segment extends approximately 170 km south from the Sovanco Fracture Zone to the Cobb Offset (Lupton et al., 1985). The 90 km long southern portion of this segment was the site for the two vertical casts (X-55 and X-55B) discussed below. *Alvin* dives in this region in 1984 confirmed the presence of a high-temperature (400°C) vent field at 2200 m water depth (Delaney et al., 1984). This venting site was located about 100 km west of the ridge axis. It was characterized by 15-20 m high black smoker sulfide chimneys and fissures, as well as large steep-

sided structures which were elongate along strike. Such structures were distributed over a distance of about 200 m at the base of the western axial valley wall (Tivey and Delaney, 1986). In addition, this vent field was bordered by an area of relatively low-temperature venting (Hammond et al., 1984; Delaney et al., 1984; Tivey and Delaney, 1986).

Both vertical casts and tow-yos were conducted during this study. A summary of the station locations and results is given in Table 2. The tow-yo XT-10 crossed over the axial valley at North Cleft in a southwesterly direction (Fig. 4). The vertical casts X-4 and X-8 were also at North Cleft, located on the ridge axis (Fig. 4). Station X-4 was located at the northern most end of the North Cleft Segment. X-8 was approximately 12 km south of X-4 along the ridge axis, near the XT-10 tow path, and only 11 km northwest of the center of the megaplume sampled in 1986 (Baker et al., 1987). However, no evidence of an event plume of that magnitude was observed during the VENTS '89 cruise. Stations X-55 and X-55B were located on the Endeavour Segment, over the vent field discovered in 1984 (Delaney et al., 1984; Hammond et al., 1984).

Transect XT-10

During this tow-yo over the North Cleft Segment, the instrument package was towed in a southwesterly direction across the ridge axis. Over 3700 data points for iron and manganese were obtained on this tow. Temperature anomaly, light

scattering (beam attenuation), iron and manganese were contoured over the XT-10 transect (Figs. 5a-d) using the contouring program *Surfer* (Golden Software). The similarities between the contours of temperature anomaly and light attenuation indicate that there is a high correlation between excess heat and the number of hydrothermal particles. This is a common feature of hydrothermal plumes, in fact light attenuation anomalies have been found to be, at times, more sensitive than temperature in identifying hydrothermal plumes (Baker et al., 1985).

The distribution of manganese, which reaches a maximum concentration of 260 nM at the heart of the plume, shows tightly coupled co-variation with temperature and light attenuation anomalies. The Mn:excess heat anomaly (Q) ratio along transect XT-10 was constant with a slope of 3.81 nmol cal^{-1} ($r^2 = 0.96$, Fig. 6). Together with the overall uniformity of this plume, the constant Mn:Q relationship suggests that there was conservative mixing between only two endmembers, seawater and one hydrothermal source. This Mn:Q relationship is in good agreement with the ratio observed previously for steady state plumes at Cleft Segment (1.9-4.1 nmol cal^{-1}; Massoth et al., 1989). It is, however, lower than the ratio observed in the high temperature source fluids at North Cleft sampled by G. Massoth (5.01-5.45 nmol cal^{-1}; pers. comm.) (Fig. 6).

Dissolved iron concentrations reached a maximum value of 75 nM during the XT-10 tow-yo (Fig. 7). This is in sharp contrast to the calculated concentration of 685 nM, which was based solely on conservative mixing of source hydrothermal fluids

(Massoth, pers. comm.) with ambient seawater (corrected for changes in heat capacity). This discrepancy may be explained by rapid iron oxidation (half life of approximately 9 hours, see below), followed by particle scavenging and removal from the dissolved phase. There is only a weak correlation between the contours of dissolved iron and the other more conservative tracers, manganese and temperature anomaly, as a result of the loss of dissolved iron (Fig. 5). The Fe:Q ratio observed during this tow-yo was 0.90 nmol cal^{-1} ($r^2 = 0.45$, Fig. 7). The low Fe:Mn ratio (1 nM Fe:10 nM Mn) observed during this transect also suggests that this was an older plume from which most of the original iron had been removed.

The plume at XT-10 displays some of the characteristics of an event plume, based on its shape (oblate spheroid), rise height (100 m higher in the water column than the observed steady state plumes), and uniform metal:Q relationships (Baker, 1990; Massoth et al., 1990). Although XT-10 showed lower Me:Q ratios than observed at a station 12 km to the north (X-4, see below), these ratios are higher than those observed in steady state plumes from this region (Massoth et al., 1990). This would indicate that this plume is not a steady state feature, and that the sources for plumes in this area are temporally variable. However, this event plume was much smaller in scale than the megaplume sampled in 1986 (Baker et al., 1987).

Cast X-8

This vertical cast was performed over the axial valley near the middle of, and

one day before the XT-10 transect. Presumably, it sampled the same plume. A submersible pumping system was also deployed on this cast, above the rosette. Therefore, after the initial downcast to confirm the location of the center of the plume, the instrument package was maneuvered over a two hour period to maintain its position in the core of the plume, and then returned to the bottom where one Niskin was tripped. Upon reaching the bottom, the instrument package failed. No other discrete samples were collected, and no further data were recorded on this cast. A comparison of the vertical profiles of temperature anomaly and dissolved manganese for cast X-8 (Fig. 8a,b) and several profiles through the center of the plume during XT-10 (Fig. 9a,b) reveals that both the vertical location of the plume core, as well as the observed temperature anomalies were similar, suggesting that these casts either sampled portions of the same plume or that two distinct plumes resulted from similar venting events. However, the manganese concentrations, and thus the Mn:Q relationships during cast X-8 (Fig. 10) were somewhat higher than those observed during the XT-10 tow-yo: 4.52 nmol cal^{-1} for X-8 vs 3.81 nmol cal^{-1} for XT-10 (Fig. 6). Both of these ratios are below that observed in high temperature sources in this region (5.23 nmol cal^{-1}; Massoth, pers. comm.). This may be due to either fine scale spatial variations in the Mn:Q ratios between vents or temporal variability in the ratios from the same vent.

Further, an excursion in the Mn:Q relationship was observed at the center of the X-8 plume (Fig. 8b). Critical evaluation of these cast data indicates that this

excursion was not an instrumental artifact. This suggests that another vent source with a lower Mn:Q ratio had penetrated into the X-8 plume. It is likely that this feature resulted from the same type of event which produced the existing plume because this excursion occurs within the plume core which, in both cases (XT-10 and X-8), is higher in the water column than has previously been observed for steady-state plumes in this region. This can be seen in a comparison of the plume core profiles of temperature anomaly and manganese from tow XT-10 (Fig. 9a,b) and from the vertical cast X-8 (Fig. 8a,b). While the iron values, as well as Fe:Q ratios at X-8 (Fig. 11) were similar to those at XT-10, these data did not reveal a similar excursion in the Fe:Q relationship because of the low concentrations that were observed.

Although cast X-8 was located along the ridge crest near the transect of the XT-10 tow-yo, no such excursions in the Mn:Q ratio were measured during XT-10, which was conducted only 1 day after the X-8 cast. This feature may have been missed during XT-10 due to tidal fluctuations which could advect such features over several kilometers. It may also indicate that these features exist on relatively fine spatial scales, or that mixing is rapid enough to disperse such features within hours of the event. Thus, it is unlikely that such a feature could be resolved using discrete sampling strategies.

Cast X-4

Cast X-4 was a vertical profile in the axial valley, 12 km north of the center of the plume sampled during the XT-10 tow-yo. The cast consisted of an initial downcast, and then two hours at a constant depth while a pumping system was maintained in the core of the plume. After pumping, the instrument package was again lowered to a depth below the plume, and discrete samples were collected on the upcast through the plume. Iron values as high as 980 nM were observed at a depth of 2150 m in this plume (Fig. 12). This concentration of iron is 84% of the predicted concentration (corrected for changes in heat capacity and dilution) extrapolated from the hydrothermal endmember concentration observed by Massoth (pers. comm.) to the maximum temperature anomaly observed during this cast (0.096°C). Fe:Q ratios were highly variable in this plume (Fig. 13), and curvature in the plot of iron vs temperature anomaly (Fig. 14) again suggests the oxidation and removal of large amounts of iron from the dissolved phase. This curvature could also be attributed to the entrainment and mixing of a second hydrothermal source with low Me:Q values within this plume. However, since curvature in the iron vs temperature anomaly relationship (Fig. 14) may be due to either rapid removal of Fe or multiple sources having distinct Fe:Q ratios, such mixing can only be resolved through examination of the more conservative chemical tracer Mn and its relationship to excess heat at X-4.

The Mn:Q ratios measured during this vertical cast (Fig. 15) were more variable than those encountered on tow XT-10. The high Fe:Mn ratios observed (10 nM Fe:6

nM Mn) suggest that the X-4 plume was younger than the plume sampled during XT-10, and that it was in close proximity to its sources. Since an age of approximately 17 hours was estimated for this plume (see below), and manganese is believed to behave conservatively in near field plumes (Cowen et al., 1990; Mottl and McConachy, 1990; Cowen et al., 1986; Klinkhammer et al., 1985; Lupton et al., 1980), variations in the Mn:heat ratio indicated the entrainment and mixing of multiple sources.

The maxima in the vertical profiles of both Mn and Fe occur at approximately 2150 m (Fig. 16, 12). This is 150 m deeper than the maxima observed during tow-yo XT-10 (Fig. 9) and vertical cast X-8 (Fig. 8), which were conducted over a vent field of similar (water) depth, approximately 2300 m. This would indicate that the plume sampled during cast X-4 was not an event plume of the type described by Baker and Massoth (Baker et al., 1990; Massoth et al., 1990; Baker et al., 1987).

Large excursions in both the Mn and Fe vertical profiles and the metal:temperature anomaly profiles were observed during this cast (Fig. 16, 12, 17, 13). These excursions in the Me:Q ratios indicate that the ascending plume was composed of at least two types of hydrothermal source fluids. One of the fluids must be characterized by high Mn:Q ratios ($\approx$ 6 nmol cal^{-1}), while the other has much lower Mn:Q ratios ($\approx$ 0.5 nmol cal^{-1}). These sources must have been in close proximity in the vent field in order to be entrained together within the same ascending plume.

These endmember predictions have been substantiated by unreported but recently discovered venting at this North Cleft vent field. Sampling and observations by G. Massoth using the deep sea submersible *Alvin* indicate the presence of high temperature vents with Mn:Q ratios of 5.01 to 5.45 nmol cal^{-1} and nearby low temperature diffuse flow vents characterized by Mn:Q ratios of 0.49 to 1.01 nmol cal^{-1} (Massoth, pers. comm.). These North Cleft endmember ratios for both Mn and Fe are plotted in Figures 6, 7, 10, 11, 14, and 15 for comparison to the ratios observed in the overlying plumes. Figure 15 shows that the highest Mn:Q ratios observed in the plume at X-4 (6.3 nmol cal^{-1}) are similar to those observed at high temperature vents in this region, while the lower Mn:Q ratios observed at this station (approximately 0.5 nmol cal^{-1}) correspond to the low temperature hydrothermal endmember ratios.

Casts X-55 and X-55B

Two vertical cast were performed at this site on the Endeavour Segment of the Juan de Fuca Ridge (Fig. 3) over a vent field discovered in 1984 (Delaney et al., 1984; Hammond et al., 1984). Cast X-55, like X-4 and X-8, consisted of an initial downcast, followed by two hours at a constant depth where the pumping system was maintained in the core of the plume, a return to the bottom, and discrete sample collection on the upcast through the plume. Cast X-55B, which was conducted 2 hours after cast X-55, was dedicated to ^{222}Rn measurements and, therefore,

hours after cast X-55, was dedicated to ^{222}Rn measurements and, therefore, corresponding discrete samples were used for ^{222}Rn determinations, and metal samples were not collected on this cast. These casts at the Endeavour Segment provided an opportunity to compare differences in Me:Q ratios between vent sites (Endeavour vs N. Cleft). In addition, conducting two casts at this site facilitated the examination of the precision and stability of the Scanner. Finally, the determination of manganese on both channels during cast X-55B allowed us to examine reproducibility between detectors.

Dissolved manganese at X-55 (determined on channel 1) reached a maximum concentration of 130 nM at a depth of 2000 m, approximately 200 m above the vent field. Discrete samples collected during this cast provided a further check on the calibration of the Scanner. These values, plotted together with Scanner results for the vertical profile of Mn (Fig. 18), again, show excellent agreement between analytical methods.

The highest Mn concentrations were observed at a maximum temperature anomaly of 0.06 °C, corresponding to a Mn:Q ratio of 1.27 nmol cal^{-1} in this plume (Fig. 19). This ratio is higher than the 350°C endmember Mn:Q ratio of 0.45 nmol cal^{-1} observed at this vent field (D. Butterfield and R. McDuff, as cited by Kadko et al., 1990), indicating that either a different source with a higher Mn:Q ratio was contributing to the plume sampled during this cast, or that the thermochemical signature of this vent field is temporally variable.

Negative temperature anomaly values in Figure 19 reflect the difficulty in selecting a "background" potential temperature (theta) value to use in the calculation of this anomaly in the hydrothermal plume environment. These negative values do not, however, change the trend in the Mn:Q relationship.

During cast X-55B, Mn was determined on both channels. The detectors were connected in series, channel 2 followed by channel 1. Channel 1, although it was calibrated independently from cast X-55, revealed excellent reproducibility for this detector between casts (Fig. 18, 19, 20, 21). The highest Mn concentrations detected on this channel were approximately 120 nM. While the maximum temperature anomaly observed during this cast (0.08°C) was greater than that measured during cast X-55, the Mn:Q ratio calculated from this channel, 1.24 nmol cal^{-1}, was comparable to that calculated from the previous cast.

Channel 2 produced manganese concentrations greater than those measured on channel 1 on either cast (Fig. 22). The highest Mn concentrations from this channel were approximately 140 nM at 0.08°C (Fig. 23). This corresponds to a Mn:Q ratio of 1.57 nmol cal^{-1}, slightly greater than the ratio calculated from channel 1. The small discrepancy ($\approx$20 nM) in manganese concentrations may be attributed to variations in response between detectors resulting from differences in construction and components.

All of the Mn:Q ratios observed in this plume at the Endeavour Segment (1.22 to 1.59 nmol cal^{-1})were considerably lower than those measured in plumes at North

Cleft (3.7 to 6.3 nmol cal^{-1}, including only the high temperature component at X-4). Measurements of the composition of the source fluids at Endeavour (D. Butterfield and R. McDuff, as cited in Kadko et al., 1990) and Cleft Segments (Massoth, pers. comm.) indicate that lower Mn:Q ratios are also found in the hydrothermal endmembers at Endeavour. This difference may be attributed to variations in source composition, the partitioning of and varying contribution of phase separated fluids, or the percent contribution of high-temperature and low-temperature venting to the composite plume. More simply, this discrepancy may also be attributed to differences in age (an age has not yet been determined for the plume sampled at the Endeavour Segment.)

Plume Age

Total dissolved:particulate iron ratios at XT-10 were much smaller than those observed at X-4 (Massoth, pers. comm.). The plume waters sampled during XT-10 were apparently older, and this age difference has allowed more dissolved iron to precipitate into the particulate form.

Plume ages can be calculated from the oxidation of iron(II) to iron(III) via the simplified reaction

$$Fe^{2+}_{diss} \underset{}{\overset{k}{\rightarrow}} Fe^{3+}_{diss} \rightarrow Fe^{3+}_{part} \qquad (2)$$

based on the observed iron(II) (Elrod et al., 1990) and total iron concentrations

measured in discrete samples (dissolved + particulate; Massoth, pers. comm.). The simplified rate equation for this reaction has the rate constant k and may be considered to be pseudo-first-order in [Fe(II)] under constant environmental conditions, and takes the form:

$$-\partial[Fe(II)]/\partial t = k_1[Fe(II)] \qquad (3)$$

Since the oxidation rate of Fe(II) varies as a function of pH, O_2, temperature, ionic strength, and pressure, this reaction rate must be calculated at *in situ* conditions. After Millero et al. (1987):

$$-\partial[Fe(II)]/\partial t = k[Fe(II)][O_2][OH^-]^2 \qquad (4)$$

$$\log k = 21.56 - (1545/T) - (3.29 I^{1/2}) + (1.52 I) \qquad (5)$$

where T is the temperature (°K), and I is ionic strength (M). We have used the measurements of Millero et al. (1987) to estimate the rate at which Fe(II) is oxidized to Fe(III). For the *in situ* pH (7.74), temperature (1.7°C) and oxygen (70.1 μM) conditions within the plume (Massoth, pers. comm.), a pseudo-first-order oxidation rate constant (k_1) of $1.29*10^{-3}$ min^{-1} was derived. This value yields a half life for Fe(II) (with respect to oxidation) of 9 hours ((ln 2)/k = 9 hours). The solution to equation (3) yields

$$[Fe(II)]_t = [Fe(II)]_i e^{-k_1 t} \quad (6)$$

Plume age is then given by:

$$t = \frac{\ln([Fe(II)]_i / [Fe(II)]_t)}{k_1} \quad (7)$$

where $[Fe(II)]_t$ is the concentration of Fe(II) observed at time t, $[Fe(II)]_i$ is the initial iron(II) concentration in the plume, which is assumed to be equal to the observed total iron (dissolved + particulate), k_1 is the rate constant (min^{-1}), and t is time (min.). Average ratios of $[Fe(II)]_t/[Fe(II)]_i$ for XT-10 and X-4 were 0.0135 and 0.106. These ratios yielded plume ages of about 46 and 17 hours at the time of sampling for the plumes at XT-10 and X-4, respectively. These plume ages were corrected for the time between bottle closure and sample acidification (9.56 and 11.76 hours for XT-10 and X-4 respectively). Because of the turbulent nature of the plume sampled at X-4, portions of this plume may be as young as 1 hour, based solely on rise time to the observed height in the water column (Little et al., 1987). Since these are average ratios, the times calculated represent an average age for the composite plume and do not necessarily reflect the age variability within the plume.

These estimates are based on the following conditions and assumptions: The oxidation of Fe(II) to Fe(III) plus Fe_{part} is the principal reaction occurring in this portion of the plume, as opposed to precipitation and removal of FeS which

dominates the reactions occurring in the near ascending plume. Rise times are fast, on the order of 1 hour or less (Little et al., 1987), and are therefore small with respect to the estimates based on Fe(II) oxidation. All of the iron was initially in the +2 oxidation state, no particulate iron was lost from the plume, and relatively little of the FeS_2 precipitates from the near field ascending plume contributes to the particulate iron in the upper plume -- most of the particulate iron in the plume is present in the form of iron oxides and oxyhydroxides. Significant contributions of Fe-sulfide minerals to the particulate component would tend to increase these age estimates.

These assumptions are supported by the observations of others. Feely et al. (1990) note that the extremely high iron concentrations and Fe:S ratios found at Cleft Segment would lead to higher percentages of iron oxides and oxyhydroxide in plume particulates. Further, Mottl and McConachy (1990) describe extremely high particle concentrations within the lower 13 m of plumes at the East Pacific Rise, and conclude that particle settling may contribute to fractionation of particles from the mixed plume solutions from which they precipitated. This would, in turn, suggest that a large proportion of the near field precipitates, which include Fe-sulfides, remain in the lower portions of plumes.

Although corrections have been made to account for the *in situ* K_w, pH, and O_2 determined directly, the rate constants in these calculations apply at 1 atm total pressure. No data are yet available to correct the rate constants to *in situ* pressure.

Because increased pressure would tend to dissociate iron complexes ($FeCl_2$, $FeSO_4$), an increased amount of free iron would be available for oxidation, thereby increasing the reaction rate. However, Laidler (1965) notes that the effect of pressure on the rate constant is dependent on the volume of activation. However, the intermediates of the iron oxidation reaction are not well known. Thus, it is difficult to predict the ultimate effect of the higher pressure at which these reactions occur. Although tentative, these estimates provide a good indication of the relative ages both within and between plumes. These estimates could be refined through mineralogical characterization of the suspended particles, a better understanding of the pressure effects on the rate constant, and the use of the Scanner for simultaneous *in situ* analysis of dissolved Fe(II) and total dissolved iron. This latter refinement is a current capability of the Scanner.

Conclusions

Chemical analyses of dissolved manganese and total dissolved iron performed *in situ* have provided high resolution data allowing chemical mapping of several plumes along the Juan de Fuca Ridge. In addition, these data have provided details of the range and variability of the concentrations of these metals in the plumes and between venting sites, and also of their relationship to excess temperature. Excursions in the metal concentrations, as well as interleaving of the Me:Q ratios, suggest turbulent entrainment of sources with differing metal concentrations and Me:Q relationships.

In addition, this variability indicates that these sources with distinct thermochemical signatures must be in close spatial and temporal proximity in the vent field to be entrained within the same ascending plume. Due to the fine scale distributions and variations in the Me:Q relationships observed for these casts, it is unlikely that discrete sampling techniques could resolve these features with the resolution necessary to provide sufficient confidence to such determinations. In addition, the Scanner's configuration is flexible, allowing it to be adapted to a variety of chemical analyses and be deployed from almost any research vessel. Thus, *in situ* chemical mapping of hydrothermal plumes has proven to be an effective prospecting tool which could be applied on a larger scale and may preclude, to some extent, the need for costly submersible search and verification of venting sources and types.

Acknowledgments

We wish to thank Chief Scientist E. Baker for his patience and encouragement; R. Feely for accommodating our participation in the NOAA/PMEL VENTS '89 expedition, Leg 1; E. Baker and S. Walker for providing CTD/T data; G. Massoth, K. Roe and V. Elrod for analysis of discrete water samples for dissolved Fe and Mn; G. Lebon for modifications to the PMEL rosette to accommodate the Scanner and for particulate Fe determinations by XRF analysis; the David and Lucille Packard Foundation for funding the presentation of the methods section at the AGU-ASLO Ocean Sciences Meeting, February 1990; The Oceanography Society for funding the presentation of this work at the Second Scientific Meeting, March 1991; and the crew and officers of the NOAA Ship *Discoverer*, R/V *Ricketts*, and R/V *Point Sur*. This work was supported by the Ocean Sciences Division of the NSF grant OCE-8609437 to K. Johnson, the Office of Naval Research grant N00014-89-J-1010 to K. Johnson and K. Coale, and the NOAA VENTS Program.

References

Atwater T. (1970) Implications of plate tectonics for the Cenozoic tectonic evolution of western North America. Geological Society of America Bulletin, **81**, 3513-3536.

Baker E. T. (1990) Detection and sampling of hydrothermal event plumes. In: RIDGE Events, Vol. 1, No. 2, U. S. RIDGE Office, Seattle.

Baker E. T. and G. J. Massoth (1986) Hydrothermal plume measurements: a regional perspective. Science, **234**, 980-982.

Baker E. T. and D. Z. Piper (1976) Suspended particulate matter: collection by pressure filtration and elemental analysis by thin-film X-ray fluorescence. Deep-Sea Research, **23**, 181-186.

Baker E. T. and G. J. Massoth (1987) Characteristics of hydrothermal plumes from two vent fields on the Juan de Fuca Ridge, northeast Pacific Ocean. Earth and Planetary Science Letters, **85**, 59-73.

Baker E. T., J. W. Lavelle and G. J. Massoth (1985) Hydrothermal particle plumes over the Juan de Fuca Ridge. Nature, **316**, 342-344.

Baker E. T., G. J. Massoth and R. A. Feely (1987) Cataclysmic hydrothermal venting on the Juan de Fuca Ridge. Nature, **329**, 149-151.

Betteridge D., E. L. Dagless, B. Fields, and N. F. Graves, (1978) A highly sensitive flow-through phototransducer for unsegmented continuous-flow analysis

demonstrating high-speed spectrophotometry at the parts per 10^9 level and a new method of refractometric determinations. Analyst, **103**, 897-908.

Bolger G. W., P. R. Betzer and V. V. Gordeev (1978) Hydrothermally-derived manganese suspended over the Galapagos Spreading Center. Deep-Sea Research, **25**, 721-733.

Boström K., M. N. P. Peterson, O. Joensuu and D. E. Fisher (1969) Aluminum-poor ferromanganoan sediments on active oceanic ridges. Journal of Geophysical Research, **74**, 3261-3270.

Chapin T. P., K. S. Johnson and K. H. Coale (1991) Rapid determination of manganese in seawater by flow injection analysis with chemiluminescence detection. Analytica Chimica Acta, in press.

Chester R. and K. J. T. Murphy (1990) Metals in the Marine Atmosphere. In: Heavy metals in the marine environment. R. W. Furners and P. S. Rainbow (Eds.) CRC Press, Boca Raton, FL, 256 pp.

Chin C., K. Coale, K. Johnson, G. Massoth, E. Baker and R. Feely (1990) Development and application of an *in situ* spectrophotometric method for the determination of manganese in hydrothermal vent plumes. EOS, **71**, 143.

Chin C. S., K. S. Johnson and K. H. Coale (in press) Spectrophotometric determination of dissolved manganese in natural waters with 1-(2-pyridylazo)-2-naphthol: application to analysis *in situ* in hydrothermal plumes. Marine Chemistry.

Coale K. H., C. S. Chin, G. J. Massoth, K. S. Johnson and E. T. Baker (1991) *In situ* chemical mapping of dissolved iron and manganese in hydrothermal plumes. Nature, **352**, 325-328.

Cowen J. P., G. J. Massoth and E. T. Baker (1986) Bacterial scavenging of Mn and Fe in a mid- to far-field hydrothermal plume. Nature, **322**, 169-171.

Craig H., W. B. Clark and M. A. Beg (1975) Excess ^{3}He in deep water on the East Pacific Rise. Earth and Planetary Science Letters, **26**, 125-132.

Delaney J. R., R. E. McDuff and J. E. Lupton (1984) Hydrothermal fluid temperatures of 400°C on the Endeavour Segment, northern Juan de Fuca. EOS, **65**, 973.

Edmond J. M., C. Measures, R. E. McDuff, L. H. Chan, R. Collier, B. Grant, C. I. Gordon and J. B. Corliss (1979) Ridge crest hydrothermal activity and the balances of the major and minor elements in the ocean: the Galapagos data. Earth and Planetary Science Letters, **46**, 1-18.

Elrod V. A., K. H. Coale, K. S, Johnson, G. J. Massoth (1990) Determination of iron in seawater by FIA using chemiluminescence detection: shipboard mapping of hydrothermal plumes. EOS, **71**, 143.

Elrod V. A., K. S. Johnson and K. H. Coale (1991) Determination of subnanomolar levels of iron(II) and total dissolved iron in seawater by flow injection analysis with chemiluminescence detection. Analytical Chemistry, **63**, 893-898.

Feely R. A., G. J. Massoth, E. T. Baker, J. P. Cowen, M. F. Lamb, K. A. Krogslund

(1990) The effect of hydrothermal processes on midwater phosphorus distributions in the northeast Pacific. Earth and Planetary Science Letters, **96**, 305-318.

German C. R., G. P. Klinkhammer, J. M. Edmond, A. Mitra and H. Elderfield (1990) Hydrothermal scavenging of rare-earth elements in the ocean. Nature, **345**, 516-518.

Hammond S. E., J. S. Lee, A. Malahoff, R. Feely, R. W. Embley and J. Franklin (1984) Discovery of high-temperature hydrothermal venting on the Endeavour Segment of the Juan de Fuca Ridge. EOS, **65**, 1111.

Jenkins W. J., J. M. Edmond and J. B. Corliss (1978) Excess ^{3}He and ^{4}He in Galapagos submarine hydrothermal waters. Nature, **272**, 156-158.

Johnson K. S., Sakamoto-Arnold, C. M., and Beehler, C. L. (1989) Continuous determination of nitrate concentrations *in situ*. Deep-Sea Research, **36**, 1407-1413.

Johnson K. S., Beehler, C. L. and Sakamoto-Arnold, C. M. (1986a) A submersible flow analysis system. Analyt. Chim. Acta, **179**, 245-257.

Johnson K. S., Beehler, C. L., Sakamoto-Arnold, C. M. and Childress, J. J. (1986b) *In situ* measurements of chemical distributions in a deep-sea hydrothermal vent field. Science, **231**, 1139-1141.

Kadko D. C., N. D. Rosenberg, J. E. Lupton, R. W. Collier and M. D. Lilley (1990) Chemical reaction rates and entrainment within the Endeavour Ridge

hydrothermal plume. Earth and Planetary Science Letters, **99**, 315-335.

Kadko D., M. P. Bacon and A. Hudson (1987) Enhanced scavenging of ^{210}Pb and ^{210}Po by processes associated with the East Pacific Rise near 8°45'N. Earth and Planetary Science Letters, **81**, 349-357.

Kappel E. S. and W. B. F. Ryan (1986) Volcanic episodicity and a non-steady state rift valley along northeast Pacific spreading centers: evidence from Sea MARC I. Journal of Geophysical Research, **91**, 13,925-13,940.

Kappel E. S. and W. R. Normark (1987) Morphometric variability within the axial zone of the southern Juan de Fuca Ridge: interpretation from Sea MARC II, Sea MARC I and deep-sea photography. Journal of Geophysical Research, **92**, 11,291-11,302.

Klinkhammer G. P. (1980a) Observations of the distribution of manganese over the East Pacific Rise. Chemical Geology, **29**, 211-226.

Klinkhammer G. (1980b) Determination of manganese in seawater by flameless atomic absorption spectrometry after pre-concentration with 8-hydroxyquinoline in chloroform. Analytical Chemistry, **52**, 117-120.

Klinkhammer G. P. and A. Hudson (1986) Dispersal patterns for hydrothermal plumes in the South Pacific using manganese as a tracer. Earth and Planetary Science Letters, **79**, 241-249.

Klinkhammer G. P., M. Bender and R. F. Weiss (1977) Hydrothermal manganese in the Galapagos Rift. Nature, **269**, 319-320.

Klinkhammer G., H. Elderfield and A. Hudson (1983) Rare earth elements in seawater near hydrothermal vents. Nature, **305**, 185-188.

Klinkhammer G., H. Elderfield, M. Greaves, P. Rona and T. Nelsen (1986) Manganese geochemistry near high-temperature vents in the Mid-Atlantic Ridge rift valley. Earth and Planetary Science Letters, **80**, 230-240.

Laidler K. J. (1965) Chemical Kinetics. Second edition. McGraw-Hill, New York. 566 pp.

Landing W. M. and K. W. Bruland (1980) Manganese in the North Pacific. Earth and Planetary Science Letters, **49**, 45-56.

Landing W. M. and K. W. Bruland (1987) The contrasting biogeochemistry of iron and manganese in the Pacific Ocean. Geochimica et Cosmochimica Acta, **51**, 29-43.

Little S. A., K. D. Stolzenbach and R. P. Von Herzen (1987) Measurements of plume flow from a hydrothermal vent field. Journal of Geophysical Research, **92**, 2587-2596.

Lupton J. E. and H. Craig (1981) A major helium-3 source at 15°S on the East Pacific Rise. Science, **214**, 13-18.

Lupton J. E., G. P. Klinkhammer, W. R. Normark, R. Haymon, K. C. MacDonald, R. F. Weiss and H. Craig (1980) Helium-3 and manganese at the 21°N East Pacific Rise hydrothermal site. Earth and Planetary Science Letters, **50**, 115-127.

Lupton J. E., J. R. Delany, H. P. Johnson and M. K. Tivey (1985) Entrainment and

vertical transport of deep-ocean water by buoyant hydrothermal plumes. Nature, **316**, 621-623.

Martin J. H. and R. M. Gordon (1988) Northeast Pacific iron distributions in relation to phytoplankton productivity. Deep-Sea Research, **35**, 177-196.

Martin J. H., G. A. Knauer and W. W. Broenkow (1985) VERTEX: the lateral transport of manganese in the northeast Pacific. Deep-Sea Research, **32**, 1405-1427.

Massoth G. J., E. T. Baker, K. K. Roe and G. T. Lebon (1990) Non-steady-state venting at Cleft Segment, Juan de Fuca Ridge: A rationale for whole-segment and temporal plume assessment, EOS, **71**, 143.

Millero F. J., S. Sotolongo and M. Izaguirre (1987) The oxidation kinetics of Fe(II) in seawater. Geochimica et Cosmochimica Acta, **51**, 793-801.

Mottl M. J. and T. F. McConachy (1990) Chemical processes in buoyant hydrothermal plumes on the East Pacific Rise near 21°N. Geochimica et Cosmochimica Acta, **54**, 1911-1927.

Normark W. R., J. L. Morton, R. A. Koski, D. A. Clague and J. R. Delaney (1983) Active hydrothermal vents and sulfide deposits on the southern Juan de Fuca Ridge. Geology, **11**, 158-163.

Palmer M. R. and J. M. Edmond (1989) The strontium isotope budget of the modern ocean. Earth and Planetary Science Letters, **92**, 11-26.

Raff A. D. and P. G. Mason (1961) Magnetic survey off the west coast of North

America, 40°N latitude to 52°N latitude. Geological Society of America Bulletin, **72**, 1267-1270.

Reijn J. M., W. E. van der Linden and H. Poppe (1981) Dispersion in open tubes and tubes packed with large glass beads: The single bead string reactor. Analytica Chimica Acta, **123**, 229-237.

Rosenberg N. D., J. E. Lupton, D. Kadko, R. Collier, M. D. Lilley and H. Pak (1988) Estimation of heat and chemical fluxes from a seafloor hydrothermal vent field using radon measurements. Nature, **334**, 604-607.

Savitzky A. and M. J. E. Golay (1964) Smoothing and differentiation of data by simplified least squares procedures. Analytical Chemistry, **36**, 1627-1639.

Shimmield G. B. and N. B. Price (1988) The scavenging of U, ^{230}Th and ^{231}Pa during pulsed hydrothermal activity at 20°S, East Pacific Rise. Geochimica et Cosmochimica Acta, **52**, 669-677.

Stookey L. L. (1970) Ferrozine -- A new spectrophotometric reagent for iron. Analytical Chemistry, **42**, 779-781.

Trefry J. H. and S. Metz (1990) Role of hydrothermal precipitates in the geochemical cycling of vanadium. Nature, **342**, 531-533.

U.S.G.S. Juan de Fuca Study Group (1986) Submarine fissure eruptions and hydrothermal vents on the southern Juan de Fuca Ridge: preliminary observations from the submersible *Alvin*. Geology, **14**, 823-827.

van den Berg J. H. M., R. S. Deelder and H. G. M. Egberink (1980) Dispersion

phenomena in reactors for flow analysis. Analytica Chimica Acta, **114**, 91-104.

Vine F. J. and J. T. Wilson (1965) Magnetic anomalies over a young oceanic ridge off Vancouver Island. Science, **150**, 485-489.

Von Damm K. L. (1990) Seafloor hydrothermal activity: black smoker chemistry and chimneys. Annual Review of Earth and Planetary Sciences, **18**, 173-204.

Von Damm K. L. and J. L. Bischoff (1987) Chemistry of hydrothermal solutions from the southern Juan de Fuca Ridge. Journal of Geophysical Research, **92**, 11334-11346.

Von Damm K. L., J. M. Edmond, B. Grant, C. I. Measures, B. Walden and R. F. Weiss (1985) Chemistry of hydrothermal solutions at 21°N, East Pacific Rise. Geochimica et Cosmochimica Acta, **49**, 2197-2220.

Weiss R. F. (1977) Hydrothermal manganese in the deep sea: scavenging residence time and $Mn/^{3}He$ relationships. Earth and Planetary Science Letters, **37**, 257-262.

Wilson J. T. (1965) Transform faults, oceanic ridges and magnetic anomalies southwest of Vancouver Island. Science, **150**, 482-485.

Figure Captions

Figure 1) Schematic diagram of the Scanner manifold for the determination of dissolved manganese and total dissolved iron *in situ*. Flow rates for the reagents and sample are shown in mL/min. Sample was drawn continuously, mixed with the reagents, and then delivered to the detectors. Glass bead columns were used to increase mixing of the sample with the reagents. Selection valves on the Scanner were used to perform a calibration sequences *in situ* at programmed time intervals. An ascorbic acid line is used for the determination of total dissolved iron, whereas without this line, only Fe(II) is detected.

Figure 2) An *in situ* calibration sequence from the tow-yo XT-3 over the Cobb Segment of the Juan de Fuca Ridge. Detector response, in detector voltage units, is plotted vs time in minutes. The Scanner was programmed to run a seawater blank (surface seawater, $\approx$ 0.5 nM Mn), 1.0 μM Mn, and 2.0 μM Mn standards once every hour of operation.

Figure 3) Location of the Cleft, Cobb, and Endeavour Segments of the Juan de Fuca Ridge in the northeastern Pacific Ocean.

Figure 4) Station locations along the North Cleft Segment are plotted over contours

of the hydrothermal temperature anomaly (contour interval = 0.01°C). Vertical cast X-4 was the northern most station on this segment. The broken line indicates the XT-10 tow-yo path. Vertical cast X-8 was located along the XT-10 tow path.

Figure 5) Measured properties for the tow-yo XT-10 across the North Cleft Segment, contoured along a vertical section over the tow track. Left side of each panel represents 44° 52.8'N, 130° 13.0'W on the eastern flank of the ridge; right side of each panel represents 44° 50.6'N, 130° 21.0'W over the western valley wall. a) Tow track of the CTDT/rosette/Scanner package, as it was towed in a southwesterly direction across the axial valley (see Fig. 4), is plotted together with the contoured section of temperature anomaly, D-theta, an indicator of the plume's location and strength. b) Light attenuation anomaly, as measured with a beam transmissometer secured to the CTD package, shows a high correlation between the distribution of hydrothermal particles (primarily iron oxyhydroxides) and the temperature anomaly. c) Iron concentrations contoured over the XT-10 transect at 10 nM intervals show weak correlation with the other conservative tracers temperature anomaly and manganese due to its rapid oxidation and removal from the dissolved phase. d) The more conservative chemical tracer, manganese, contoured over the XT-10 transect at 25 nM intervals shows excellent agreement with temperature anomaly and beam attenuation.

Figure 6) Manganese (nM) vs temperature anomaly (°C) from both the Scanner and discrete samples from transect XT-10 shows excellent agreement between methods. This Mn:temperature anomaly relationship is quite linear (r^2 = 0.96) with a slope of 3.81 nmol cal^{-1}. Mn:Q ratios in source fluids sampled by G. Massoth (5.23 nmol cal^{-1}) (pers. comm.), corrected for changes in heat capacity, are also shown in this figure.

Figure 7) Iron vs temperature anomaly along the XT-10 transect shows extremely low slope (0.9 nmol cal^{-1})relative to the source fluids (12.1 nmol cal^{-1};Massoth, pers. comm.). The noise in this data reflects concentrations near our detection limit for iron and the nonconservative behavior of iron in these plumes. The concentrations measured *in situ* are in good agreement with the GFAAS results determined at PMEL.

Figure 8) a) Vertical profile of the hydrothermal temperature anomaly measured during cast X-8. The highest temperature anomalies observed were approximately 0.065°C, and were measured at about 2000 m. b) Vertical profile of dissolved manganese measured during cast X-8. The highest manganese concentrations (340 nM) were also observed at 2000 m, however, an excursion in the manganese concentrations occurred in the core of this plume. This was presumably the result of the penetration of a younger plume, with lower Mn:Q ratios, into the core of the

existing plume.

Figure 9) a) This plot shows several vertical profiles of the temperature anomaly measured over at the center of the plume during the XT-10 tow-yo. The highest temperature anomalies (0.065°C) were, again, measured at 2000 m. These similarities suggest that XT-10 and X-8 either sampled the same plume, or sampled plumes resulting from similar types of events. b) The highest manganese concentrations measured during XT-10, 260 nM, were lower than those observed at X-8. In addition, the excursion in manganese concentration at the center of the plume was also absent.

Figure 10) Manganese vs temperature anomaly for the vertical cast X-8. The Mn:Q ratio in this plume was 4.52 nmol cal^{-1}. This ratio was higher than that observed during XT-10, yet still below the ratio measured in high-temperature hydrothermal source fluids (5.23 nmol cal^{-1}; Massoth, pers. comm.).

Figure 11) Iron vs temperature anomaly for cast X-8. Iron concentrations measured during this cast were similar to those seen during tow XT-10. However, because these concentrations were very low, any excursion in the Fe:Q ratio similar to that seen in the Mn:Q relationship is within the noise of this data set.

Figure 12) Vertical profile of iron concentrations measured during cast X-4. Excursions and variability in these concentrations indicate the turbulent entrainment within the ascending plume. The core of this plume can be seen at approximately 2150 m, where the Fe concentrations are as high as 980 nM.

Figure 13) Vertical profile of the Fe/temperature anomaly ratio at X-4. Excursions and variability in the Fe/Q relationship indicate the turbulent entrainment of hydrothermal sources with different Fe:Q ratios within the ascending plume.

Figure 14) Iron vs temperature anomaly at X-4, plotted together with discrete sample values. Curvature in this plot may indicate either the oxidation and removal of iron from the dissolved phase, or entrainment and mixing of a second hydrothermal source with low Fe:Q values within this plume.

Figure 15) Manganese vs temperature anomaly for cast X-4 from both Scanner and discrete samples. Because of the conservative behavior of Mn in near field plumes, the curvature in this plot indicates the entrainment of a second hydrothermal source with low Mn:Q values.

Figure 16) Vertical profile of the manganese concentrations measured during cast X-4. The core of this plume can be seen at 2150 m, where Mn concentrations reach

640 nM. Variability in these concentrations indicate that the ascending portion of this plume was sampled during this cast.

Figure 17) Manganese/temperature anomaly profile at X-4. Large excursions in the Mn:Q profile indicate that the ascending plume was composed of at least two hydrothermal source fluids with different Mn:Q ratios.

Figure 18) Vertical profile of the manganese concentration measured during the vertical cast X-55 over the Endeavour segment. Both Scanner and discrete sample values are plotted, and there is very good agreement between data sets.

Figure 19) Manganese vs temperature anomaly at X-55. Scanner and discrete sample values are in good agreement. The Mn:Q ratio observed in this plume, 1.27 nmol cal^{-1}, is higher than the ratio measured for the high temperature sources in this region (0.45 nmol cal^{-1}; D. Butterfield and R. McDuff, as cited by Kadko et al., 1990).

Figure 20) Vertical profile of the manganese concentration at X-55B, channel 1. No discrete samples were collected on this cast. However, there is excellent agreement between this cast and X-55, conducted a few hours earlier.

Figure 21) Manganese vs temperature anomaly for X-55B, channel 1. The slope of the Mn:temperature anomaly relationship during this cast (1.24 nmol cal^{-1})is similar to that measured at X-55.

Figure 22) Vertical profile of the manganese concentration at X-55B measured on channel 2. This profile shows the same trend as that produced by channel 1.

Figure 23) Manganese vs temperature anomaly for X-55B, channel 2. The slope of the Mn:temperature anomaly relationship produced by this channel (1.57 nmol cal^{-1}) is slightly higher than that from channel 1. This result is attributed to differences in response between detectors.

Figure 24) Regressions of manganese vs temperature anomaly for all stations, plotted together with source ratios from North Cleft (both high- and low-temperature) and Endeavour Segments (see text). The ranges in the Mn:temperature relationships shown here represent ± 1 S.D.

Table 1: Comparison of hydrothermal, fluvial, and atmospheric fluxes (moles year^{-1}).

	Hydrothermal Contributions				Relative Hydrothermal Contribution[g]
	Source Fluids 21°N, EPR[a]	Other Venting Sites	Fluvial Input[b]	Atmospheric Deposition[c]	
Li	$1.2\text{-}1.9\times10^{11}$	$9.5\text{-}16\times10^{10}$[d]	1.4×10^{10}		91
Na	$-8.6\text{-}1.9\times10^{12}$	+,- [d,k]	6.9×10^{12}		-76
K	$-1.9\text{-}2.3\times10^{12}$	1.3×10^{12}[d]	1.9×10^{12}		-20
Rb	$3.7\text{-}4.6\times10^{9}$	$1.7\text{-}2.8\times10^{9}$[d]	5×10^{8}		99
Be	$1.4\text{-}5.3\times10^{5}$	$1.6\text{-}5.3\times10^{6}$[d]	3.3×10^{7}		5
Mg	-7.5×10^{12}	-7.7×10^{12}[d]	5.3×10^{12}		-143
Ca	$2.4\text{-}15\times10^{11}$	$2.1\text{-}4.3\times10^{12}$[d]	1.2×10^{13}		14
Sr	$-3.1\text{-}+1.4\times10^{9}$	0[d]	2.2×10^{10}		-4
Ba	$1.1\text{-}2.3\times10^{9}$	$2.5\text{-}6.1\times10^{9}$[d]	1.0×10^{10}		23
F	-1.0×10^{10}		1.6×10^{11}		-6
Cl	$0\text{-}-1.2\times10^{13}$	$-31\text{-}+7.8\times10^{12}$[d]	6.9×10^{12}		-212
SiO_2	$2.2\text{-}2.8\times10^{12}$	3.1×10^{12}[d]	6.4×10^{12}		30
Al	$5.7\text{-}7.4\times10^{8}$		6.0×10^{12}	2.4×10^{11}	<0.1
SO_4	-4.0×10^{12}	-3.8×10^{12}[d]	3.7×10^{12}		-105
H_2S	$9.4\text{-}12\times10^{11}$	+[d]			
$\sum S$	$-2.8\text{-}3.1\times10^{11}$	-[d]			

	Hydrothermal Contributions				Relative Hydrothermal Contribution[g]
	Source Fluids 21°N, EPR[a]	Other Venting Sites	Fluvial Input[b]	Atmospheric Deposition[c]	
Mn	$1.0\text{-}1.4\times10^{11}$	$5.1\text{-}16\times10^{10}$[d]	4.9×10^{10}	1.3×10^{9}	69
Fe	$1.1\text{-}3.5\times10^{11}$	+[d]	2.3×10^{10}	6.3×10^{10}	73
Co	$3.1\text{-}32\times10^{6}$		1.1×10^{8}	4.1×10^{7}	10
Cu	$0\text{-}6.3\times10^{9}$	-[d]	5.0×10^{9}	5.5×10^{8}	36
Zn	$5.7\text{-}15\times10^{9}$		1.4×10^{10}	3.0×10^{9}	38
Ag	$0\text{-}5.4\times10^{6}$		8.8×10^{7}		3
Cd	$2.3\text{-}26\times10^{6}$	-[d]	2.8×10^{7}	$<3.0\times10^{7}$	20
Pb	$2.6\text{-}5.1\times10^{7}$		1.5×10^{8}	1.3×10^{9}	3
V		-1.4×10^{8}[e]*	5.0×10^{8}[e]	$<6.9\times10^{8}$	-12
Cr		-[d], -[e]*	3.5×10^{8}	$<9.5\times10^{8}$	-
Ni		-[d]	4.9×10^{8}	$<1.2\times10^{9}$	-
P		-4.2×10^{9}[f]*	3.2×10^{10}[f]	3.2×10^{9}[f]	-12
As	$0\text{-}6.5\times10^{7}$	-[e]*	7.2×10^{8}		4
Se	$0\text{-}1.0\times10^{7}$	-[d]	7.9×10^{7}		6
^{3}He		≤1080[h]		~1080[h]	+
^{210}Pb ^{210}Po ^{234}U ^{238}U ^{230}Th ^{231}Pa		-[i] -[i] -[i] -[i] -[i]			-
REE		-[j]			-

Footnotes to Table 1

[a]EPR data from Von Damm et al. (1985).

[b]Fluvial fluxes from Von Damm et al. (1985) and Edmond et al. (1979a,b) and references therein.

[c]Atmospheric fluxes from Chester and Murphy (1990) and references therein. These values represent net global total atmospheric input, and are not corrected for % soluble.

[d]GSC data from Edmond et al.(1979a,b).

[e]MAR data from Trefry and Metz (1990) and references therein.

[f]JDFR data from Feely et al. (1990) and references therein. Atmospheric value is soluble P in atmospheric particulates.

[g]Relative hydrothermal contribution calculated as follows: where HT contribution is positive, Relative hydrothermal contribution = (HT source/all sources)x100, and all sources = hydrothermal + fluvial + atmospheric. Where HT contribution is negative, Relative hydrothermal contribution = (HT sink/all sources)x100, and all sources = fluvial + atmospheric.

[h]Data from Craig et al. (1975). The studies of Clarke et al. (1969), Craig et al. (1975), Lupton and Craig (1975; 1981), and Craig and Lupton (1976) have indicated that hydrothermal venting is a major source of ^{3}He to the world's ocean.

[i]These radionuclides have a strong *in situ* production term from the radiodecay of their parent isotopes. Hydrothermal source fluids, fluvial, and atmospheric input are small in comparison (Kadko et al., 1987; Shimmield and Price, 1988).

[j]Data from Klinkhammer et al. (1983) and German et al. (1990).

[k] + = gain, - = loss, * = removal mechanism is scavenging by hydrothermal precipitates in plumes.

Table 2: Summary of VENTS '89 station locations and results.

Cast type	Station	Date	Location[a]	Latitude, Longitude[b]	Metals[c]	Discrete[d]
Tow-yo[e]	XT-2	7/29/89	Endeavour	47°49' N, 129°11' W to 48°16' N, 129°57' W	Fe_{total} Mn	+
Tow-yo[e]	XT-3	7/31/89	Cobb	47°45' N, 129°00' W	Mn	+
Vertical	X-4	8/04/89	N. Cleft	44°57.7' N, 130°13.5' W	Mn Fe_{total}	+
Vertical	X-8	8/12/89	N. Cleft	44°51.6' N, 130°16.4' W	Mn Fe_{total}	
Tow-yo	XT-10	8/13/89	N. Cleft	44°52.8' N, 130°13.0' W to 44°50.6' N, 130°21.0' W	Mn Fe_{total}	+
Vertical	X-55	8/22/89	Endeavour	47°57.5' N, 129°06.3' W	Fe_{total} Mn	+
Vertical	X-55b	8/22/89	Endeavour	47°57.5' N, 129°06.3' W	Mn Mn	

Footnotes to Table 2

[a]Segment of the JDFR along which the cast was conducted.

[b]Ship's latitude and longitude.

[c]Metals analyzed *in situ* by the Scanner.

[d]Indicates that discrete samples were collected concurrently using the rosette.

[e]Used for calibration purposes.

Scanner Manifold Configuration for Iron and Manganese Determinations

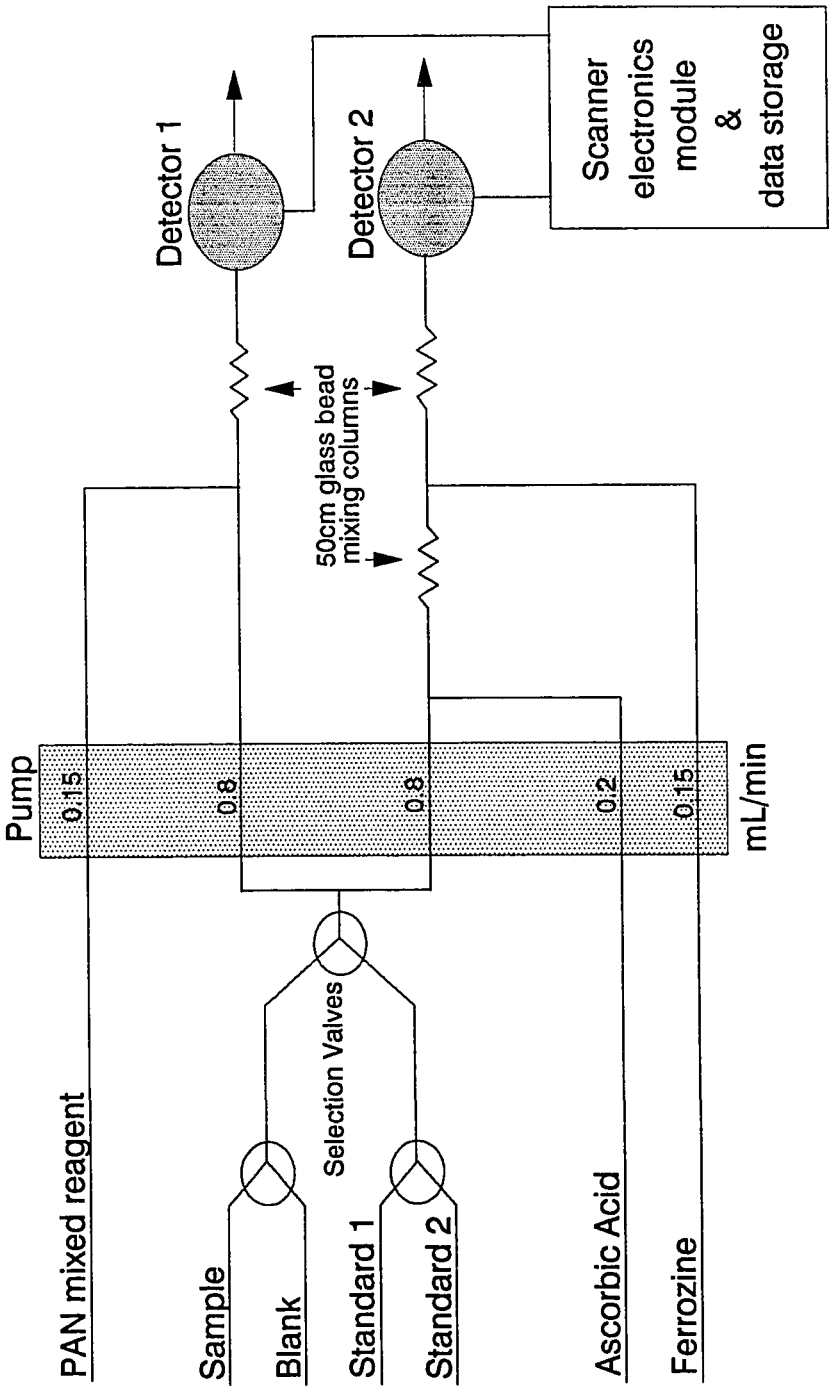

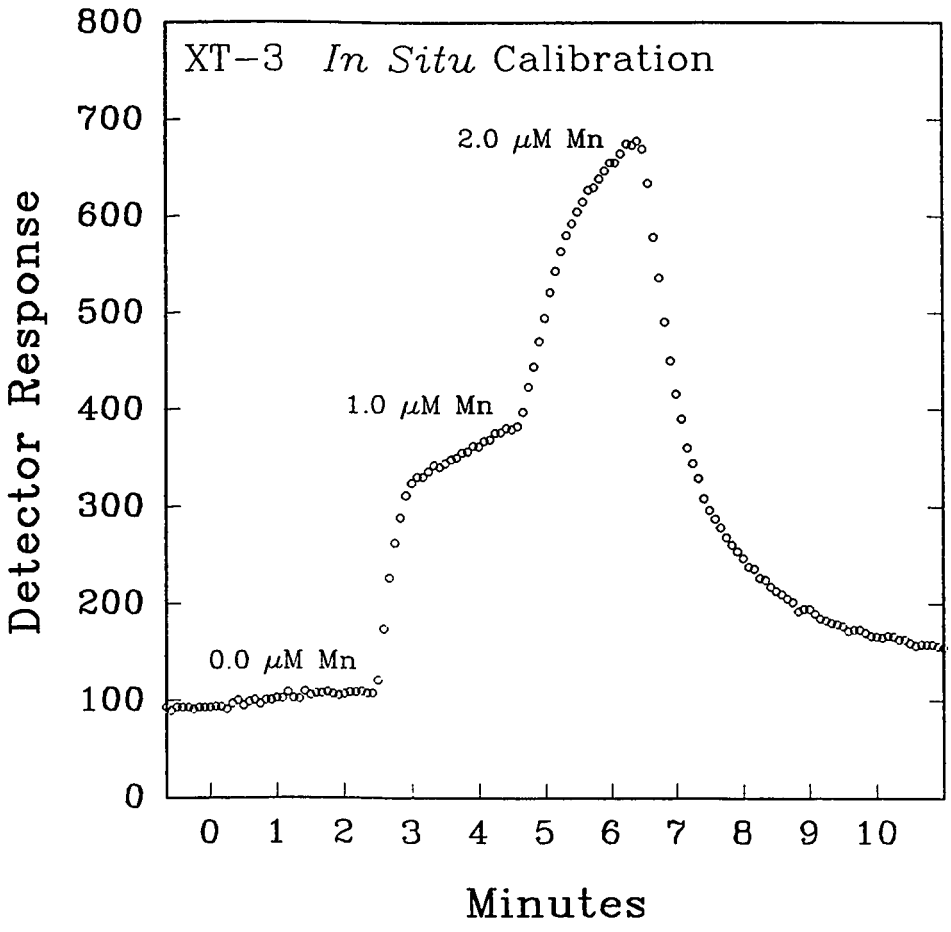
XT−3 *In Situ* Calibration
2.0 μM Mn
1.0 μM Mn
0.0 μM Mn
Detector Response
800
700
600
500
400
300
200
100
0
0 1 2 3 4 5 6 7 8 9 10
Minutes

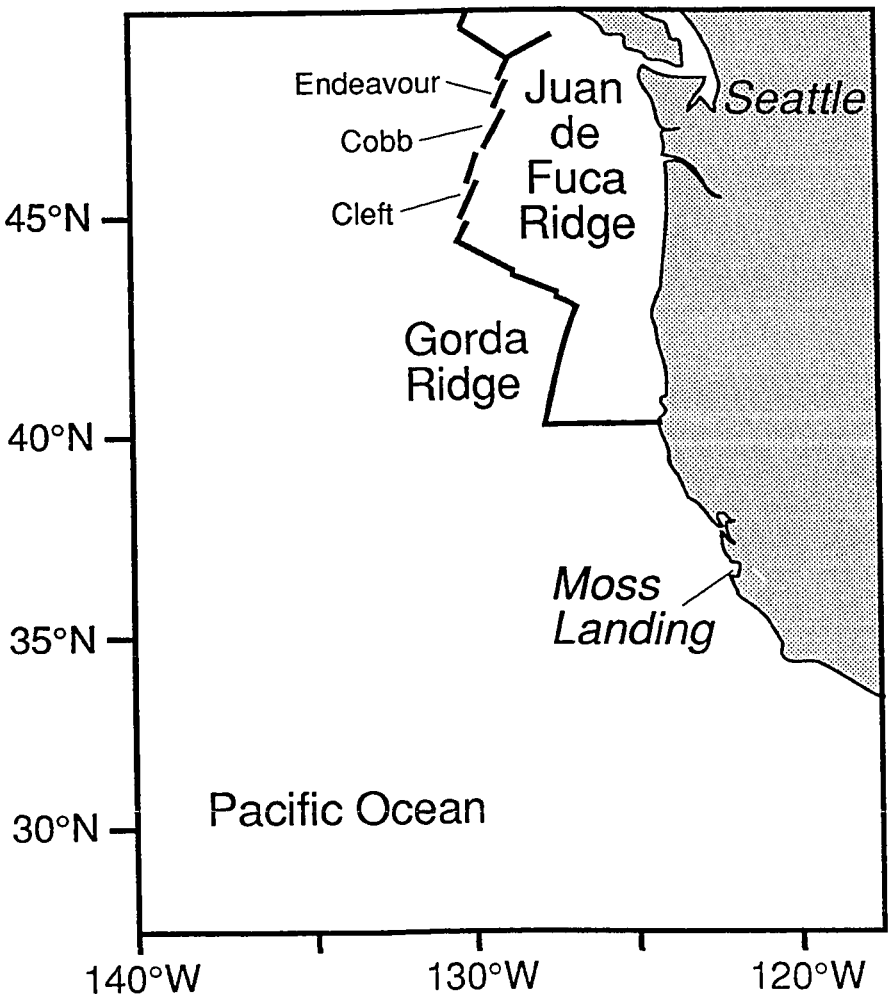
Endeavour
Cobb
Cleft
Juan
de
Fuca
Ridge
Seattle
Gorda
Ridge
Moss
Landing
Pacific Ocean
45°N
40°N
35°N
30°N
140°W
130°W
120°W

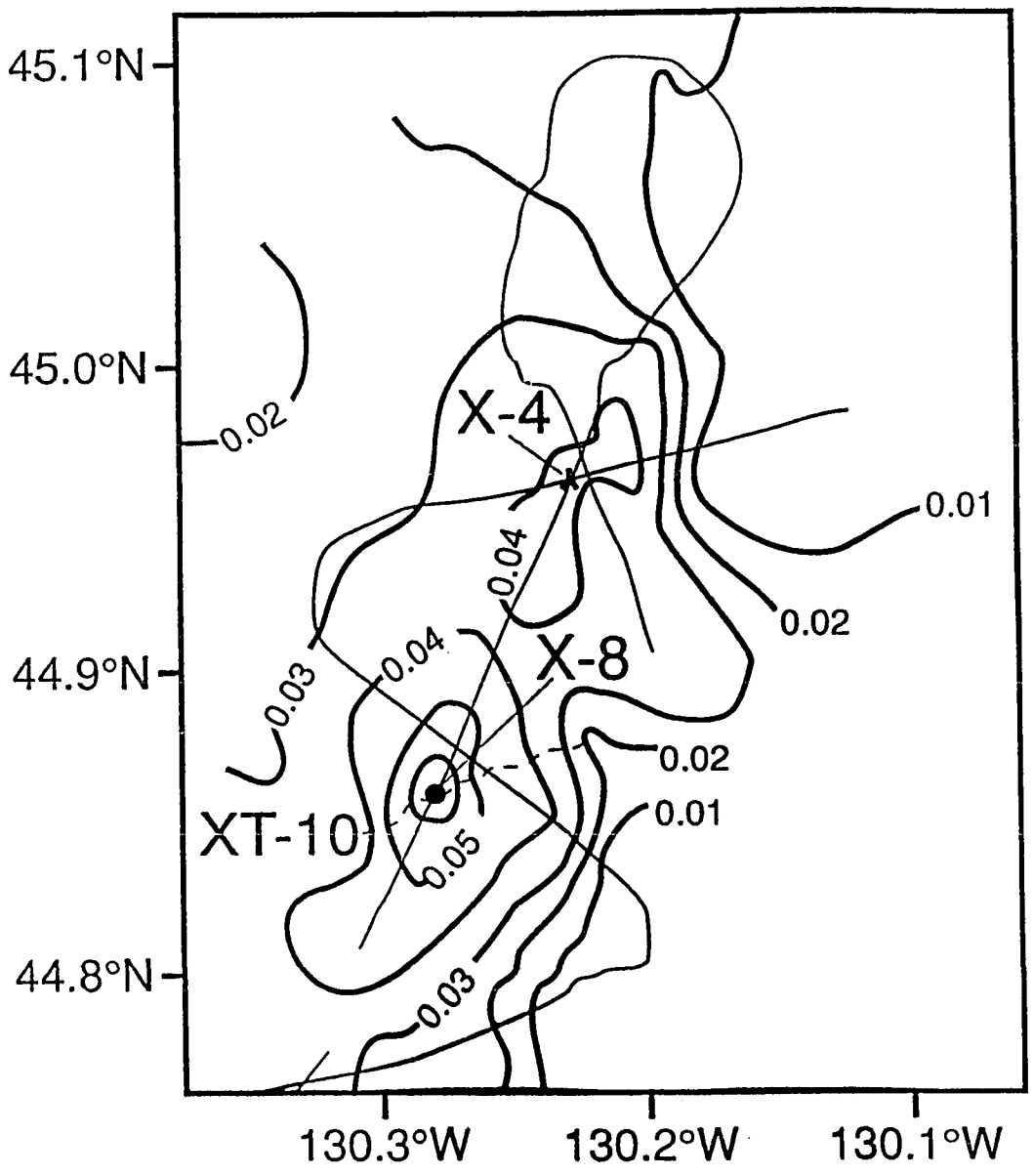
45.1°N
45.0°N
44.9°N
44.8°N
130.3°W
130.2°W
130.1°W
X-4
X-8
XT-10
0.02
0.01
0.04
0.02
0.04
0.03
0.02
0.01
0.05
0.03

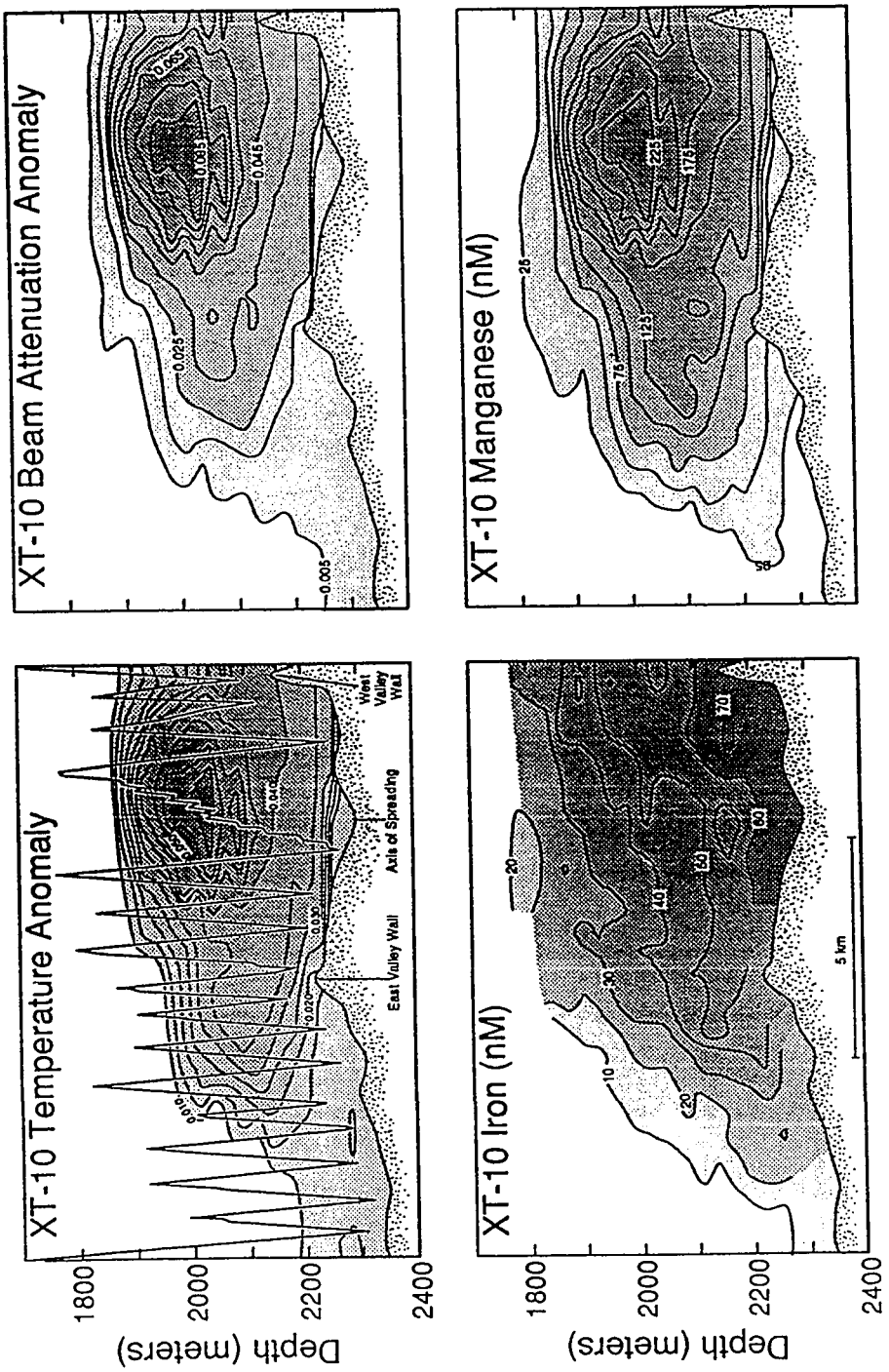
XT-10 Temperature Anomaly
XT-10 Beam Attenuation Anomaly
XT-10 Iron (nM)
XT-10 Manganese (nM)
Depth (meters)
1800
2000
2200
2400
West Valley Wall
East Valley Wall
Axis of Spreading
5 km

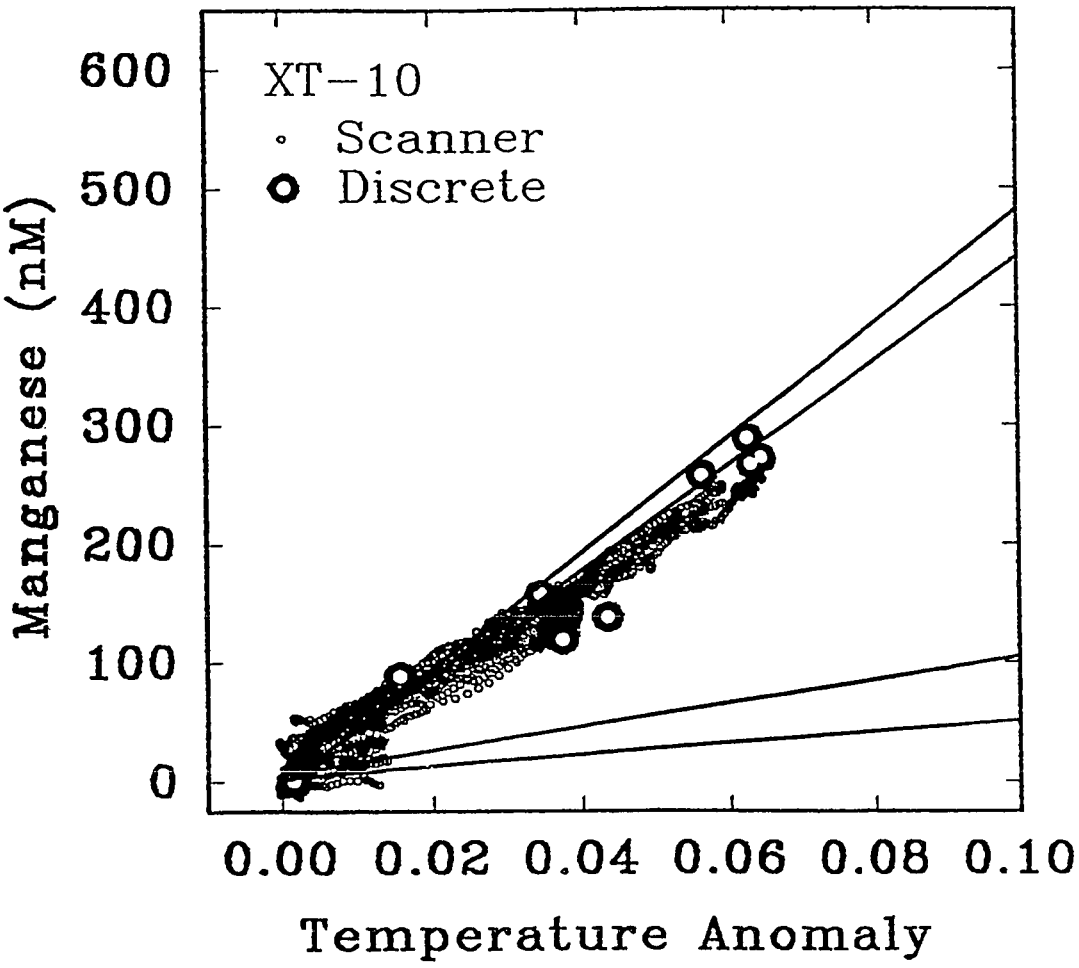
XT−10
Scanner
Discrete
600
500
400
300
200
100
0
Manganese (nM)
0.00
0.02
0.04
0.06
0.08
0.10
Temperature Anomaly

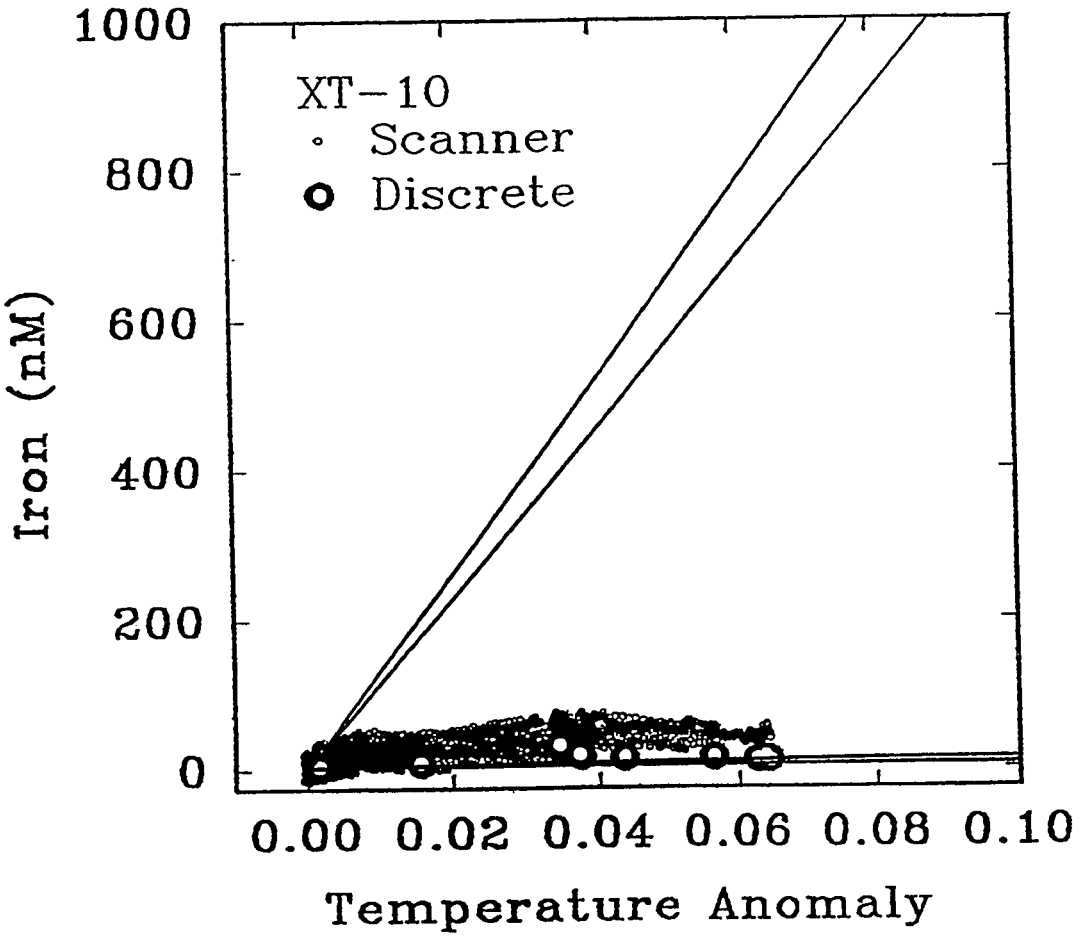
1000
800
600
400
200
0
Iron (nM)
XT-10
Scanner
Discrete
0.00 0.02 0.04 0.06 0.08 0.10
Temperature Anomaly

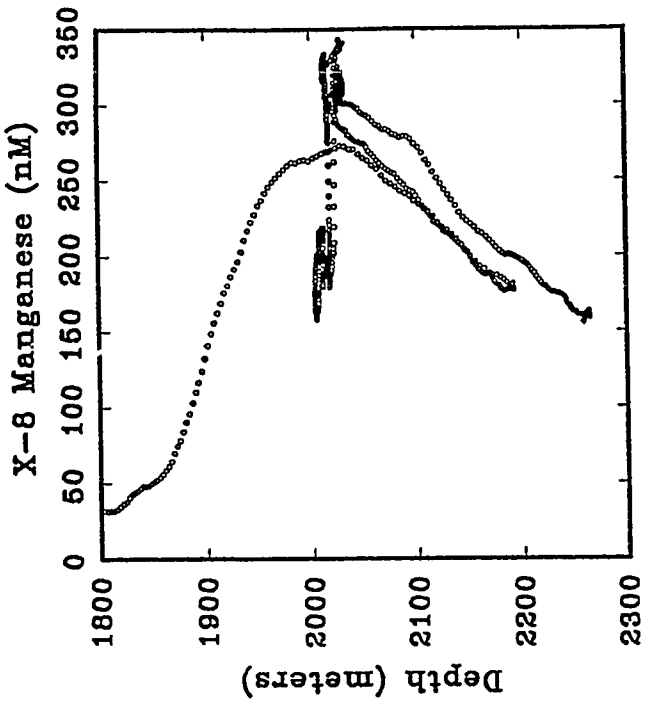
X-8 Manganese (nM)
0
50
100
150
200
250
300
350
1800
1900
2000
2100
2200
2300
Depth (meters)

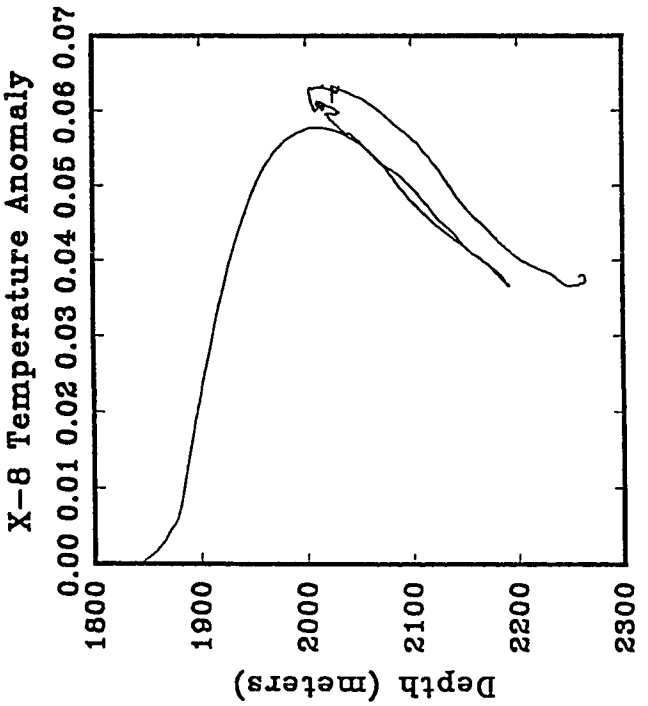
X-8 Temperature Anomaly
0.00
0.01
0.02
0.03
0.04
0.05
0.06
0.07
1800
1900
2000
2100
2200
2300
Depth (meters)

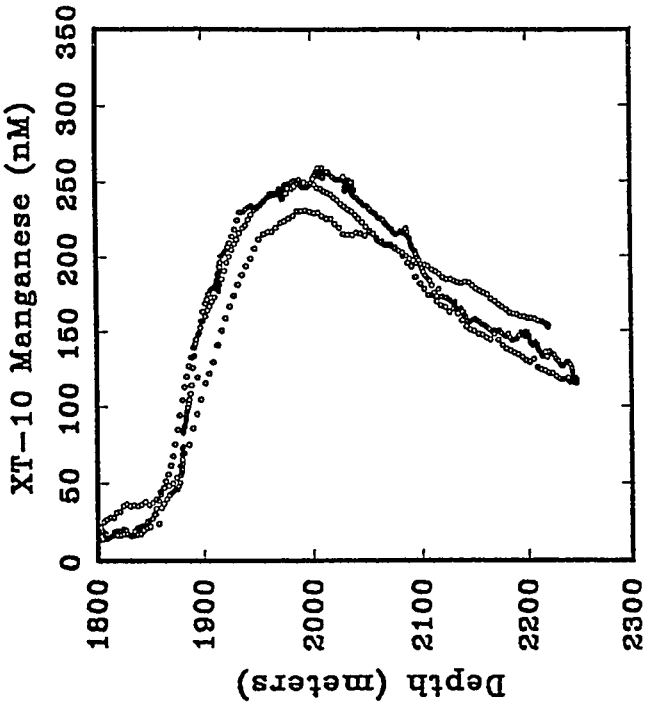
XT−10 Manganese (nM)
0
50
100
150
200
250
300
350
1800
1900
2000
2100
2200
2300
Depth (meters)

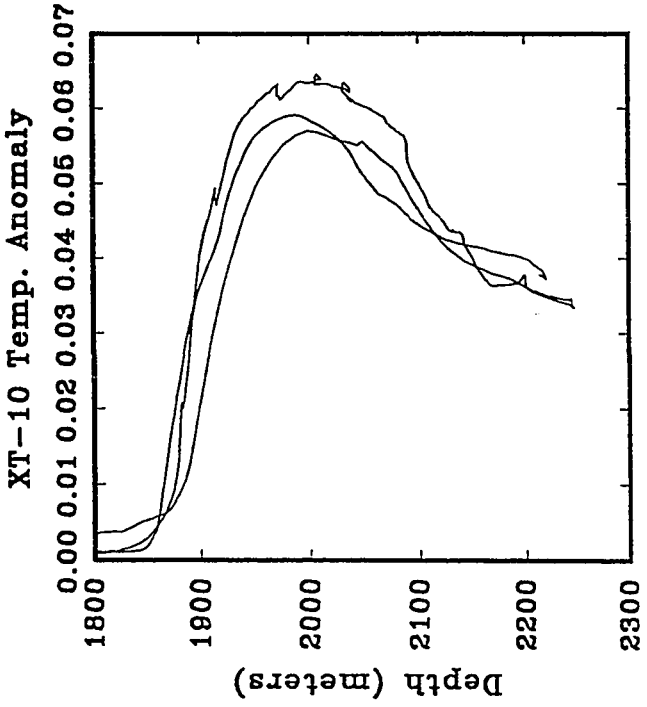
XT−10 Temp. Anomaly
0.00
0.01
0.02
0.03
0.04
0.05
0.06
0.07
1800
1900
2000
2100
2200
2300
Depth (meters)

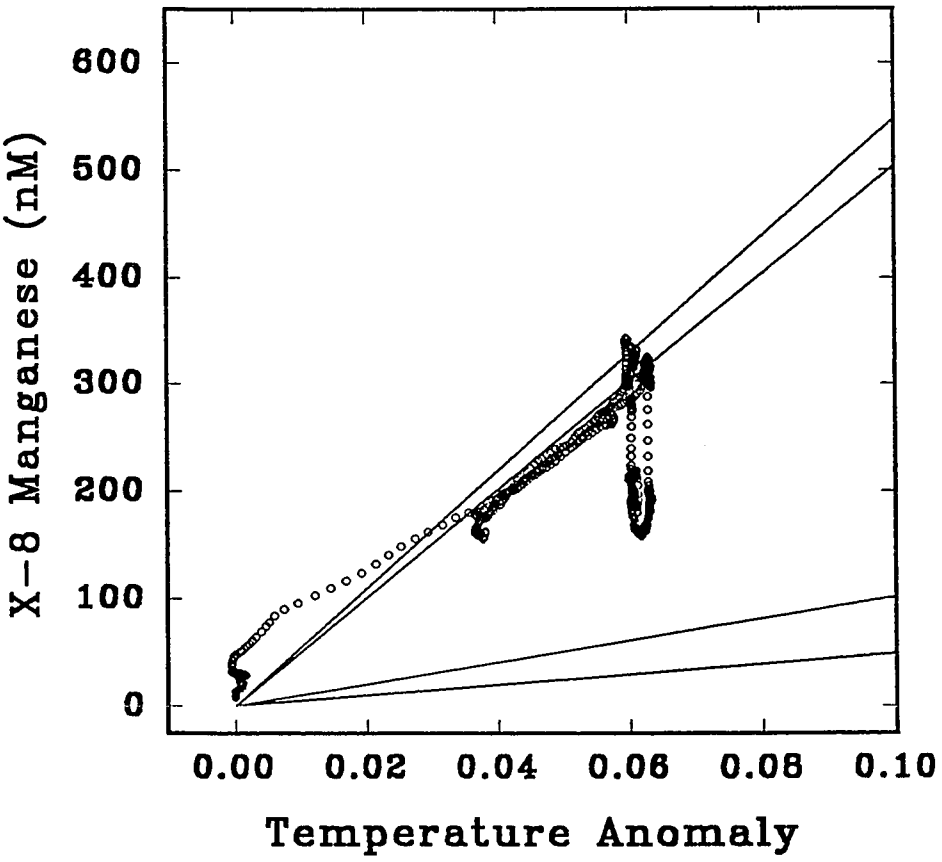
X-8 Manganese (nM)
600
500
400
300
200
100
0
0.00
0.02
0.04
0.06
0.08
0.10
Temperature Anomaly

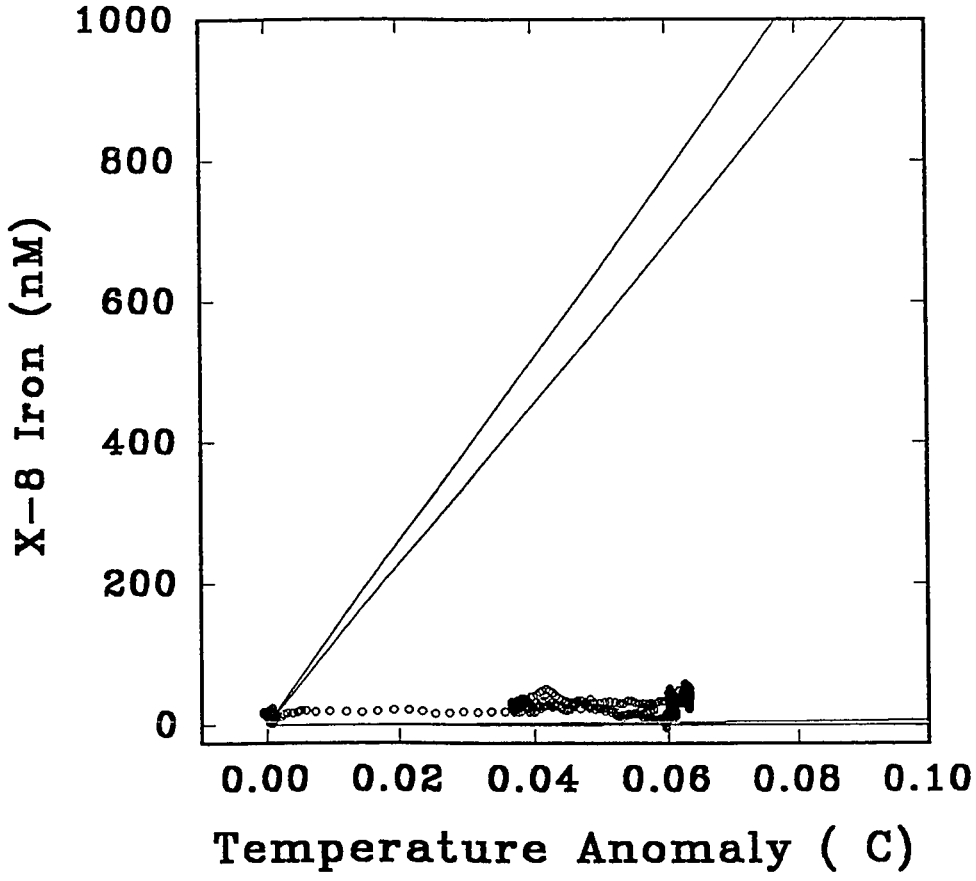
1000
800
600
400
200
0
X-8 Iron (nM)
0.00
0.02
0.04
0.06
0.08
0.10
Temperature Anomaly (C)

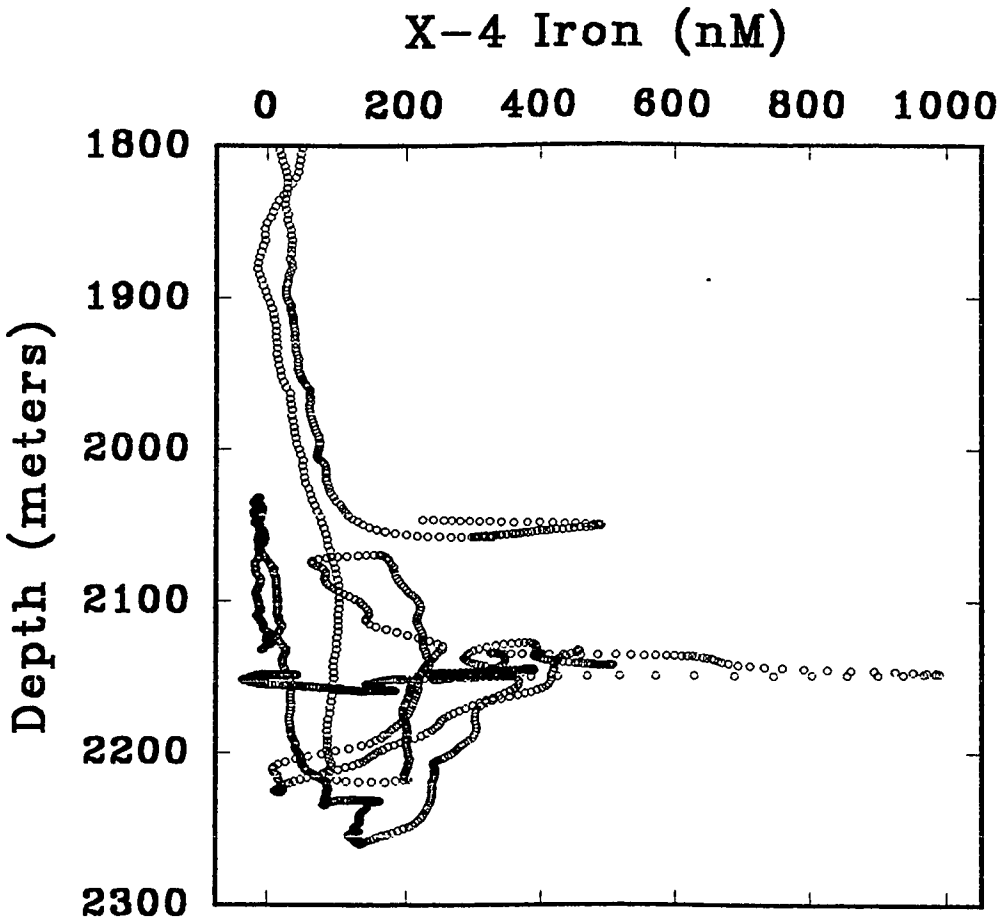
X-4 Iron (nM)
0
200
400
600
800
1000
1800
1900
2000
2100
2200
2300
Depth (meters)

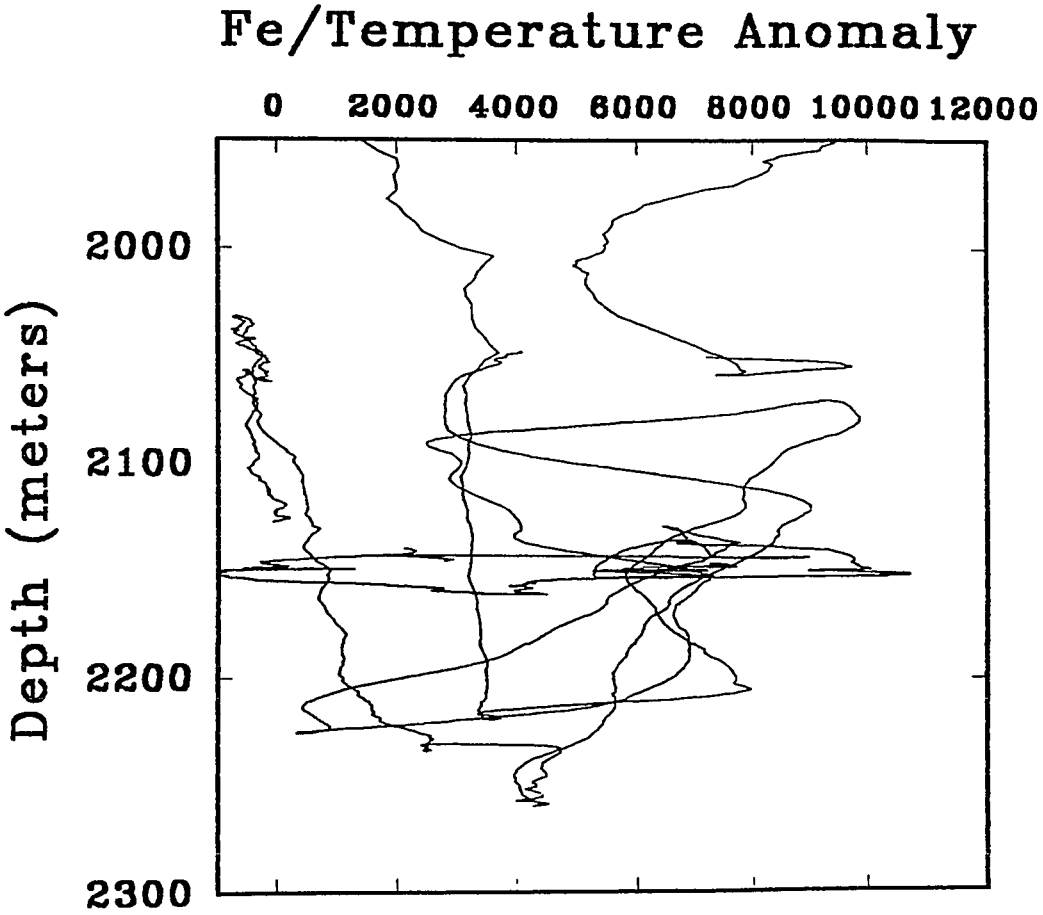
Fe/Temperature Anomaly
0
2000
4000
6000
8000
10000
12000
Depth (meters)
2000
2100
2200
2300

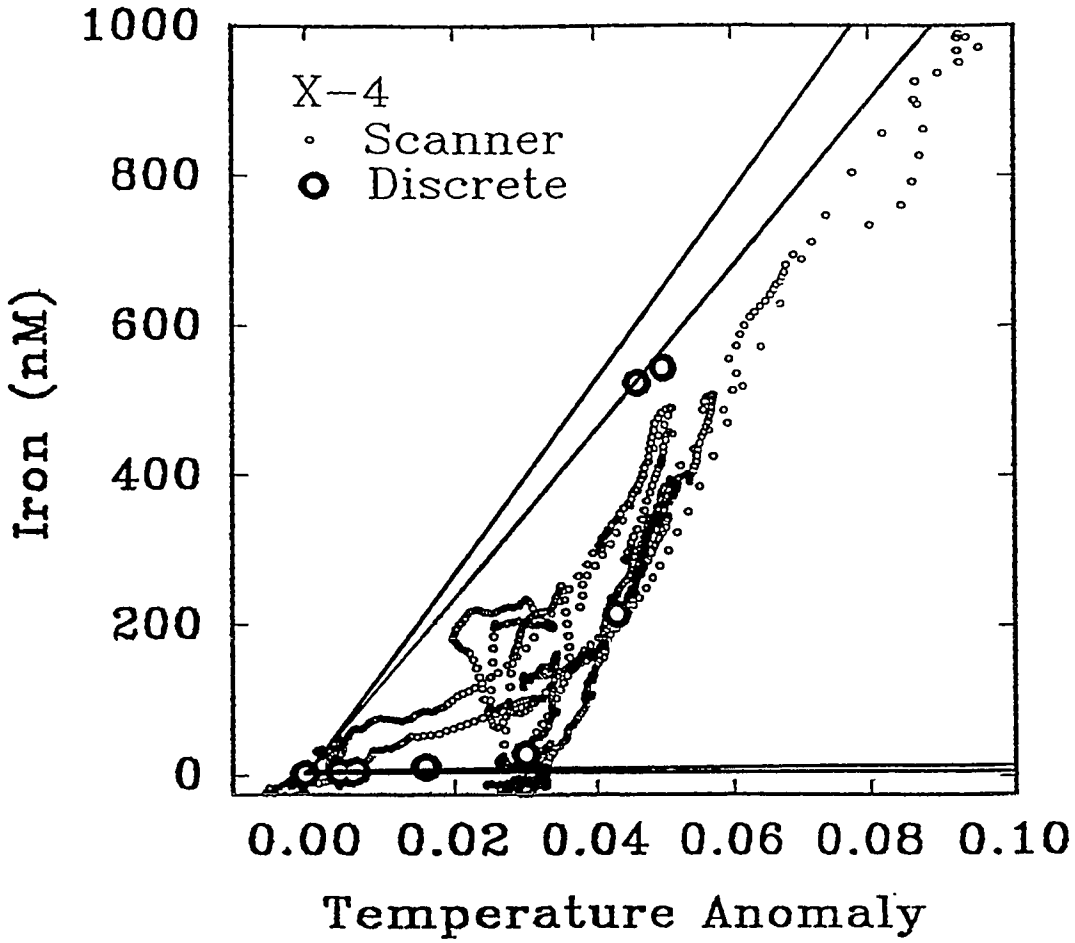
X-4
Scanner
Discrete
1000
800
600
400
200
0
Iron (nM)
0.00
0.02
0.04
0.06
0.08
0.10
Temperature Anomaly

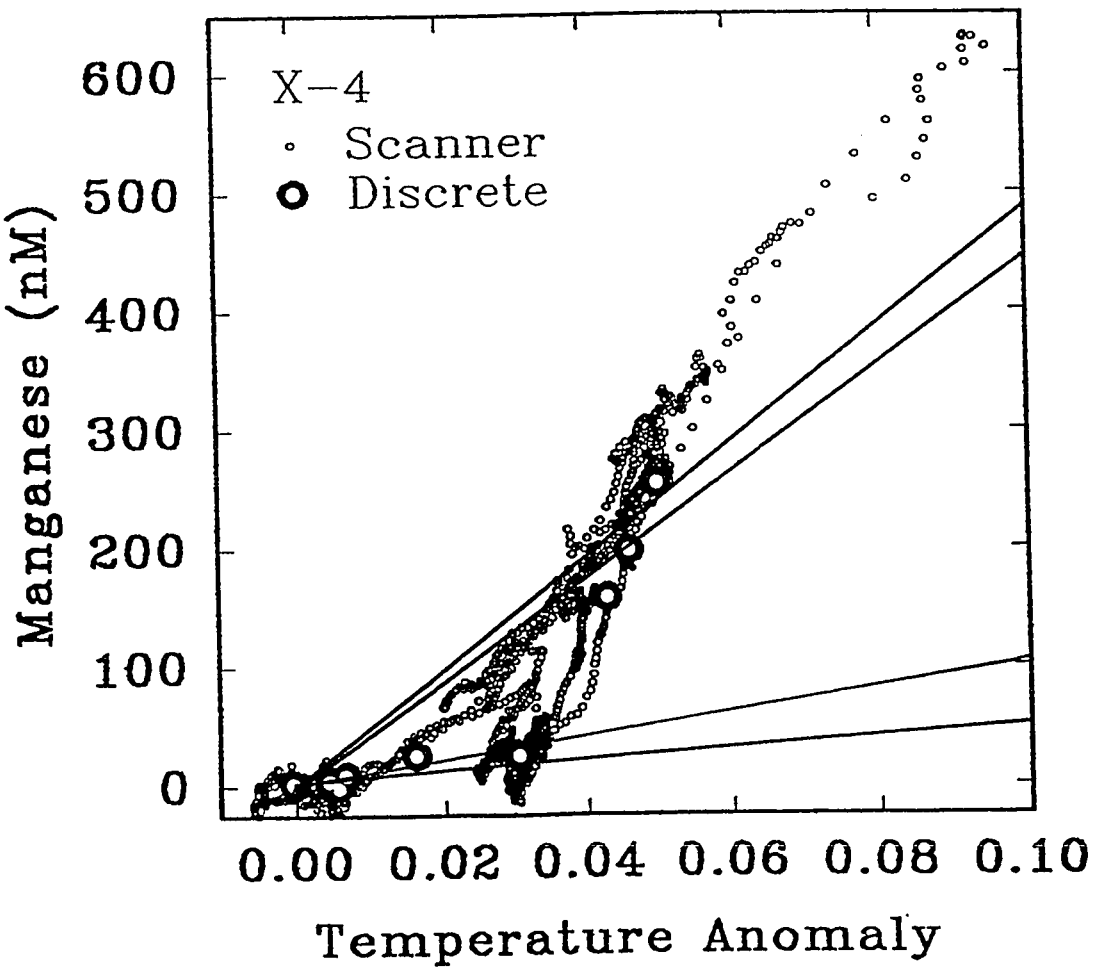
X−4
Scanner
Discrete
600
500
400
300
200
100
0
Manganese (nM)
0.00
0.02
0.04
0.06
0.08
0.10
Temperature Anomaly

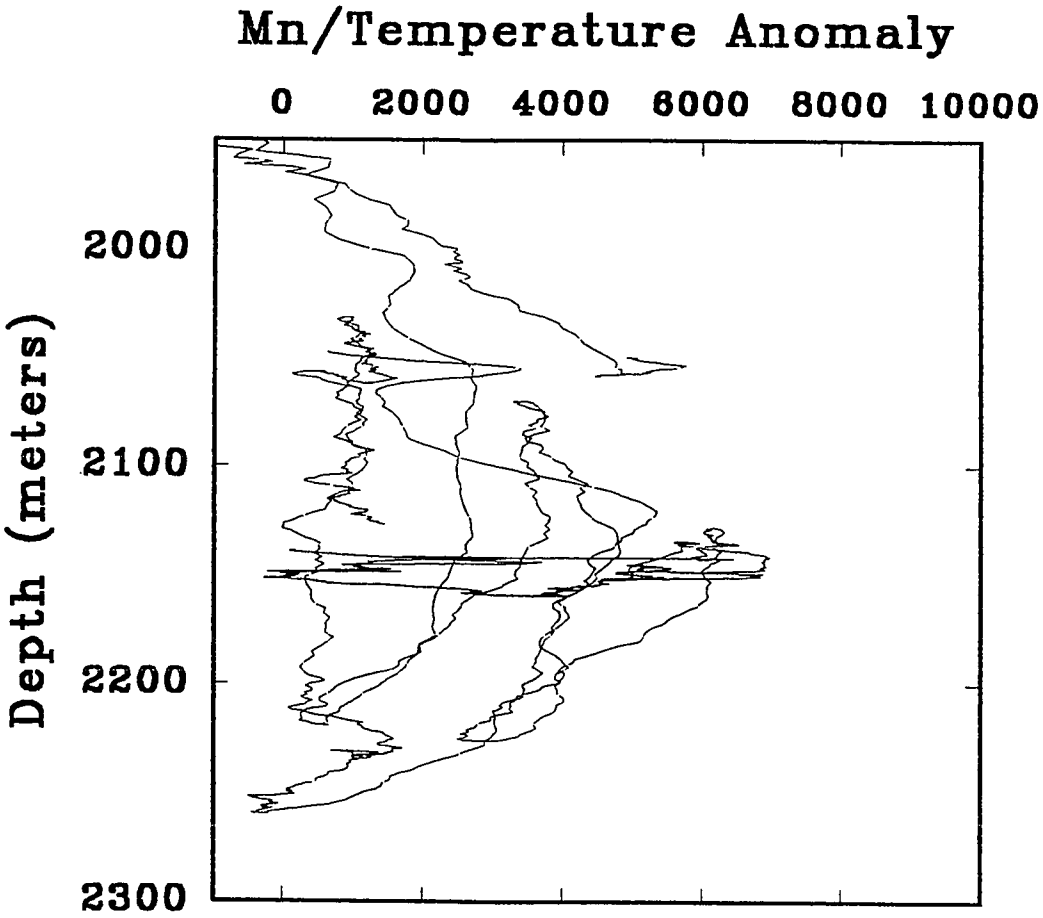
Mn/Temperature Anomaly
0
2000
4000
6000
8000
10000
Depth (meters)
2000
2100
2200
2300

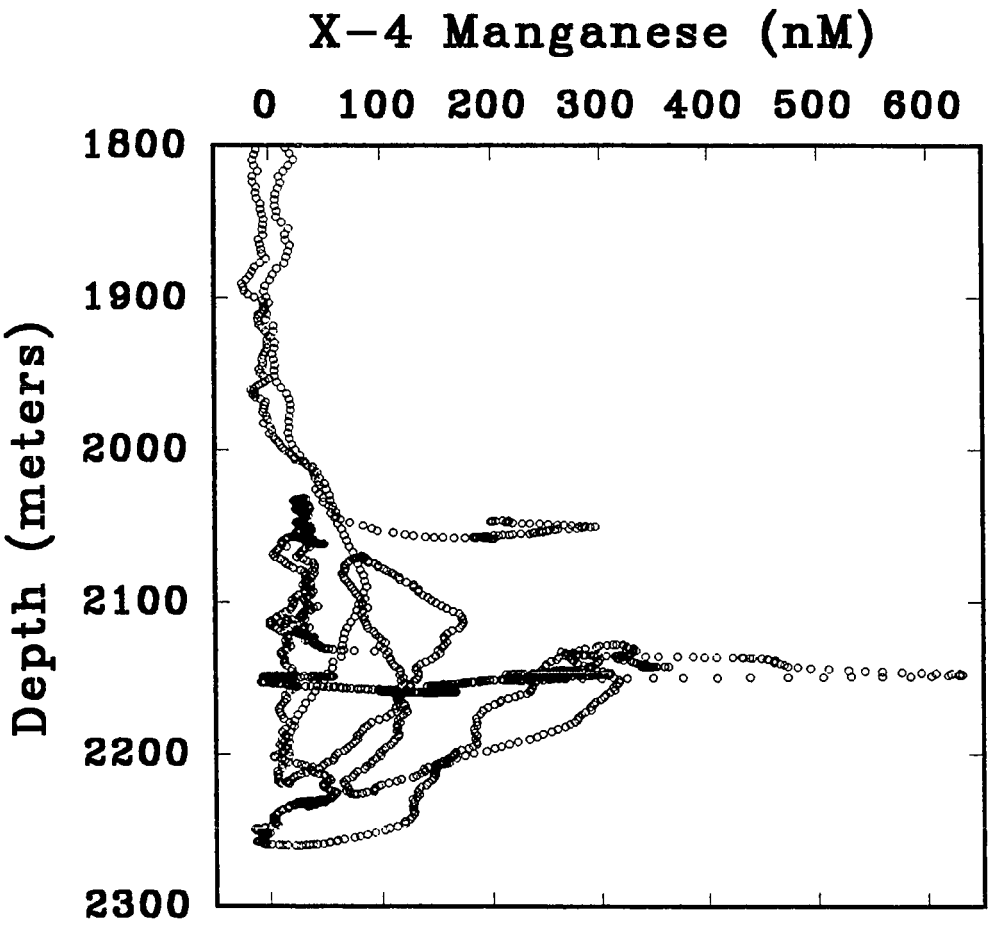
X-4 Manganese (nM)
0
100
200
300
400
500
600
1800
1900
2000
2100
2200
2300
Depth (meters)

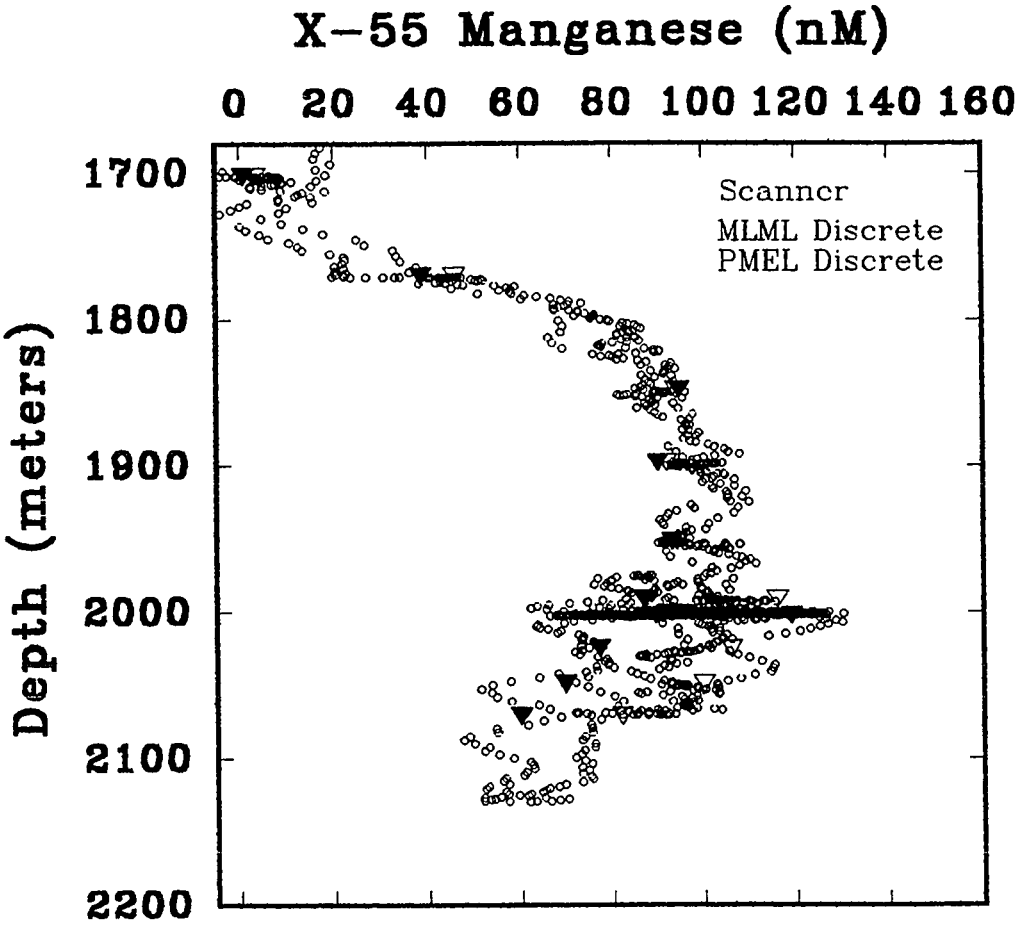
X-55 Manganese (nM)
0 20 40 60 80 100 120 140 160
Depth (meters)
1700
1800
1900
2000
2100
2200
Scanner
MLML Discrete
PMEL Discrete

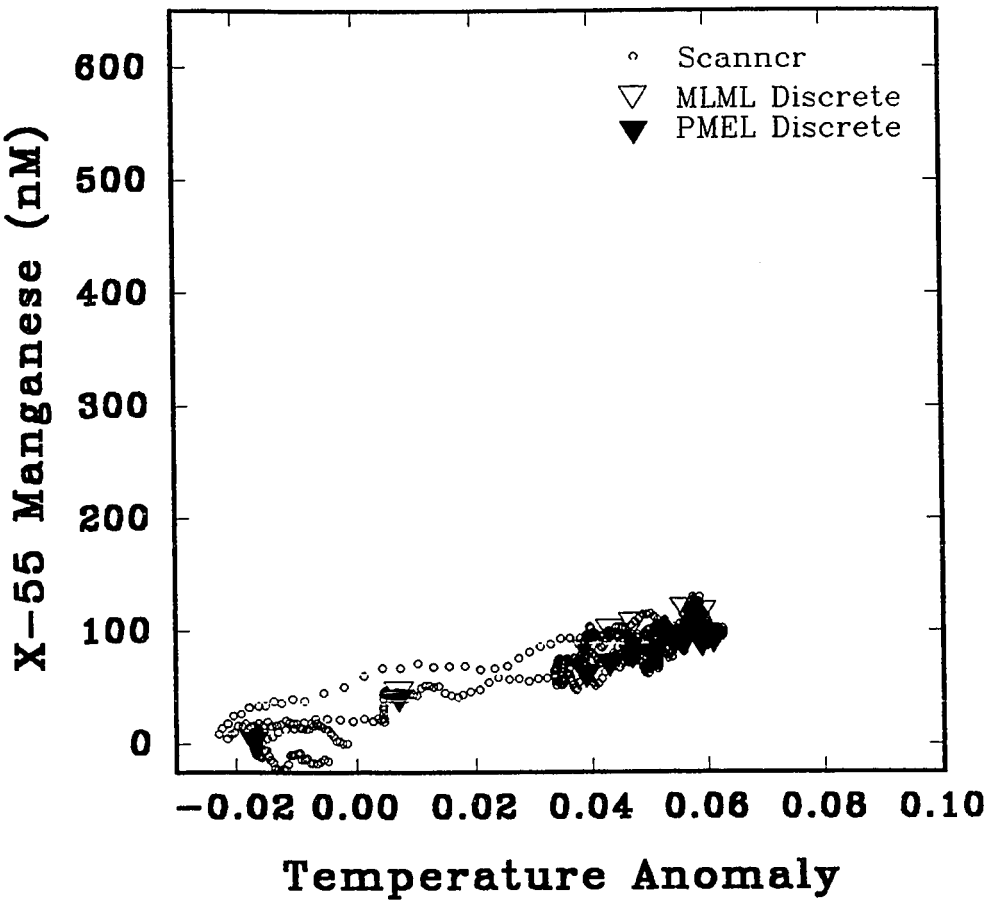
Scanner
MLML Discrete
PMEL Discrete
X-55 Manganese (nM)
600
500
400
300
200
100
0
−0.02 0.00 0.02 0.04 0.06 0.08 0.10
Temperature Anomaly

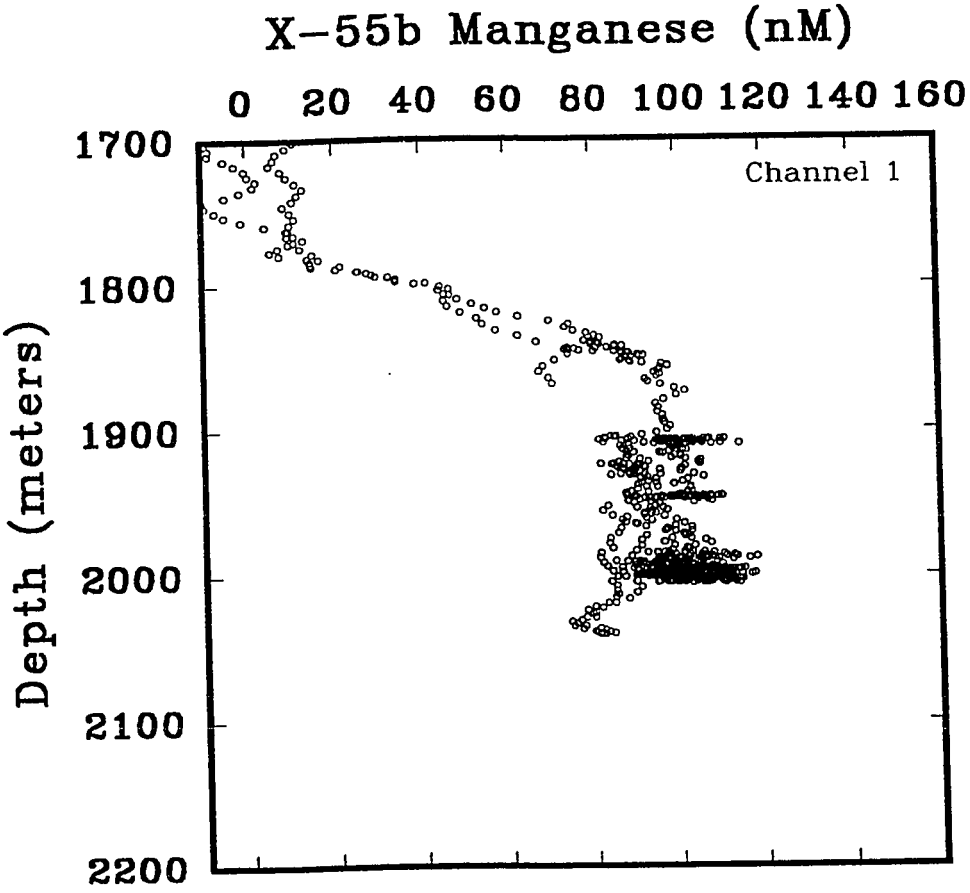
X-55b Manganese (nM)
0 20 40 60 80 100 120 140 160
1700
1800
1900
2000
2100
2200
Depth (meters)
Channel 1

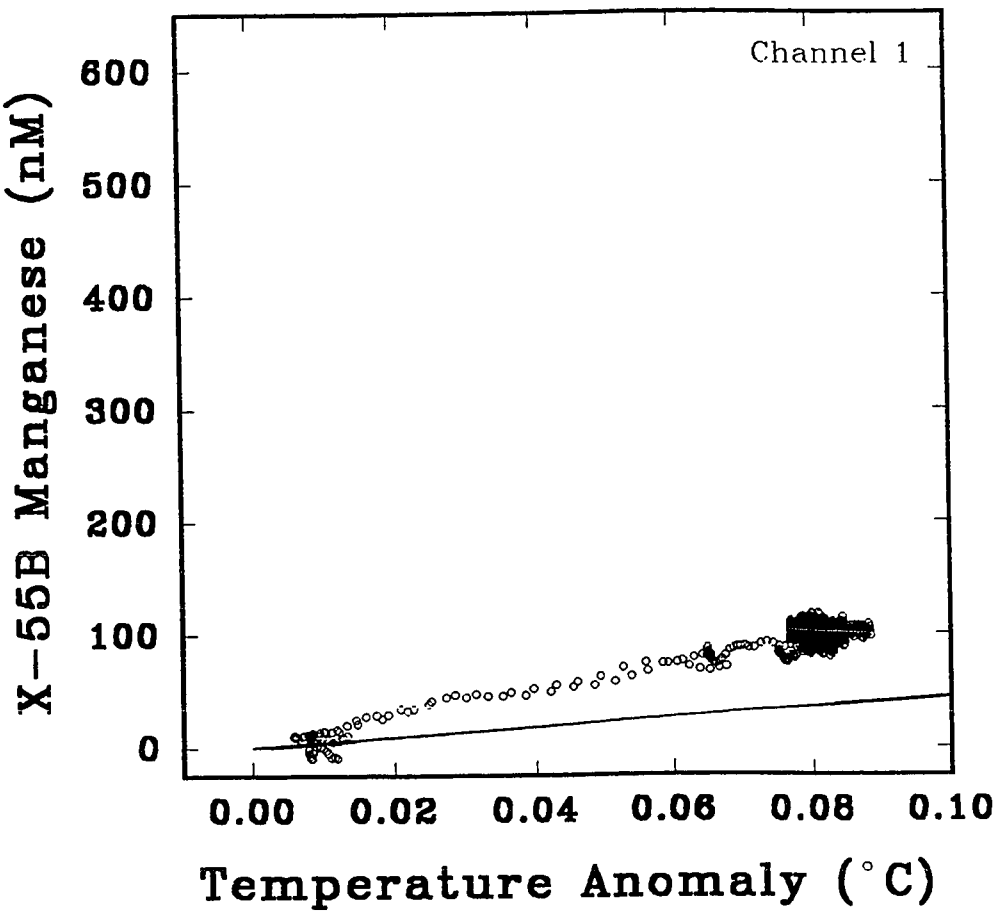
Channel 1
X-55B Manganese (nM)
600
500
400
300
200
100
0
0.00
0.02
0.04
0.06
0.08
0.10
Temperature Anomaly (°C)

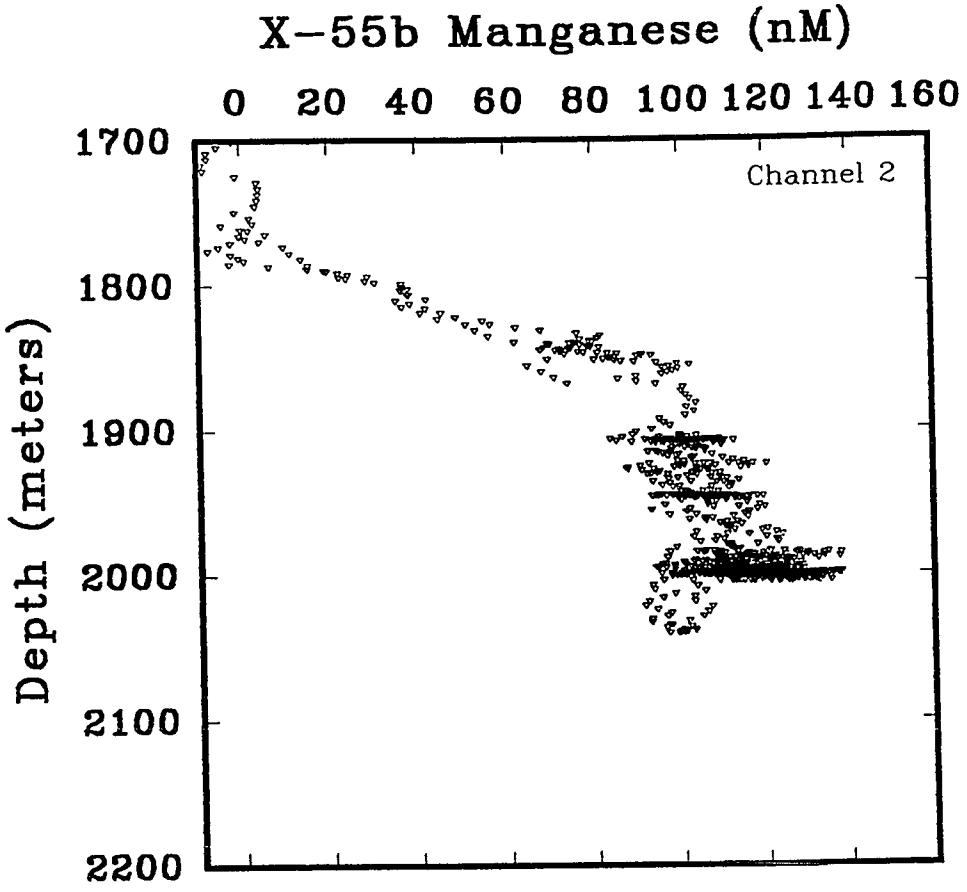
X-55b Manganese (nM)
0 20 40 60 80 100 120 140 160
1700
1800
1900
2000
2100
2200
Depth (meters)
Channel 2

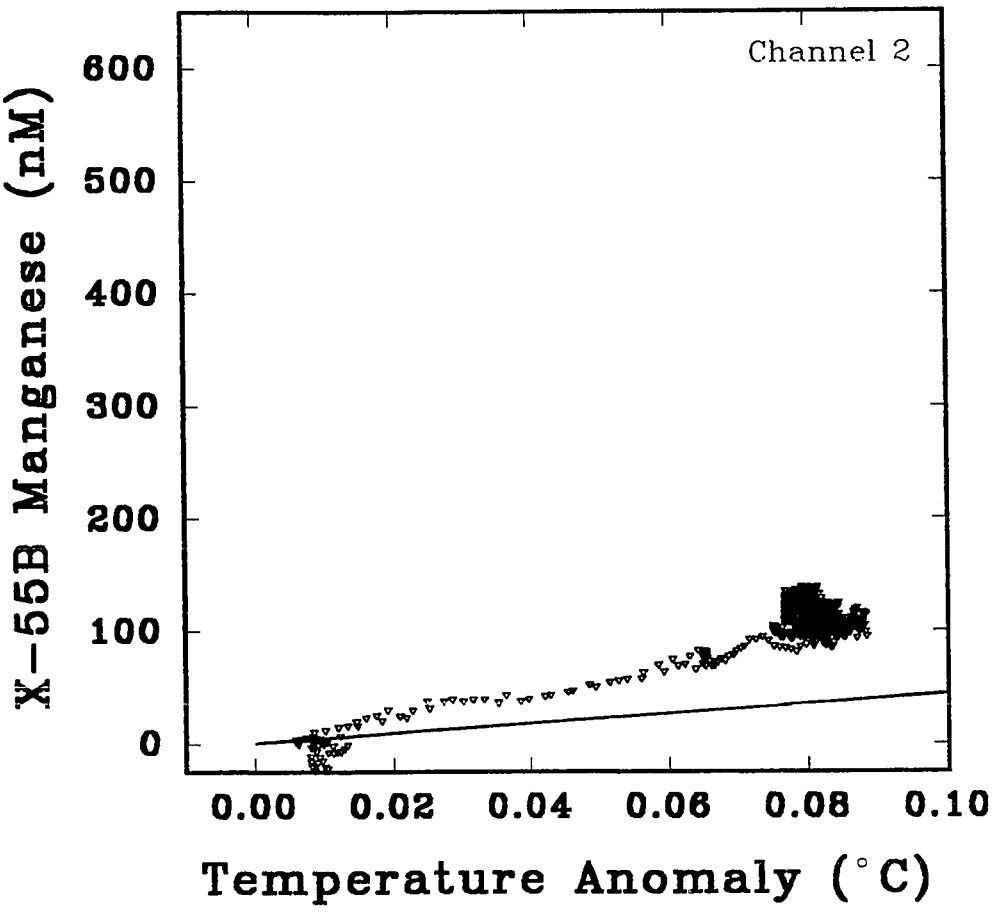
Channel 2
X-55B Manganese (nM)
600
500
400
300
200
100
0
0.00
0.02
0.04
0.06
0.08
0.10
Temperature Anomaly (°C)

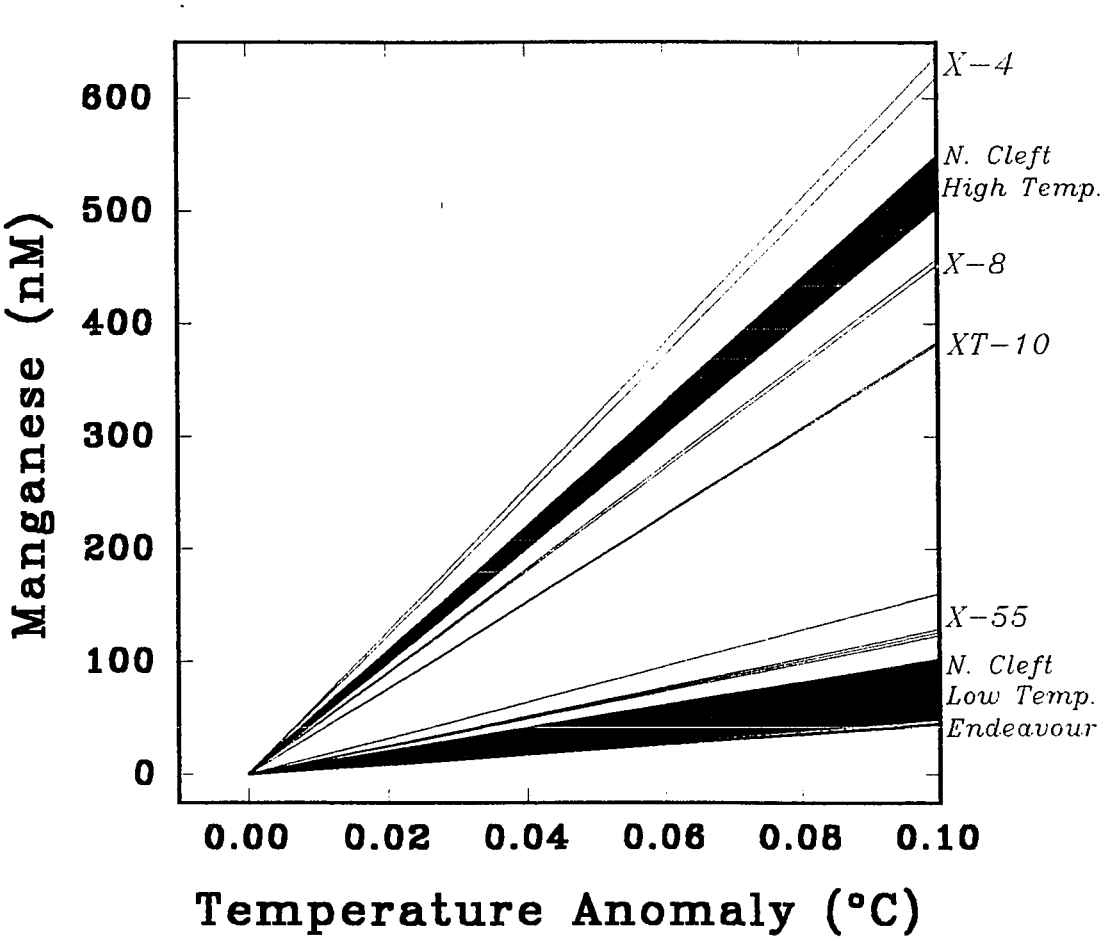
Manganese (nM)
600
500
400
300
200
100
0
0.00
0.02
0.04
0.06
0.08
0.10
Temperature Anomaly (°C)
X−4
N. Cleft
High Temp.
X−8
XT−10
X−55
N. Cleft
Low Temp.
Endeavour

CHAPTER 4

Conclusions

Spatial and temporal variability in thermochemical fluxes, and the extreme thermal conditions at individual vents can make it difficult to determine mass fluxes by direct observation. However, hydrothermal plumes integrate this variability and observations of the composite plume can be used to estimate thermal and chemical fluxes from vent fields (Baker and Massoth, 1986; Rosenberg et al., 1988). Therefore, mapping of hydrothermal plumes is one of the most effective strategies for assessing the mass and thermal budgets of venting sites.

High resolution chemical mapping of dissolved manganese and total dissolved iron performed *in situ* using the Scanner has proven to be an effective tool in elucidating chemical processes in hydrothermal plumes along the Juan de Fuca Ridge. These data have provided details of the range and variability of the concentrations of these metals both in the plumes and between venting sites (Fig. 1). Details of the relationship of these metal concentrations to excess temperature have provided evidence of multiple source mixing.

In Figure 1 the results from all stations are summarized. Regressions of the manganese data vs temperature anomaly from each cast are displayed as a range (± 1 S.D.). The hydrothermal source ratios (corrected for changes in heat capacity) from the North Cleft (high T Mn:Q = 5.01 to 5.45 nmol cal^{-1}, low T = 0.49 to 1.01 nmol cal^{-1}; Massoth, pers. comm.) and Endeavour Segments (high T = 0.45 nmol cal^{-1}; D. Butterfield and R. McDuff, as cited in Kadko et al., 1990) are also plotted

for comparison to the plume ratios. There is a striking differences between the Mn:Q ratios observed both in plumes as well as in high temperature source fluids at North Cleft and at Endeavour. The highest Mn:Q ratios observed in this study were measured during the vertical cast X-4 at the northern most end of the North Cleft Segment. These ratios (6.15 to 6.33 nmol cal^{-1}) were higher than those observed in hydrothermal source fluids at this venting site. Ratios observed during both a tow-yo (XT-10, 3.79 to 3.82 nmol cal^{-1}) and a vertical cast (X-8, 4.49 to 4.54 nmol cal^{-1}) 12 km south of X-4 were slightly lower than the high temperature source ratios. Mn:Q ratios observed during two casts at the Endeavour Segment (X-55 and X-55B, 1.22 to 1.59 nmol cal^{-1}) were slightly higher than the ratios measured in high temperature source fluids at this vent field. They were, however, significantly lower than the any of the high temperature ratios measured at North Cleft, and comparable to the North Cleft low temperature source ratio. Differences between the Mn:Q ratios observed in plumes and in hydrothermal source fluids may indicate that the Mn:Q signatures of the sources contributing to the dispersing plume are temporally variable, or that other undiscovered venting sites are contributing to these plumes. Such temporal variability could be examined more closely by conducting more detailed Scanner deployments, to obtain higher spatial and temporal resolution. Alternatively, this variability could be monitored using arrays of moored chemical sensors of the type currently being developed by Johnson and Jannasch.

References

Baker E. T. and G. J. Massoth (1986) Hydrothermal plume measurements: a regional perspective. Science, **234**, 980-982.

Kadko D. C., N. D. Rosenberg, J. E. Lupton, R. W. Collier and M. D. Lilley (1990) Chemical reaction rates and entrainment within the Endeavour Ridge hydrothermal plume. Earth and Planetary Science Letters, **99**, 315-335.

Rosenberg N. D., J. E. Lupton, D. Kadko, R. Collier, M. D. Lilley and H. Pak (1988) Estimation of heat and chemical fluxes from a seafloor hydrothermal vent field using radon measurements. Nature, **334**, 604-607.

Figure Caption

Figure 1) Regressions of manganese vs temperature anomaly for all stations, plotted together with source ratios from North Cleft (both high- and low-temperature) and Endeavour Segments (see text). The ranges in the Mn:temperature relationships shown here represent ± 1 S.D.

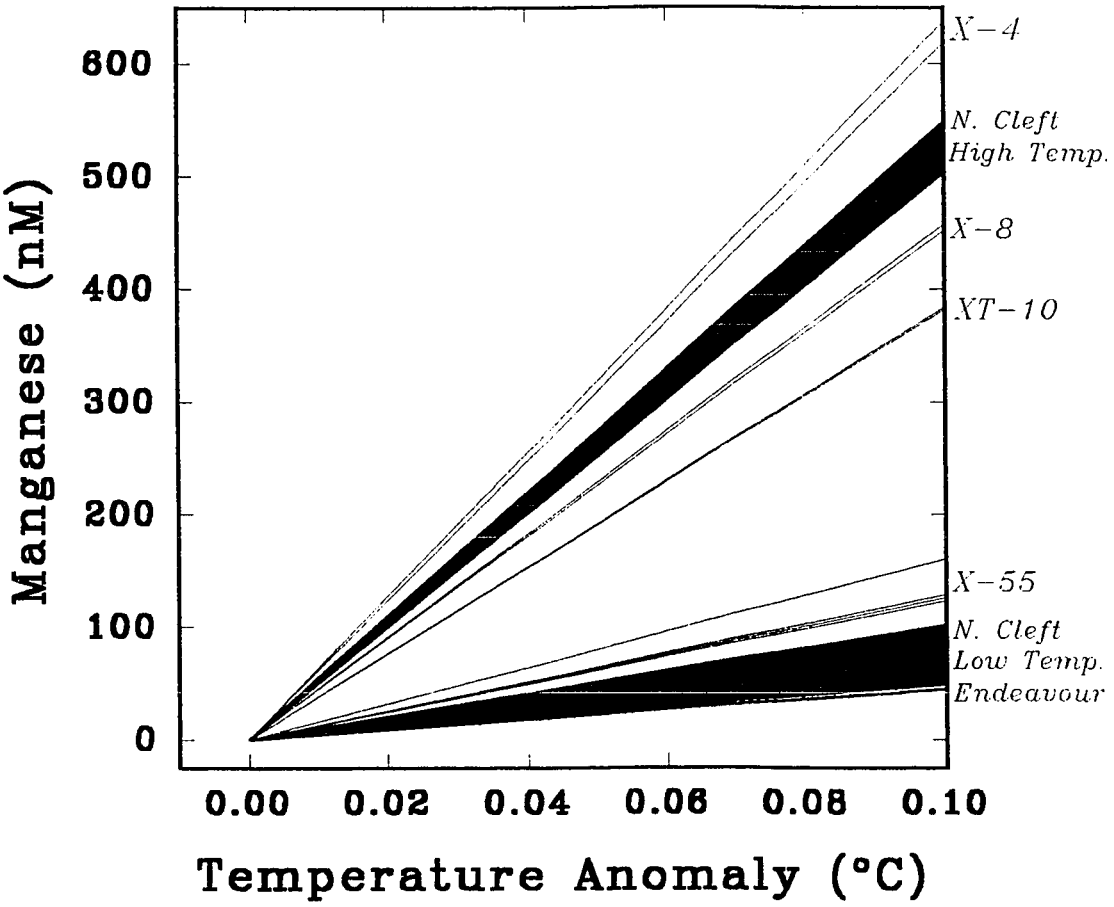
Manganese (nM)
600
500
400
300
200
100
0
0.00
0.02
0.04
0.06
0.08
0.10
Temperature Anomaly (°C)
X-4
N. Cleft
High Temp.
X-8
XT-10
X-55
N. Cleft
Low Temp.
Endeavour

APPENDIX 1

In Situ Chemical Mapping of Dissolved Iron and Manganese In Hydrothermal Plumes

Kenneth H. Coale[1], Carol S. Chin[1], Gary J. Massoth[2], Kenneth S. Johnson[1,3] and Edward T. Baker[2]

1) Moss Landing Marine Laboratories, P. O. Box 450, Moss Landing, CA 95039, (U. S. A.)

2) Pacific Marine Environmental Laboratory, NOAA, 7600 Sand Point Way NE, Seattle, WA 98115 (U. S. A.)

3) Monterey Bay Aquarium Research Institute, 160 Central Avenue, Pacific Grove, CA 93950, (U. S. A.)

Hydrothermal vents along mid-ocean ridges are a major source of elements such as Li, Si, Mn and Fe to the world's oceans[1]. This venting produces both episodic and steady state hydrothermal plumes of unique thermochemical signatures within the mid-water column. The particulate phases within these plumes (predominantly iron oxides and hydroxides) also scavenge P, V, As, Pb, Po and several rare earth elements from seawater[4,5,6,7]. Thus, on a global scale, hydrothermal plumes are both a major source for some elements and a major sink for others. Ultimately, the particulate metals precipitated from plumes form extensive regions of metalliferous sediments over the crests and flanks of mid-ocean ridges[2,3]. Although the metalliferous sediment coverage is vast and well documented, only a tiny fraction of the vents responsible for these sediments have been located (Fig 1a). To date, both the number and location of hydrothermal vents and the detailed distribution of chemical constituents within the resultant plumes are poorly understood due to under-sampling of the mid-ocean ridges and the overlying waters. In this work, the first high resolution transects of the dissolved chemical constituents iron and manganese, together with temperature anomalies and light attenuation, were mapped in hydrothermal plumes in near real time using a novel submersible chemical analyzer (Scanner)[8,9] and a Conductivity/Temperature/Depth/ Transmissometer instrument package (CTDT)[10]. This effort has demonstrated not only that this *in situ* analytical capability is a useful prospecting tool, but also that the thermochemical signature of the plume is diagnostic of the source hydrothermal processes. The

metal:temperature anomaly ratio revealed systematic and continuous variations that demonstrate rapid removal of iron from the dissolved phase, while manganese behaves nearly conservatively in the near field. Variations in the Mn:temperature ratio require three end-member mixing between seawater, "black smoker" effluent water, and an unreported but recently discovered low Mn:heat source water.

Measurements were made during the VENTS '89 cruise, Leg 1 (July 27 to August 25, 1989) aboard the R/V Discoverer. The Scanner was secured to a CTDT/rosette package and towed across the Cleft segment at the southern end of the Juan de Fuca Ridge (Fig. 1b, 1c). *In situ* measurements of dissolved manganese and total dissolved iron (Fe(II) plus Fe(III)) were performed continuously and the data were recorded every 5 seconds. The instrument package was raised and lowered during "tow-yos"[11] while the ship steamed slowly at a speed of 1-2 knots. Dissolved manganese was analyzed colorimetrically using 1-(2-pyridyalzo)-2-naphthol (PAN)[12] and total dissolved iron was determined with ferrozine[13] after reducing iron(III) to iron(II) with ascorbic acid. A filter on the sample inlet allowed only dissolved metals ($< 10\ \mu$m) to be analyzed. Simultaneous measurements of conductivity, temperature, depth and light attenuation (an indicator of hydrothermal plume particles) were also obtained with the CTDT mounted on the rosette[10]. In addition, 10 discrete samples were obtained with the rosette on each tow. These samples were analyzed for dissolved ($<0.2\ \mu$m) and particulate manganese and iron[14]. Similar results for dissolved metal determinations performed *in situ* and in the laboratory (see below)

indicate that the colorimetric analyses used *in situ* are insensitive to metal in the particulate phase.

The track of the Scanner/CTDT package across the ridge crest during the XT-10 "tow-yo," and the corresponding contours of the hydrothermal temperature anomaly, light attenuation, manganese and iron are shown in Fig. 2a-d. This tow produced the first high resolution survey of Mn and Fe in a vent plume. Over 3700 sets of analyses for both metals were performed *in situ* during this tow. The contoured section of manganese shows excellent agreement with the distributions of temperature anomaly and light attenuation. The highest metal concentrations (259 nM Mn and 75 nM Fe) were found at a depth of about 2000 m (260 m above the bottom) and were centered over the axial valley of the ridge.

The correspondence between the dissolved iron contours and other physical parameters was poor (Fig. 2c). A plot of dissolved iron versus temperature anomaly for XT-10 (Fig. 3a) has a slope of only 900 nM $°C^{-1}$ (r^2 = 0.45). This corresponds to an iron:excess heat anomaly (Q) ratio of 0.90 nmol cal^{-1}. The ratio of iron:Q (corrected for changes in heat capacity[15]) in hydrothermal source fluids from vent fields located approximately 25 km further south on Cleft Segment ranges from 22.9 to 78.0 nmol cal^{-1}[16]. About 97% of the original dissolved iron had been removed from this plume if the source fluids resemble those of the south Cleft Segment. This accounts for the weak correlation of iron with other parameters.

A regression of manganese vs temperature anomaly shows a linear relationship

with a slope of 3.78 nmol cal^{-1} (r^2 = 0.96, Fig. 3b), in good agreement with the Mn:Q ratio determined previously for steady-state plumes in this area (1.9-4.1 nmol cal^{-1})[17]. The linear relationship suggests that Mn is not being rapidly removed. The Mn:Q ratio measured in this plume is, however, lower than that found in any of the black smoker vents that have been sampled at south Cleft (4.7-15.0 nmol cal^{-1})[16,18]. The composition of the black smoker source vents for the plume sampled during the XT-10 tow must be different from previously measured values, or there must be an additional source of low Mn:Q water that is entrained in the plume. The effects of these processes can be resolved by examining data from other tows in this area.

The results from a vertical cast (X-4, Fig. 3c,d) at a site 12 km to the north show considerably different trends, particularly for iron, than were found during XT-10 (Fig. 3a,b). The trends in the metal:temperature anomaly plots at both stations are confirmed by the excellent agreement between the *in situ* and laboratory analyses of dissolved manganese and iron (Fig. 3, large symbols). The metal:Q relationships at X-4 are clearly not linear. In addition, the highest Fe:Q ratio at station X-4 (10.6 nmol cal^{-1}) was 12 times greater than the average value found during the XT-10 tow. The high iron values suggest that the plume at X-4 was considerably younger than that sampled during XT-10. Analyses of the rosette samples show concentrations of particulate iron collected during the XT-10 tow that are as high as 475 nM (98% of the total dissolved + particulate concentration in this discrete sample), while they reached only 226 nM at X-4 (29% of the total

concentration). Estimates of the ages of the plumes at the time of sampling were derived using the temperature/pH/salt effect-corrected iron oxidation rate law[19], the observed Fe(II) concentrations[20] and the assumption that no particulate iron had been lost from the plume. This iron oxidation rate constant of $1.29*10^{-3}$ min^{-1} was derived from the equations of Millero and coworkers[19] for the *in situ* pH (7.74), temperature (1.7°C) and oxygen (70.1 μM) conditions within the plume. Ages were further corrected for time between bottle closure and sample acidification (9.56 and 11.76 hours for XT-10 and X-4 respectively). Average $Fe(II)/Fe_{total}$ for XT-10 and X-4 of 0.0135 and 0.106 yield plume ages of about 46 and 17 hours at XT-10 and X-4, respectively. Although some Fe may have been removed in the lower ascending plume, this removal is thought to take place within the first 25 meters, or first few minutes of mixing[21]. These ages, although tentative, demonstrate the utility of Fe(II)/Fe(III) as an age tracer.

The highest Mn:Q ratios at X-4 (6.7 nmol cal^{-1}) are within the range of values that have been found in black smoker vents at the south Cleft Segment (4.7-15.0 nmol cal^{-1})[16,18]. However, the lowest Mn:Q ratios at X-4 are well below this range. Chemical scavenging cannot remove sufficient Mn to produce these low ratios. There is no evidence for significant manganese removal in the buoyant plume at the Juan de Fuca Ridge, at the East Pacific Rise[21,22,23] or in the near field plume at XT-10 (Fig. 3b). Furthermore, bacterial removal of manganese is not rapid enough to account for this deficiency[22].

We postulate that the curvature in the X-4 Mn:excess temperature relationship is produced by mixing high Mn:Q discharge from black smoker vents with a low Mn:Q discharge. There are several possible sources for the low Mn:Q water. Venting of fluids that have undergone phase separation and segregation could provide a low Mn:Q signature to these plumes[24]. Phase separated fluids have been sampled from Axial Volcano, which is located between Cleft and Endeavour Segments on the Juan de Fuca Ridge[24,25]. The condensed vapor phase fluids have distinctively low chloride concentrations and are depleted in metals relative to heat (Mn:Q = 0.61 nM cal^{-1}; Fe:Q = 0.03 nM cal^{-1})[24,25]. Low temperature water/rock interactions in which seawater is heated but fewer metals are extracted from the basalt could also produce a low Mn:Q signature[26]. The mixing of ambient seawater with varying proportions of black smoker type fluids and condensed vapor phase or low temperature fluids could produce the signals observed both at XT-10 and X-4.

Alternatively, episodic large scale venting that has produced two megaplume events in this area[18,26] could also have influenced our observations. These megaplumes are characterized by Mn:Q values (0.2-0.7 nmol cal^{-1})[18,27] much lower than the steady state plumes in these areas (1.9-4.1 nmol cal^{-1})[17]. Although XT-10 shows some characteristics of rapid, megaplume type venting (homogeneous Me:Q, oblate spheroid shape, higher in the water column), the overall magnitude of this feature was small in comparison to a full scale megaplume event and the metal:heat

ratios were higher.

XT-10 appears to be the result of a relatively rapid discharge from a basically homogenous source. In contrast, the inhomogeneity in the thermochemical signatures of X-4 indicate not only that there are multiple sources for this plume, but that the sources are in close spatial and temporal proximity in order to be entrained in the same portion of this relatively young and turbulent plume. Hydrothermal fluids with distinct Mn:Q ratios must be present in the vent field that produces this plume. Recent submersible dives by one of us (GJM) have confirmed the presence of both a low and high Mn:Q source in this area, conforming to the ratios found in the overlying plume[28]. ^{3}He could also be used to evaluate, more definitively, the inputs from low and high temperature sources and distinguish the contribution from phase separated fluids. To date, however, there is no *in situ*, high resolution capability for determining ^{3}He, and Mn is thought to behave similarly and conservatively in the near field[21,22,23].

In situ determinations of the concentrations of dissolved iron and manganese in hydrothermal plumes coupled with high resolution CTDT data have increased our understanding of the variability in metal:Q ratios typically under-represented by conventional point source sampling techniques. This capability has enabled us to map the near field distributions of these metals and has revealed metal:Q relationships that require three endmember mixing of sources in close spatial and temporal proximity. Although there is no substitute for hydrothermal endmember

sampling by submersibles, this rapid, low cost, remote detection capability can provide high resolution distributions more representative of the full range of metal:Q values that contribute to the composite plume. This has allowed us, from the plume perspective, to recognize that quantitatively important and thermochemically distinct sources contribute to the dispersing plume. Thermochemical characterization of the resultant hydrothermal plume, however, may preclude, to some extent, the need for submersible search and verification of the source fluids. The Scanner configuration is flexible and can accommodate one channel for the determination of Fe(II) and the other for Fe_{total}. This potential for the Scanner to be used for *in situ* age determinations in plume environments is quite promising. Furthermore, this technique demonstrates the feasibility of mapping iron and manganese concentrations and metal:heat relationships over mid-ocean ridges of the world's oceans and could therefore provide a more accurate accounting of the global cycling of elements through hydrothermal systems.

References

(1) Edmond, J. M., Von Damm, K. L., McDuff, R. E. & Measures, C. I. Nature **297**, 187-191 (1982).

(2) Bostrom, K., Peterson, M. N. P., Joensuu, O. & Fisher, D. E. J. geophys. Res. **74**, 3261-3270 (1969).

(3) Edmond, J. M. et al. Earth planet. Sci. Lett. **46**, 1-18 (1979).

(4) Feely, R. A. et al. Earth planet. Sci. Lett. **96**, 305-318 (1990).

(5) Trefrey, J. H. & Metz, S. Nature **342**, 532-533 (1990).

(6) Kadko, D., Bacon, M. P. & Hudson, A. Earth planet. Sci. Lett. **81**, 349-357 (1987).

(7) German, C. R., Klinkhammer, G. P., Edmond, J. M., Mitra, A. & Elderfield, H. Nature **345**, 515-518 (1990).

(8) Johnson, K. S., Beehler, C. L. & Sakamoto-Arnold, C. M. Analyt. Chim. Acta **179**, 245-257 (1986).

(9) Johnson, K. S., Beehler, C. L. & Sakamoto-Arnold, C. M. Science **231**, 1139-1141 (1986).

(10) Baker, E. T. & Massoth, G. J. Science **234**, 980-982 (1986).

(11) Baker, E. T. & Massoth, G. J. Earth planet. Sci. Lett. **85**, 59-73 (1987).

(12) Chin, C. S., Johnson, K. S. & Coale, K. H. Mar. Chem. in press (1991).

(13) Stookey, L. L. Anal. Chem. **42**, 779-781 (1970).

(14) Klinkhammer, G. Anal. Chem. **52**, 117-120 (1980).

(15) Bischoff, J. L. & Rosenbauer, R. J. Am. J. Sci. **285**, 725-763 (1985).

(16) Von Damm, K. L. & Bischoff, J. L. J. geophys. Res. **92**, 11334-11346 (1987).

(17) Massoth, G. J., Baker, E. T., Roe, K. K. & Lebon, G. T. EOS **71**, 143 (1989).

(18) Massoth, G. J. et al. EOS **69**, 147 (1988).

(19) Millero, F. J., Sotolongo, S. & Izaguirre, M. Geochim. cosmochim. Acta **51**, 793-801 (1987).

(20) Elrod, V. et al. EOS **71**, 143 (1989).

(21) Mottl, M. J. & McConachy, T. F. Geochim. cosmochim. Acta **54**, 1911-1927 (1990).

(22) Cowen, J. P., Massoth, G. J. & Feely, R. A. Deep Sea Res. **34**, 1619-1637 (1990).

(23) Lupton, J. E. et al. Earth planet. Sci. Lett. **50**, 115-127 (1980).

(24) Massoth, G. J. et al. Nature **340**, 702-705 (1990).

(25) Butterfield, D. A., Massoth, G. J., McDuff, R. E., Lupton, J. E. & Lilley, M. D. J. geophys. Res. **95**, 12,895-12,921 (1990).

(26) Kadko, D. C., Rosenberg, N. D., Lupton, J. E., Collier, R. W. & Lilley, M. D. Earth planet. Sci. Lett. **99**, 315-335 (1990).

(27) Baker, E. T. et al. J. geophys. Res. **94**, 9237-9250 (1989).

(28) Massoth, G. J. et al. EOS, **71**, 1619 (1990).

Figure Captions

Figure 1a) Map of the world's oceans showing locations of known hydrothermal vents (stars, showing scarcity of known vent sites), and the distribution of metalliferous sediment coverage where $Al/Al+Fe+Mn < 60$ (indicating vast extent of hydrothermally derived sediments, after Bostrom[2]). 1b) Location of the Cleft Segment along the Juan de Fuca Ridge. 1c) Areal map of the hydrothermal temperature anomaly (in °C) at the north Cleft Segment and tow track of the CTDT package used to map the spatial extent of the plumes in this area. The XT-10 tow track is shown by dashed line. The axial valley orientation is N 20°E and directly underlies the temperature anomaly maxima.

Figure 2) Measured properties for the tow-yo XT-10, contoured over the tow track. Left hand side of each panel represents 44° 52.8'N, 130° 13.0'W on the eastern flank of the ridge; right hand side of each panel represents 44° 50.6'N, 130° 21.0'W over the western valley wall. a) Tow track of the CTDT/Rosette/Scanner package, as it was towed in a southwesterly direction across the axial valley (see Fig. 1c), is plotted together with the contoured section of the excess temperature anomaly, D-theta[10], an indicator of the plume's location and strength. The contour interval is 0.01 °C. b) Light attenuation anomaly, as measured with a beam transmissometer secured to the CTDT package, shows a high correlation between the distribution of

hydrothermal particles (primarily iron oxyhydroxides) and the temperature anomaly. The contour interval is 0.01 m^{-1}. c) Iron concentrations contoured over the XT-10 transect at 10 nM intervals show weak correlation with the other conservative tracers temperature anomaly and manganese due to its rapid oxidation and removal. These concentrations are near the Scanner detection limit for iron (18 nM). The noise, therefore, represents both plume heterogeneity and analytical variability at these low levels. d) The more conservative tracer, manganese, contoured over the XT-10 section at 25 nM intervals shows excellent agreement with temperature anomaly and light attenuation. The detection limit is 18 nM.

Figure 3) Plots of dissolved metals vs temperature anomaly for the stations XT-10 and X-4. Scanner metal analyses performed *in situ* colorimetrically[12], whereas discrete dissolved samples were analyzed by column extraction followed by GFAAS[14] at PMEL. Particulate samples were analyzed by XRF using thin film procedures also at PMEL. a) Iron vs temperature anomaly along XT-10 shows extremely low slope relative to the source fluids. The variability in this data reflects concentrations near our detection limit for iron and the nonconservative behavior of iron in these plumes. The concentrations measured *in situ* are in good agreement with the GFAAS results determined at PMEL. b) Manganese (nM) vs excess temperature anomaly (°C) from both the Scanner and discrete samples from XT-10. This Mn:temperature anomaly relationship is quite linear ($r^2 = 0.96$) with a slope of 3.78 nmol cal^{-1}, less

than that observed in the nearest known source fluids. c) Iron vs temperature anomaly is plotted for X-4. d) Manganese vs temperature anomaly plotted for X-4. This station shows much more curvature indicating inhomogeneous mixing of multiple sources, some of which bear Mn:heat ratios similar to those observed in the black smokers to the south (see text).

Acknowledgements

We wish to thank R. Feely for accommodating our participation on the NOAA Vents '89 cruise, leg I; S. Walker for processing the CTDT data; V. Elrod and K. Roe for analysis of discrete water samples for dissolved Fe and Mn, G. Lebon for modifications to the PMEL rosette to accommodate the Scanner and for particulate Fe determinations by XRF analysis, and the crew and officers of the R/V *Discoverer*. This research was supported by the Ocean Sciences Division of the NSF, the Office of Naval Research, and the NOAA VENTS Program.

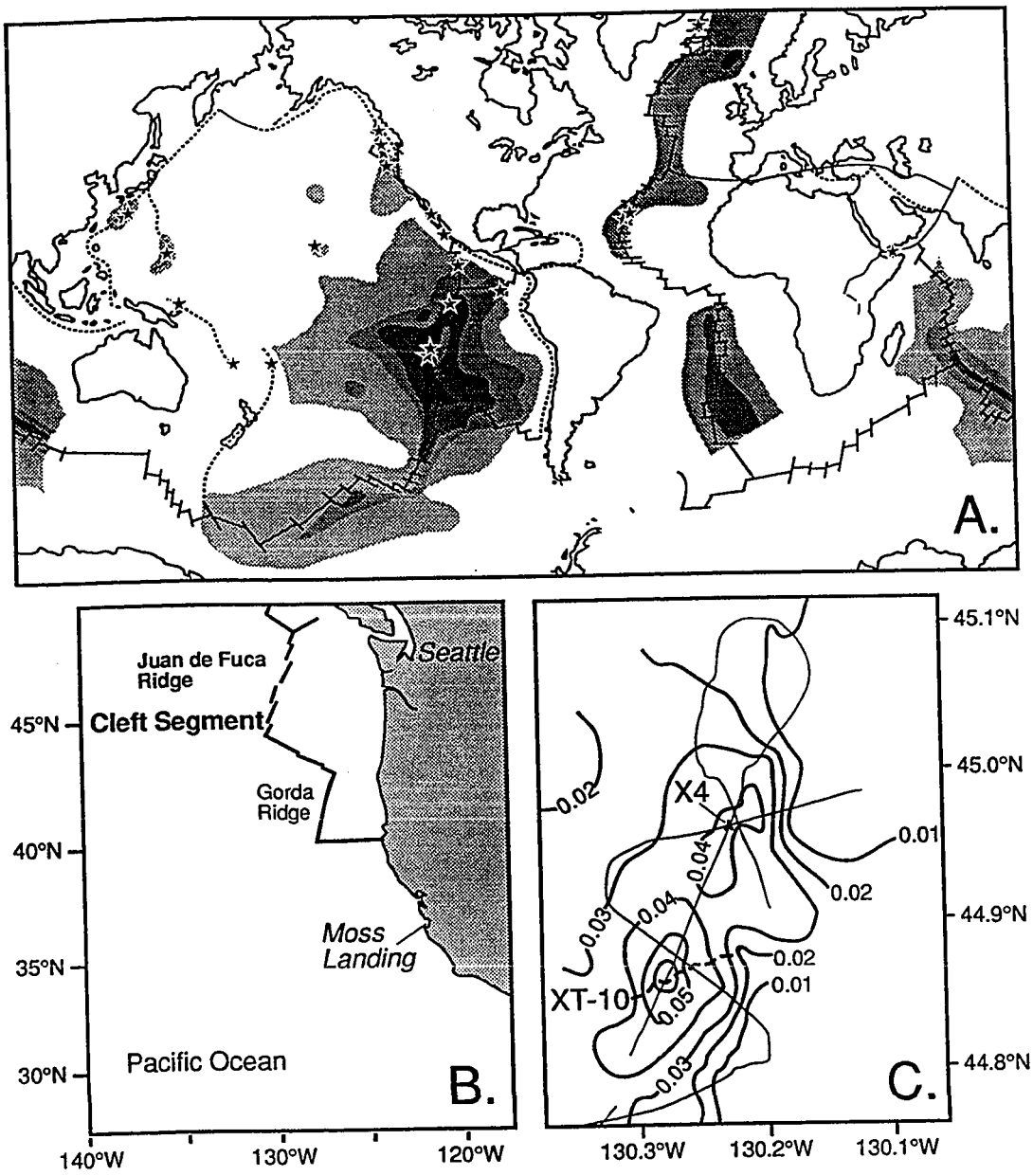
A.
Juan de Fuca
Ridge
Seattle
45°N
Cleft Segment
Gorda
Ridge
40°N
Moss
Landing
35°N
Pacific Ocean
30°N
B.
140°W
130°W
120°W
45.1°N
45.0°N
44.9°N
44.8°N
X4
0.02
0.01
0.04
0.02
0.03
0.04
0.02
XT-10
0.01
0.05
0.03
C.
130.3°W
130.2°W
130.1°W

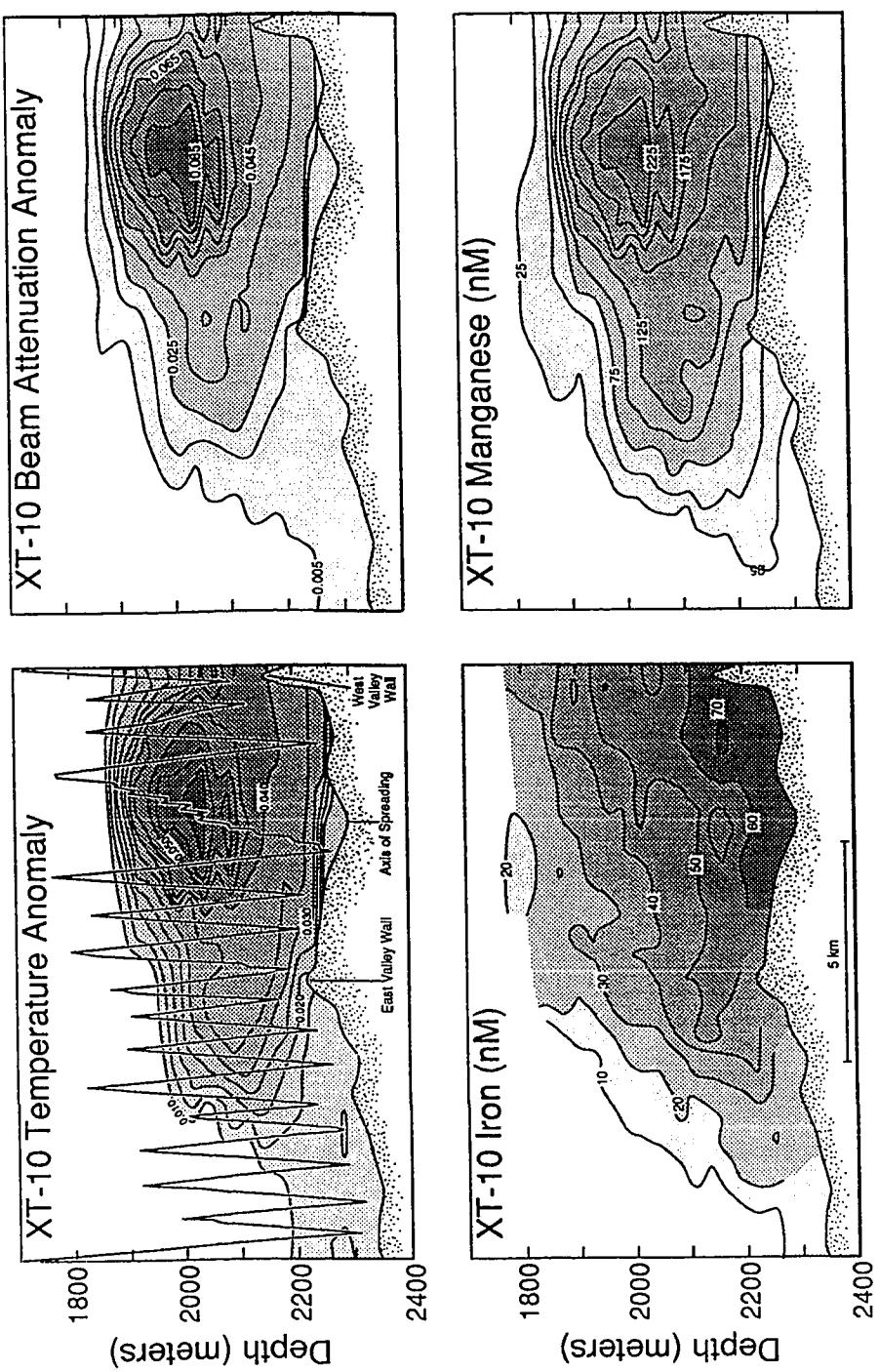
XT-10 Temperature Anomaly
XT-10 Beam Attenuation Anomaly
XT-10 Iron (nM)
XT-10 Manganese (nM)
Depth (meters)
1800
2000
2200
2400
West Valley Wall
East Valley Wall
Axis of Spreading
5 km

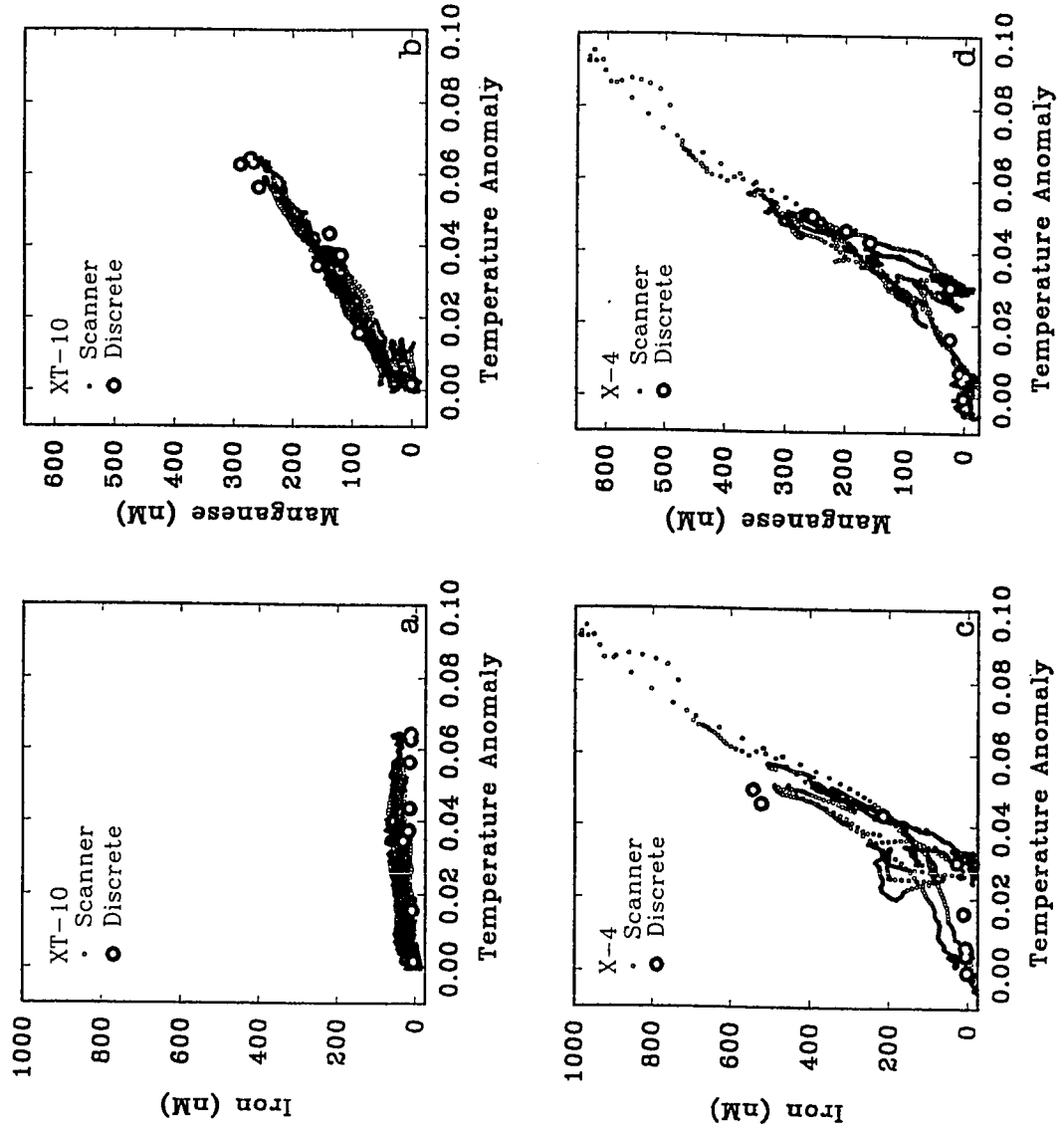
XT−10
Scanner
Discrete
Iron (nM)
Manganese (nM)
Temperature Anomaly
a.
b.
X−4
c.
d.